Regulation of cell signalling by iRhoms



Boris Sieber

Brasenose College
University of Oxford

A thesis submitted to the University of Oxford
for the degree of Doctor of Philosophy

Trinity Term 2019

Table of contents

Acknowledgments **5**

Abstract **6**

Abbreviations **8**

1. Introduction **12**

1.1. iRhoms **12**

1.1.1. The rhomboid-like superfamily 12

1.1.2. iRhoms structure and expression 15

1.2. TACE **20**

1.2.1. TACE structure and function 20

1.2.2. TACE maturation and trafficking 22

1.2.3. TACE activation 24

1.3. Proteostasis of ER proteins **29**

1.3.1. iRhoms and protein turnover 29

1.3.2. Degradation routes for transmembrane proteins in the ER 32

1.3.2.1. ERAD 32

1.3.2.2. ER-phagy 35

1.4. Pathological importance of iRhoms and TACE **40**

1.4.1. iRhoms and TACE in inflammation and immunity 40

1.4.2. iRhoms and TACE in cancers 41

1.4.2.1. iRhom1 in cancer cells 41

1.4.2.2. iRhom2 in cancer cells 42

1.4.2.3. TACE in cancers 44

1.5. Ras proto-oncogenes **45**

1.5.1. Ras mutations 45

1.5.2. Ras effectors and cell transformation 47

1.5.3. Oncogenic KRas in lung cancer 49
1.6. Aim of the projects 51
2. Material and methods 53
2.1. Molecular biology methods 53
2.1.1. Molecular cloning 53
2.1.1.1. Polymerase chain reaction (PCR) 53
2.1.1.2. Restriction digest 54
2.1.1.3. Agarose gel electrophoresis and gel purification 55
2.1.1.4. DNA assembly 55
2.1.1.5. Transformation 57
2.1.1.6. Plasmid preparation 57
2.1.1.7. Sequencing 57
2.1.2. mRNA isolation and quantitative PCR 58
2.1.3. Isolation of genomic DNA 59
2.1.4. CRISPR/Cas9 constructs 60
2.2. Cell biology methods 61
2.2.1. Cell lines and culture 61
2.2.2. DNA transfection 62
2.2.3. siRNA transfection 63
2.2.4. Lentiviral transduction 64
2.2.5. CRISPR/Cas9 knockout 65
2.3. Biochemical methods 66
2.3.1. Cell lysis 66
2.3.2. Bicinchoninic acid (BCA) assay 66
2.3.3. Co-immunoprecipitation 66
2.3.4. Concanavalin A enrichment 67
2.3.5. Deglycosylation assay 67
2.3.6. SDS-PAGE and western blot 67
2.3.7. Alkaline phosphatase assay 70

2.3.8. Immunofluorescence staining and confocal microscopy 71

3. Regulation of TACE activity 74

3.1. Introduction 74

3.2. Results 75

3.2.1. The stimulated activation of TACE requires iRhom phosphorylation 75

3.2.2. Generating HEK293T iRhom1/2 DKO to study Ras-induced shedding DKO 81

3.2.3. Oncogenic Ras induces shedding in an iRhom2-dependent manner 86

3.2.4. Oncogenic Ras induces iRhom2 phosphorylation, which is required for shedding and 14-3-3 binding 93

3.3. Discussion and future plans 97

4. iRhom-driven degradation of EGFR ligands 104

4.1. Introduction 104

4.2. Results 106

4.2.1. iRhoms reduce Myc-EGF level in a dose-dependent manner 106

4.2.2. iRhom-driven degradation is rescued by proteasomal and lysosomal inhibitors 107

4.2.3. iRhoms drive degradation of Myc-EGF from the ER in a Beclin 1-dependent manner 112

4.2.4. Systems to study the role of endogenous iRhoms in Myc-EGF degradation 124

4.3. Discussion 134

5. Discussion 137

5.1. Regulation of TACE activity 137

5.1.1. KRas-induced activation of TACE by phosphorylation of iRhom2 N-terminus 138

5.1.2. TACE activity in KRas tumourigenesis in the lung 140

5.1.3. EGFR dependence of KRas-induced tumourigenesis 142

5.1.4. Downstream effectors of KRas as therapeutic targets 145

5.2. iRhom-driven degradation of EGFR ligands 149

5.2.1. iRhom-driven degradation of Myc-EGF from the endoplasmic reticulum (ER) in a Beclin-1 dependent manner 149
5.2.2. Dual degradation of ER proteins 150
5.2.3. ER-phagy 155
5.2.4. The role of endogenous iRhoms in Myc-EGF degradation 158
Appendix 160
References 164

Acknowledgments

First, I would like to thank my supervisor, Matthew Freeman, for the support and guidance throughout this DPhil. I am very grateful for the opportunity to work in your lab on these projects.

Many thanks to the current and past members of the Freeman lab: Shaked Ashkenazi, Iqbal Dulloo, Stefan Düsterhöft, Adam Grieve, Lucie Kafková, Ulrike Künzel, Kyojiro Ikeda, Nina Jajčanin Jozić, Clémence Levet, Viorica Liebe, Fangfang Lu, Ángela Moncada Pazos, Sonia Muliyil, Archna Shah, Xin Shen, Hongmei Xu, Lucrezia Zarcone and Boyan Zhang. I would like to particularly thank Adam, Fangfang, Uli and Hongmei for the interesting discussions, encouragements and for helping me to evolve into a DPhil student. Many thanks to Adam for the scientific discussions, and for the feedbacks on my scientific applications and reports. The (too) rare contributions of Gunther were also truly appreciated.

I am very grateful for the support of Brasenose College, the Boehringer Ingelheim Fonds and the Medical Research Council.

I would like to thank my family and my friends for your support and enthusiasm. Thanks a lot for your support and encouragements, and for coming to visit and offering me much-needed distractions from the lab.

Thank you my Dzes for believing in me and for the adventures to come.

Abstract

My first project focuses upon the regulation of TACE by oncogenic stimulation. TACE (for TNFα-activating enzyme) is a major regulator of numerous cell signalling pathways, including epidermal growth factor receptor (EGFR) signalling. TACE acts at the plasma membrane to release signalling factors into the extracellular medium. iRhom1 and iRhom2 are multi-pass membrane proteins that belong to the rhomboid-like superfamily, and they are the ultimate regulators of TACE activity. It has been recently discovered that the phosphorylation of iRhom2 is required for the stimulated activity of TACE at the plasma membrane. However, whether iRhom phosphorylation is crucial in other pathological contexts is unknown. In addition, the role of iRhom1 phosphorylation in TACE activation remains unstudied.

I have demonstrated that the phosphorylation of iRhom1 is required for TACE activity upon pharmacological stimulation. Therefore, the mechanism of TACE activation is conserved between iRhom1 and iRhom2. To study the role of iRhom phosphorylation in cancer, the role of the central proto-oncogenes Ras was investigated. Oncogenic KRas and HRas stimulate TACE activity, which demonstrates the conserved role of Ras proteins in stimulating the release of EGFR ligands by TACE. The reconstitution of double knockout (DKO) cells with iRhom2, but not with iRhom1 supports KRas-induced shedding. The specificity towards iRhom2 therefore constitutes a characteristic feature of oncogenic stimulation of TACE activity. Importantly, I have shown KRas-induced shedding requires iRhom2 phosphorylation and recruitment of the phospho-binding proteins 14-3-3. To assess the importance of these findings in lung cancer, the expression of iRhoms was genetically removed in non-small-cell lung cancer cells, thereby allowing me to test the requirement of iRhom2 phosphorylation for *in vivo* tumourigenesis.

My second project concerns another regulatory function of iRhoms: the degradation of EGFR ligands. Before being cleaved off at the plasma membrane, EGFR ligands are produced as single-pass transmembrane proteins in the endoplasmic reticulum. It was discovered that iRhoms induce the degradation of EGFR ligands by the proteasome. The role of iRhoms as negative regulators of EGFR ligands is conserved in *Drosophila* and in mammalian cells. However, the molecular mechanism by which iRhoms destabilise EGFR ligands was unknown.

I established a system in human cells and confirmed that ectopic iRhom expression triggers dose-dependent degradation of EGF. I found that the two degradation machineries of the cell support iRhom-driven degradation: the proteasome and the lysosome. Focussing on lysosomal degradation, I found that iRhoms drive EGF to lysosomal degradation directly from the ER, suggesting that this constitutes an ER-phagy route. Importantly, I found a requirement for the autophagy core protein Beclin-1 in this process. Finally, I attempted to determine the requirement of endogenous iRhoms in the degradation of EGF. Although I found an upregulation in EGF protein in iRhom-depleted cells, further validation with iRhom depletion and genetic ablation of iRhom1/2 by CRISPR/Cas9 highlighted technical issues with my approach. Therefore, further work is required to establish the involvement of endogenous iRhoms in EGF degradation.

Abbreviations

ADAM17	a disintegrin and metalloprotease 17
AP	alkaline phosphatase
Areg	amphiregulin
ATZ	α1-antitrypsin Z
BCA	bicinchoninic acid
BSA	bovine serum albumin
BTC	betacellulin
CANDIS	conserved adam seventeen dynamic interaction sequence
cDNA	complementary DNA
CHX	cycloheximide
CRISPR/Cas9	clustered regularly interspaced short palindromic repeats/CRISPR-associated protein 9
DKO	double knockout
DNA	deoxyribonucleic acid
DSB	double-strand break
ECL	enhanced chemiluminescence
EGF	epidermal growth factor
EGFR	epidermal growth factor receptor
Endo H	endoglycosidase H
ER	endoplasmic reticulum
ERAD	ER-associated degradation
Ereg	epiregulin
ER-EGF	ER-retained green-EGF
FBS	fetal bovine serum
FTase	farnesyltransferase
FTI	FTase inhibitor
GAPDH	glyceraldehyde 3-phosphate dehydrogenase
GAP	GTPase-activating protein
GDP	guanosine diphosphate
GEF	guanine nucleotide exchange factor
GnRHR	gonadotropin-releasing hormone receptor
GPCR	G protein-coupled receptor

gRNA	guide RNA
GTP	guanosine triphosphate
HB-EGF	heparin-binding epidermal growth factor
HMGR	hydroxy β-methylglutaryl-CoA reductase
HNSCC	head and neck squamous cell cancer
IP	immunoprecipitation
IRHD	iRhom homology domain
KO	knockout
LAC	lung adenocarcinoma
LAP	LC3-associated phagocytosis
LIR	LC3-interacting region
LPS	lipopolysaccharide
MEF	mouse embryonic fibroblast
MOI	multiplicity of infection
MPD	membrane proximal domain
mRNA	messenger RNA
NHEJ	non-homologous end joining
NPC	Niemann–Pick type C
NSCLC	non-small-cell lung carcinoma
NSG	non-obese diabetic (NOD) scid gamma
PAC	proteasomal assembly chaperone
PAM	protospacer adjacent motif
PCR	polymerase chain reaction
PDL	poly-D-lysine
PE	phosphatidylethanolamine
PLL	poly-L-lysine
PMA	phorbol-12-myristate-13-acetate
PNGase F	peptide N-glycosidase F
pNP	paranitrophenol
pNPP	p-Nitrophenyl phosphate
PVDF	polyvinylidene difluoride
qPCR	quantitative PCR
RNA	ribonucleic acid

SCLC	small-cell lung cancer
SP	smartpool siRNA
ST	stealth siRNA
STING	stimulator of interferon genes
TACE	TNFα-activating enzyme
TBE	tris-borate-EDTA
TGFα	transforming growth factor alpha
TGN	trans-Golgi network
TMD	transmembrane domain
TNFα	tumour necrosis factor alpha
TOC	tylosis with oesophageal cancer
TPD	TACE pro-domain
VISA	virus-induced signalling adapter

CHAPTER 1

Introduction

1. Introduction

A wide range of topics will be covered in this introduction as they represent the basis for the two functions of iRhoms that I have investigated. The first function is the role of iRhoms as cofactors of the shedding enzyme TACE (section 1.2). I have particularly assessed this role in the pathological context of Ras-induced transformation and tumourigenesis (sections 1.4 and 1.5). The second function I have investigated is the ability of iRhoms to regulate protein turnover in the endoplasmic reticulum (section 1.3).

1.1. iRhoms

1.1.1. The rhomboid-like superfamily

iRhoms are members of the rhomboid-like superfamily, which were first discovered as EGF regulators in *Drosophila melanogaster* (Freeman, 1994; Sturtevant et al., 1993). The name of the superfamily comes from the phenotype of the *Drosophila* Rhomboid-1 mutant larvae, which presents a pointed head skeleton (Jürgens et al., 1984). Rhomboid-1 is a serine protease that cleaves the EGFR ligand Spitz in *Drosophila*. As this cleavage occurs inside the transmembrane domain (TMD) of Spitz, Rhomboid-1 has defined the rhomboid-like superfamily as one of the few families containing intramembrane proteases (Lee et al., 2001; Urban et al., 2001).

The rhomboid-like superfamily is conserved across all kingdoms of life. Structurally, the best characterised member is the *Escherichia coli* protease GlpG, whose crystal structure has been determined (Ben-Shem et al., 2007; Wang et al., 2006; Wu et al., 2006). The structure of GlpG defined the rhomboid-like fold as a six TMD core with a GxxxG motif in TMD6 that interacts with TMD4 for stabilisation of

the overall fold. The rhomboid-like fold is the central determinant for the recognition of transmembrane proteins, especially the single-pass type I transmembrane proteins (Tichá et al., 2018).

Generally, there is extensive sequence divergence between rhomboid-like proteins, yet bioinformatical analyses have identified a wider rhomboid-like superfamily comprising 14 members (Lemberg and Freeman, 2007). They can be phylogenetically divided into two branches: the first branch contains the active rhomboid proteases and iRhoms (which are catalytically inactive) (Figure 1A). The activity of the rhomboid proteases relies on a catalytic dyad, constituted by serine and histidine residues (Lemberg et al., 2005). The second branch is formed of all other inactive rhomboid-like proteins that are evolutionary more distant to the active proteases and iRhoms (Figure 1A) (Adrain and Freeman, 2012).

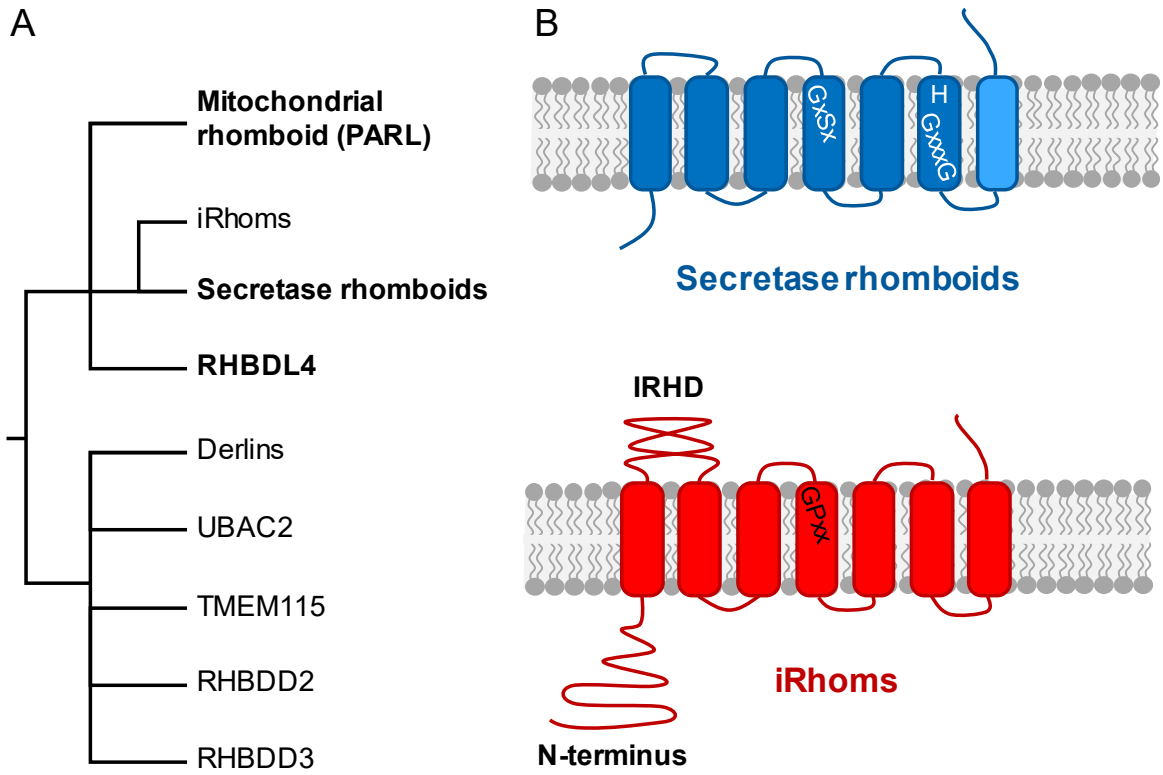


Figure 1: iRhoms in the rhomboid-like superfamily. A) Overview of the mammalian members of the rhomoid-like superfamily. The rhomboid-like superfamily is divided into two main branches according to the conservation in function and sequence. At the top is the branch with the active rhomboid proteases (in bold) and the closely related iRhoms. The lower branch contains other inactive members of the superfamily, which are evolutionary more distant to the active proteases. Of note, this figure is not a phylogram, but a representation of the classification. **B)** Comparison of the features or the mammalian secretase rhomboids and iRhoms. The schematic representation of the secretase rhomboid indicates the position of the catalytic serine (GxSx) and histidine (H). In addition, the first six transmembrane domains constituting the rhomboid fold are shown in dark blue, and the interaction motif GxxxG is indicated. The schematic representation of iRhoms shows their characteristic long, disordered cytoplasmic N-terminus and their conserved L1 loop between the first and the second transmembrane domains called the iRhom homology domain (IRHD). In addition, the presence of the proline (GPxx) impairing any proteolytic activity is indicated.

1.1.2. iRhoms structure and expression

iRhoms are evolutionarily the closest members to the rhomboid proteases. However, iRhoms are catalytically inactive, as a proline disrupts the canonical rhomboid protease active site (Lemberg and Freeman, 2007). The presence of a proline in the place of the catalytic serine of an active rhomboid is sufficient to abolish its proteolytic activity. The absence of catalytic activity of iRhoms is further attributed to their inability to cleave their interactors, such as the EGFR ligands and TACE/ADAM17 (Zettl et al., 2011).

The rhomboid-like fold of iRhoms is completed at the C-terminus by an additional TMD, which makes iRhoms seven transmembrane domain-containing proteins (Lemberg and Freeman, 2007). The two specific features of iRhoms are a long cytoplasmic N-terminus, and an extended loop (termed the L1 loop) between TMD1 and TMD2 (Figure 1B) (Lemberg and Freeman, 2007). The long cytoplasmic N-terminus undergoes numerous post-translational modifications and serves as a regulatory hub for iRhoms (see sections 1.1.3 and 1.2.3). The L1 loop in iRhoms is called the iRhom homology domain (IRHD), and is the most highly conserved region in all iRhom proteins. The IRHD contains 16 cysteines, which are proposed to create a globular fold by disulphide bonds (Lemberg and Freeman, 2007).

Mammalian cells possess two iRhoms encoded by RHBDF1 (for iRhom1) and RHBDF2 (for iRhom2) (Ensembl genome browser (Yates et al., 2016)). A comparison of the amino acid sequences demonstrated that human iRhom1 is 68% similar to human iRhom2 (Lemberg and Freeman, 2007). However, there are variations when comparing the domains within iRhoms: the IRHD shows the highest

similarity, whereas the N-termini are the most divergent regions (Dulloo et al., 2019; Lemberg and Freeman, 2007).

The main cellular localisation of iRhoms is within the endoplasmic reticulum (ER) (Grieve et al., 2017; Künzel et al., 2018; Luo et al., 2016; McIlwain et al., 2012; Zettl et al., 2011; Zou et al., 2009). However, smaller pools of iRhoms are also present in other compartments of the secretory pathway. In particular, the presence of iRhoms has been reported in the Golgi and at the plasma membrane (Grieve et al., 2017; Hosur et al., 2014; Künzel et al., 2018; Luo et al., 2016; Maney et al., 2015; McIlwain et al., 2012). Finally, it has recently been reported that iRhoms also localise at lysosomes (Künzel et al., 2018; Luo et al., 2016), which suggests that iRhoms undergo turnover from the cell surface.

In mouse tissues, qPCR analyses have demonstrated that both iRhoms are expressed in most mouse tissues (Li et al., 2015). The lung and the skin constitute important contexts for iRhom2 (Christova et al., 2013; Li et al., 2015), as illustrated by its high expression that can be detected at the protein level (Künzel et al., 2018), and by the pathological importance of iRhom2 in the skin (see section 1.4). As only iRhom2 is expressed in the immune system, this has allowed the characterisation of iRhom2 importance for the regulation of inflammation and infection (section 1.4.1). Conversely, since the non-immune cells of the brain exclusively express iRhom1, this represents an interesting context to investigate the *in vivo* importance of iRhom1 function.

1.1.3. iRhoms regulation

One major way that all rhomboid-like proteins are regulated is via spatiotemporal regulation of their expression. iRhoms expression is upregulated by different stimuli (Figure 2). In macrophages, iRhom2 mRNA increases upon viral infection (Luo et al., 2016) or after treatment by the bacterial cell wall component LPS, which mimics bacterial infection (Adrain et al., 2012; McIlwain et al., 2012). The increase of iRhom2 mRNA upon LPS treatment has been demonstrated in mouse tissues after intraperitoneal injection (Lu et al., 2017). Treatment with translation inhibitors or stressors of the endoplasmic reticulum represents another context in which iRhoms are upregulated (Lee et al., 2015). Finally, the expression of iRhoms is also increased during cancer progression (section 1.4.2).

In addition to regulation of transcriptional expression, another control of the abundance of iRhoms in the cell is the regulation of protein stability (Figure 2). It has been shown that iRhoms protein stability is increased upon proteasomal inhibition (Hosur et al., 2014; Zettl et al., 2011). There is also regulation of iRhom2 level at the plasma membrane as it is stabilised by inhibitor of endocytosis (Cavadas et al., 2017). Recently, our lab and Colin Adrain's lab have discovered that FRMD8 (also called iTAP) is required for the stability of iRhom2 proteins (Künzel et al., 2018; Oikonomidi et al., 2018). FRMD8 is a cytoplasmic protein that binds the N-terminus of iRhoms, thereby representing a novel binding partner of iRhoms. The role of FRMD8 in iRhom2 stability is demonstrated in cells upon FRMD8 overexpression, which increases iRhom2 half-life (Oikonomidi et al., 2018). In addition, depletion of FRMD8 causes a dramatic decrease in iRhom2 levels, which is rescued by lysosomal inhibitors (Künzel et al., 2018; Oikonomidi et al., 2018). FRMD8 is therefore required for iRhom2 stability at the protein level, as it prevents its

lysosomal degradation. Interestingly, FRMD8 is part of a tripartite complex with iRhom2 and TACE, and it is necessary and sufficient for iRhom2 to localise at the plasma membrane (Künzel et al., 2018; Oikonomidi et al., 2018). Overall, FRMD8 is a crucial component for the stability of iRhom2 and for its role at the plasma membrane as a TACE cofactor.

Finally, iRhoms are regulated by post-translational modifications, such as ubiquitination and phosphorylation (Figure 2). Several lysines in the N-terminus of human iRhom2 have been identified as ubiquitination sites (Dr Ulrike Künzel, unpublished data). iRhom2 has recently been shown to interact with the E2-conjugating enzyme UBE2V1 and the E3 ligase CHIP, which triggers iRhom2 polyubiquitination upon TNFα treatment (Zhang et al., 2018). In addition, iRhom2 also binds to the E3 ligases MARCH5 (Luo et al., 2017) and RNF5 (Cavadas et al., 2017; Luo et al., 2017). As a result, regulation of iRhom2 by the ubiquitination machinery constitutes an emerging theme. iRhom2 is also regulated by phosphorylation of N-terminal residues (Cavadas et al., 2017; Grieve et al., 2017). This phosphorylation, triggered by PMA and LPS stimulation, depends on the kinases ERK1/2 and p38 (Cavadas et al., 2017; Grieve et al., 2017). The importance of their activity on iRhoms for TACE regulation at the plasma membrane will be presented in section 1.2.3.

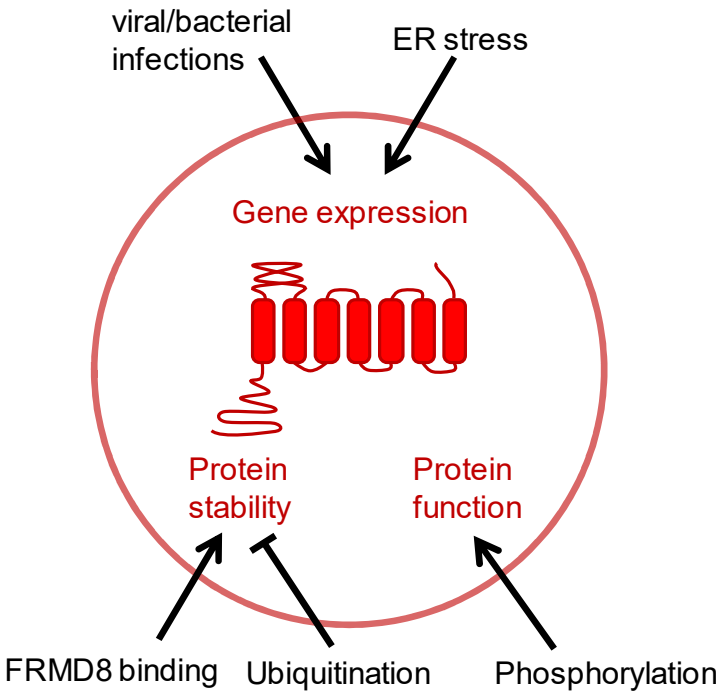


Figure 2: Regulation of iRhoms level and function. Gene expression of iRhoms is increased upon bacterial infection, viral infection or treatment with ER stressors. The stability of iRhoms proteins is increased by binding with interactors such as FRMD8, whereas polyubiquitination of iRhoms triggers their degradation. Finally, one of the best characterised post-translational modifications affecting iRhoms function on TACE is the phosphorylation of their cytoplasmic N-terminus, which is triggered either pharmacologically or by the bacterial cell wall component LPS mimicking a bacterial infection.

1.2. TACE

1.2.1. TACE structure and function

To ensure proper development, cells need to communicate by releasing signalling factors to the external environment. Upon reaching target cells, these factors bind to receptors to trigger intracellular pathways, ensuring an appropriate response by the cell. As many signalling factors are transmembrane proteins, they need to be cleaved off the plasma membrane, in a process called shedding.

Some of the most studied signalling factors are the ligands of epidermal growth factor (EGF) receptor (EGFR). They share a type I transmembrane topology with one (or several) EGF domain(s) in the extracellular N-terminus. Upon shedding, the active EGF domain is released by the signal-sending cell and it activates EGFR receptors (ERBB1-4) on the target cell. This binding triggers activation of intracellular signalling pathways such as Ras-MEK-ERK and PI3K pathways, which ultimately regulate cell proliferation, migration or differentiation (Adrain and Freeman, 2014).

One of the best characterised shedding enzymes is TNFα-activating enzyme (TACE), which also called a disintegrin and metalloprotease 17 (ADAM17). Although it was first discovered as a TNFα shedding enzyme (Black et al., 1997; Moss et al., 1997), it is now known that TACE has more than 90 substrates (Düsterhöft et al., 2019). Among these are the following EGFR ligands: amphiregulin (Areg), transforming growth factor alpha (TGFα), heparin-binding epidermal growth factor (HB-EGF), epiregulin (Ereg). In contrast to TACE, its closely related sheddase, ADAM10, is a principal shedding enzyme of the EGFR ligands epidermal growth factor (EGF) and betacellulin (BTC) (Sahin et al., 2004).

TACE is a metalloprotease with a type I transmembrane structure (Figure 3). In the extracellular N-terminus is its catalytic site that relies on a Zn^{+2} ion to catalyse shedding of substrate. At the very C-terminus is the pro-domain, which has a bifunctional role. It first acts as a chaperone during TACE biogenesis, and then later functions as an inhibitor domain, before being cleaved off by the proprotein convertase furin in the trans-Golgi network (TGN) (Endres et al., 2003; Peiretti et al., 2003; Schlöndorff et al., 2000). This step constitutes the maturation of TACE, which is followed by its trafficking to the plasma membrane, where mature TACE can be activated to shed substrates. TACE possesses three other regulatory domains in its N-terminus (Figure 3): the disintegrin-like domain, the membrane proximal domain (MPD) and CANDIS (for Conserved Adam seventeeN Dynamic Interaction Sequence) (Düsterhöft et al., 2019). At the C-terminus is the cytosolic tail, for which the regulatory role in shedding is still debated (see section 1.2.3).

To conclude, TACE represents a central enzyme at the cell surface for release of EGFR ligands. As one of the main activators of EGFR signalling, TACE has to be tightly regulated. Several of its domains are involved in this regulation. One of the best characterised is the pro-domain, which first ensures proper folding of the catalytic site before maintaining TACE into an inactive state. This regulation is removed during the maturation of TACE in the TGN.

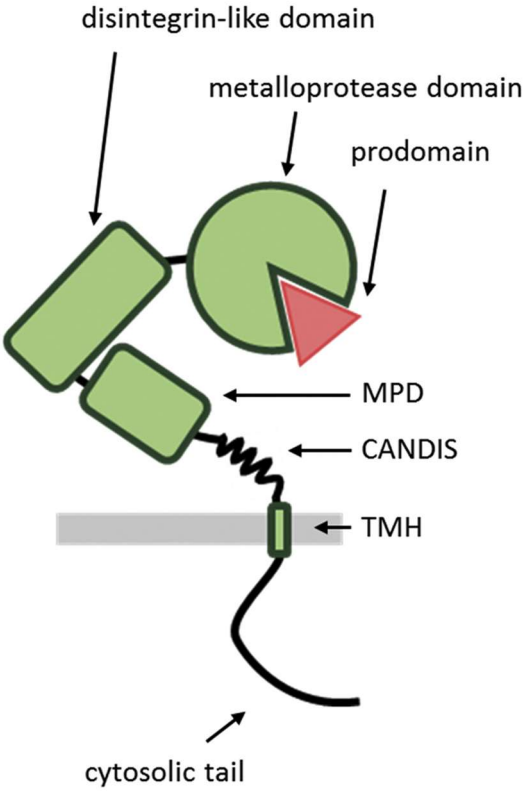


Figure 3: Structural organisation of TACE (adapted from (Düsterhöft et al., 2019)). Schematic representation of the type I transmembrane shedding enzyme TACE with its inhibitory prodomain (red) at the N-terminus and its C-terminal cytosolic tail. In addition to the catalytic metalloprotease domain, the different regulatory domains such as the disintegrin-like domain, the membrane proximal domain (MPD) and CANDIS (for Conserved Adam seventeeN Dynamic Interaction Sequence) are represented.

1.2.2. TACE maturation and trafficking

Although iRhoms have first been discovered for their role in decreasing EGFR ligands level (see section 1.3.1), the best characterised function of iRhoms is the regulation of TACE activity during two critical steps. In this section I will describe iRhoms control of TACE traffic to the Golgi, where it undergoes maturation. In the next section I will present the role of iRhoms phosphorylation at the plasma membrane in the stimulated activity of TACE.

The requirement of iRhoms for TACE maturation was first discovered for iRhom2 in macrophages, where iRhom2 is the only iRhom expressed. Stimulation by the bacterial component LPS induces TNFα shedding by TACE in these cells (Adrain et al., 2012; McIlwain et al., 2012). However, this shedding is abolished in iRhom2 KO macrophages (Adrain et al., 2012; McIlwain et al., 2012). It was shown that these cells have only immature TACE, but no mature TACE (McIlwain et al., 2012). To investigate whether this is due to an impairment of TACE trafficking, the glycosylation status of TACE was assessed in these cells. As immature TACE had a glycosylation signature characteristic of an ER-resident protein in iRhom2 knockout (KO) macrophages (Adrain et al., 2012), it demonstrated a requirement for iRhom2 in TACE traffic to the TGN. To assess whether this loss of TACE maturation and traffic was due to a defect in TACE folding, immature TACE from iRhom2 macrophages was isolated and incubated with furin proteases. As this treatment restored TACE activity (Adrain et al., 2012), it demonstrated unequivocally that iRhom2 is not required for TACE folding, but for its maturation in the TGN by furin.

iRhom2 binds to both immature and with mature TACE (Adrain et al., 2012; Grieve et al., 2017; McIlwain et al., 2012). Interestingly, the iRhom homology domain (IRHD) of iRhom2 is required for binding to immature TACE (Grieve et al., 2017). In addition, a mutation in the first transmembrane domain (TMD) of iRhom2 also abolishes TACE maturation (Li et al., 2017). These data therefore highlight the importance of TMD1 and the IRHD of iRhom2 for TACE maturation.

Except in immune cells, both iRhoms contribute to TACE maturation in most cell types. In mouse embryonic fibroblasts (MEFs), depletion of both iRhoms is required

to disrupt TACE maturation and to abrogate its shedding activity (Christova et al., 2013; Lee et al., 2015). In addition, all tested mouse tissues (except the brain) show loss of mature TACE only when iRhom1 and iRhom2 are depleted (Li et al., 2015). Overall, both iRhoms support TACE maturation in most cell types.

Finally, the importance of iRhoms for TACE maturation is illustrated in mice. iRhom1/2 double knockout (DKO) mice show a phenotype that appears to be as severe as the TACE KO mice (Christova et al., 2013; Li et al., 2015). TACE KO mice are characterised by perinatal death with developmental defects characteristic of EGFR dysregulation (Jackson et al., 2003; Peschon et al., 1998). There is a controversy about the phenotype of the iRhom1 KO mice: deletion of all iRhom1 exons except exon1 results in mice with a defect in weight gain and a shorter life expectancy (Christova et al., 2013), whereas a smaller deletion in the iRhom1 gene leads to viable mice (Li et al., 2015). This difference might explain why the iRhom1/2 DKO mice are either embryonic lethal (when most of iRhom1 is deleted) (Christova et al., 2013), or perinatal lethal (with the smaller deletion of iRhom1) (Li et al., 2015). In any case, the phenotype of iRhom1/2 DKO mice highlights the importance of iRhoms for TACE maturation *in vivo*.

1.2.3. TACE activation

Once TACE has undergone maturation, its catalytic activity requires stimulation at the plasma membrane. Several pharmacological stimuli have been discovered for TACE activation. Among them, the PKC-dependent stimuli phorbol-12-myristate-13-acetate (PMA) and lipopolysaccharide (LPS) are the most commonly used (Doedens et al., 2003; Loegering and Lennartz, 2011; Rovida et al., 2001). In addition, TACE activity can also be induced by physiological stimuli such as

histamine, which also relies on PKC activity (Lorenzen et al., 2016). Interestingly, TACE activation upon PMA stimulation is a very quick process (within approximately ten minutes) (Le Gall et al., 2010). This is much quicker than the maturation of TACE, which requires about three hours (Schlöndorff et al., 2000). As a result, an increase in TACE maturation cannot represent the mechanism by which TACE is activated upon PMA. That iRhom2 may play a role in TACE activation was indicated by two other pieces of evidence: i) iRhom2 interacts with mature TACE (Adrain et al., 2012), and ii) overexpressed iRhom2 shows plasma membrane localisation (Maney et al., 2015). But until recently, a role for iRhoms in TACE activation was not demonstrated.

It was recently discovered by our lab and Colin Adrain's lab that stimuli such as PMA and LPS induces phosphorylation of the N-terminus of iRhom2, which is required for TACE activation (Cavadas et al., 2017; Grieve et al., 2017). Although a phosphorylation-deficient version of iRhom2 still supports TACE maturation and the trafficking of the sheddase to the plasma membrane, this variant shows strong reduction of PMA-stimulated shedding by TACE in comparison to iRhom2-WT (Cavadas et al., 2017; Grieve et al., 2017). The kinases responsible for this phosphorylation are MEK1/2 and p38. These results demonstrate that phosphorylation of iRhom2 N-terminus is required for the activation of mature TACE upon stimulation. This is further supported by the treatment with MEK1/2 inhibitors, which decreases PMA-induced shedding by TACE (Grieve et al., 2017)

The most important phosphorylation residues in mouse iRhom2 can be divided into three main sites (see section 3.1). Mutation of any of the three sites in mouse iRhom2 strongly reduced TGFα shedding by TACE in MEFs (Grieve et al., 2017).

The residue showing the highest contribution was mapped as the serine 83 in site1 (Cavadas et al., 2017).

To understand the molecular mechanism by which iRhom2 phosphorylation affects TACE activity, both sets of authors focused on the phosphorylation site-binding 14-3-3 proteins, which are part of iRhom2 interactome (Cavadas et al., 2017; Grieve et al., 2017). Binding of 14-3-3 to iRhom2 strongly increased upon PMA stimulation. Mutation of the phosphorylation sites, or treatment with MEK1/2 inhibitor, strongly decreased 14-3-3 interaction to iRhom2 upon PMA (Cavadas et al., 2017; Grieve et al., 2017). To determine the sufficiency of 14-3-3 binding for TACE activation, 14-3-3 binding sites termed R18 sequences were inserted in the place of the phosphorylation sites in iRhom2 (Grieve et al., 2017), or an R18 sequence was fused to the end of the N-terminus of phosphorylation-deficient iRhom2 (Cavadas et al., 2017). Both strategies led to constitutive binding of 14-3-3 proteins and increased the constitutive (unstimulated) activity of TACE (Cavadas et al., 2017; Grieve et al., 2017). These results demonstrate that phosphorylation of the N-terminus of iRhom2 leads to recruitment of the phospho-binding proteins 14-3-3 to induce TACE activity.

Overall, the work by both sets of authors has demonstrated a novel role for iRhom2 in regulating TACE activity. This discovery raises the question on how iRhom2 phosphorylation induces TACE-dependent shedding, especially whether the effect is direct or indirect. It could be suggested that the phosphorylation of iRhom2 increases its affinity for TACE substrates, thereby allowing their presentation to the shedding enzyme. This hypothesis can be linked to the role of iRhom2 on substrate selectivity established in iRhom2 KO MEFs, which show

impairment of TACE-dependent shedding of substrates such as HB-EGF and EPR, but not of TGFα or Areg (Maretzky et al., 2013). To test whether the effect of iRhom2 phosphorylation is direct (on TACE) or indirect (on substrate presentation), cleavage of a fluorogenic, soluble peptide substrate was assessed (Caescu et al., 2009) (instead of the expression of membrane-bound alkaline phosphatase-fused substrates (Sahin et al., 2004)). As this assay shows the loss of proteolytic activity of TACE for iRhom2 pDEAD, it demonstrates that the phosphorylation of iRhom2 is necessary for the direct activation of TACE (Cavadas et al., 2017). In addition to the precise mechanism by which iRhom2 directly regulate TACE activity, several interesting questions emanate from the work of (Cavadas et al., 2017; Grieve et al., 2017): a) how does the binding of 14-3-3 proteins to iRhom2 affect TACE activity?; b) in addition to inflammation (see section 1.4.1), are there other pathological contexts in which the phosphorylation of iRhom2 is crucial?; c) is iRhom1 also phosphorylated upon stimulation, and if so, does it increase TACE activity?

Before it was demonstrated that iRhom2 is phosphorylated upon stimuli to induce TACE activity, most of the attention was focused on the phosphorylation of the cytosolic tail of TACE. A controversy still exists regarding the role of TACE phosphorylation in its stimulated activity. On one hand, the cytosolic tail of TACE has been shown to be phosphorylated (especially at threonine 735) upon stimuli in an ERK- or p38-dependent manner (Díaz-Rodríguez et al., 2002; Fan et al., 2003; Killock and Ivetić, 2010). Expression of the T735A mutant shows impaired stimulated shedding of TGFα (Xu and Derynck, 2010) or the neurotrophin receptor TrkA (Díaz-Rodríguez et al., 2002). On the other hand, it has been demonstrated that most of the cytosolic tail of TACE (including T735) is dispensable for stimulated shedding of TNFα (Schwarz et al., 2013) or TGFα (Hall and Blobel, 2012; Le Gall et

al., 2010). To solve this controversy, it is proposed that either the cytosolic tail of TACE has an inhibitory effect which is suppressed by phosphorylation of T735 (Düsterhöft et al., 2019), or that the T735A mutation directly affects TACE stability at the plasma membrane (Xu and Derynck, 2010). Overall, the importance of the phosphorylation of the cytosolic tail of TACE remains unclear, contrary to the phosphorylation of iRhom2, which clearly induces TACE activation.

1.3. Proteostasis of ER proteins

1.3.1. iRhoms and protein turnover

EGFR ligands are produced as transmembrane proteins that are proteolytically cleaved at the plasma membrane to release the active domain, in a process called shedding. EGF can be shed by ADAM10, a member of the ADAM family (Sahin et al., 2004), and by the rhomboid protease RHBDL2 (Adrain et al., 2011). In *Drosophila melanogaster* the EGFR ligands Spitz, Gurken and Keren can be cleaved by several rhomboid proteases, including Rhomboid-1 (Lee et al., 2001; Urban et al., 2001, 2002).

In contrast to the shedding of EGFR ligands, our lab has demonstrated that iRhoms act as negative regulators of EGFR signalling in *Drosophila* and mammalian cells (Zettl et al., 2011). This role is illustrated by the sleep-like phenotype of iRhom KO flies, which undergo increased periods of inactivity. A similar phenotype has been observed upon activation of EGFR signalling (Foltenyi et al., 2007), thereby suggesting that iRhom KO phenotype is due to EGFR hyperactivation. In support of this hypothesis, knockdown of EGFR or its ligand Spitz in iRhom KO flies rescued the sleep-like phenotype (Zettl et al., 2011). Using the rough eye phenotype as a readout for EGFR dysregulation (Bai et al., 2001), genetic interactions further highlight the role of iRhom in inhibiting EGFR signalling during *Drosophila* development. For example, depletion of iRhom expression suppressed the rough eye phenotype caused by EGFR inhibition (Zettl et al., 2011). As a result, developmental and behavioural evidence support the role of *Drosophila* iRhom as a negative regulator of EGFR signalling.

To investigate the mechanism for the inhibitory effect of *Drosophila* iRhom, cell culture-based experiments were performed. It was first confirmed that, contrary to Rhomboid-1, iRhom does not induce cleavage of the EGFR ligands Spitz and Gurken. Overexpression of iRhom triggered a decrease in Spitz and Gurken, but without secretion or cleavage fragments in the lysate. As a result, the reduction of EGFR ligands in presence of iRhom constitutes an inhibitory mechanism distinct from the cleavage by rhomboid proteases. Concerning the molecular mechanism of this inhibitory effect, genetic interactions in *Drosophila* suggested that it might involve components of ER-associated degradation (ERAD). The rough eye phenotype caused by EGFR inhibition was partially rescued by knockdown of Hrd1 or EDEM2. This result indicates that EGFR signalling is under the control of ERAD components during fly development. Overall, *Drosophila* iRhom is a novel regulator of EGFR signalling, which acts by decreasing EGFR ligands level, possibly via an ERAD pathway (Zettl et al., 2011).

To investigate whether mammalian iRhoms affect EGFR ligands, iRhoms were overexpressed in COS-7 cells, where they showed an ER localisation. In presence of iRhom1 or iRhom2 the level of EGF strongly decreased. This result confirms that the inhibitory effect of iRhoms on EGFR ligands is conserved in mammals. The effect of iRhoms is independent of RHBDL2 cleavage, as a variant of EGF that cannot be cleaved by RHBDL2 still decreased in the presence of iRhoms. Interestingly, inhibition of the proteasome rescued the level of EGF in presence of iRhom1, which supports the hypothesis of an ERAD-based mechanism. Concerning its specificity, expression of iRhoms led to the reduction of all tested EGFR ligands, but not of the luminal Prolactin, or of the *Drosophila* transmembrane protein Delta. In addition, the expression the ER polytopic protein Unc93b did not affect EGFR

ligands. As a result, mammalian iRhoms specifically reduce the level of EGFR ligands independently of the action of active rhomboid proteases, such as RHBDL2.

As a conclusion, iRhoms act as negative regulators of the EGFR pathway. This role is demonstrated in *Drosophila* by the sleep-like phenotype and the inhibitory effect of iRhom on EGFR signalling during development. The ability of overexpressed iRhoms to reduce EGFR ligands is conserved between *Drosophila* iRhom and mammalian iRhom1 and iRhom2. It is specific to iRhoms as a trigger, and to EGFR ligands as regulated proteins (called clients). The ER localisation of iRhoms suggests that EGFR ligands are directly targeted from the ER to a degradation machinery. Of note, the localisation of iRhoms in other cell compartments was unknown at the time of the study. The proposal of an ERAD mechanism is supported by the involvement of the proteasome. Whether other pathways for the degradation of ER localised proteins participate in the inhibitory effect of iRhoms on EGFR ligands remains an open question. Finally, identification of specific components of the pathways triggered by iRhoms for the degradation of EGFR ligands would greatly improve our understanding of how iRhoms regulate EGFR signalling in *Drosophila* and mammals.

Two recent studies have associated iRhoms to protein degradation. First, expression of iRhom1 and other members of the rhomboid-like superfamily leads to increased proteasomal activity. It was shown that iRhom1 interacts with proteasomal assembly chaperones (PACs) and stabilises them (Lee et al., 2015). Whether this interaction is specific to iRhom1, or shared with other rhomboid-like members remains to be determined. The second study concerns the adaptor for innate immunity virus-induced signalling adapter (VISA). VISA is a single-pass

transmembrane protein that is stabilised by iRhom2, due to its ability to trigger degradation of the E3 ligases MARCH5 and RNF5 (Luo et al., 2017). As a result, iRhoms seem to have opposing effects on protein turnover. On one hand, iRhom1 stabilises PACs, which increases proteasomal activity. On the other hand, iRhom2 triggers the degradation of E3 ligases, which results in the stabilisation of VISA. These seemingly contradictory effects could be due to the specific effect by either iRhom1 or iRhom2. Further evidence is required to understand whether these effects, especially the increase in proteasomal activity, might provide molecular insights into the destabilisation of EGFR ligands by iRhoms in *Drosophila* and mammalian cells.

1.3.2. Degradation routes for transmembrane proteins in the ER

Most transmembrane proteins, such as the EGFR ligands, are first assembled in the endoplasmic reticulum (ER), before trafficking to their target compartment. To ensure their correct folding, transmembrane proteins undergo quality control mechanisms. This ensures the protein homeostasis (or proteostasis) of the ER. However, when proteins fail to properly fold and accumulate in the ER, they are targeted for degradation. Two main degradation routes exist for ER transmembrane proteins: ER-associated degradation (ERAD) and ER-phagy. In addition to the degradation of misfolded proteins, these pathways degrade specific substrates in order to regulate cell signalling.

1.3.2.1. ERAD

ERAD is a process by which ER substrates are targeted for degradation by the cytoplasmic proteasomal machinery. The main role of ERAD is to act as a quality-control mechanism that prevents accumulation of misfolded proteins in the ER

lumen. Additionally, regulatory functions have also been reported for ERAD, especially in the context of cell signalling regulation. Impairment of ERAD functions is associated with multiple human diseases, including cancer formation (Walter and Ron, 2011).

The ERAD pathway can be divided into four main steps (Figure 4) (Olzmann et al., 2013). The first step is the recognition of specific features in the substrate (such as misfolding). Three branches of ERAD exist, depending on whether the recognised feature is in the cytoplasmic domain (ERAD-C), in the transmembrane domain (ERAD-M), or in the luminal domain (ERAD-L) (Ruggiano et al., 2014). Addition of a polyubiquitin chain on the substrate represents the second step of ERAD, and that requires an E3 ligase (Figure 4), which specifies substrates for certain ERAD machineries. Among the numerous ERAD-linked E3 ligases, the best characterised are Hrd1 and gp78 (Olzmann et al., 2013). During retrotranslocation, which constitutes the next step, the ubiquitinated substrate is recognised the VCP/p97 ATPase, which extracts the protein from the ER membrane (Figure 4). To do so, the substrate and its polyubiquitin chain are unfolded to move through the small central pore of VCP/p97. During the last step of ERAD, the substrate is recognised by the 26S proteasome, which leads to substrate degradation (Olzmann et al., 2013; Twomey et al., 2019).

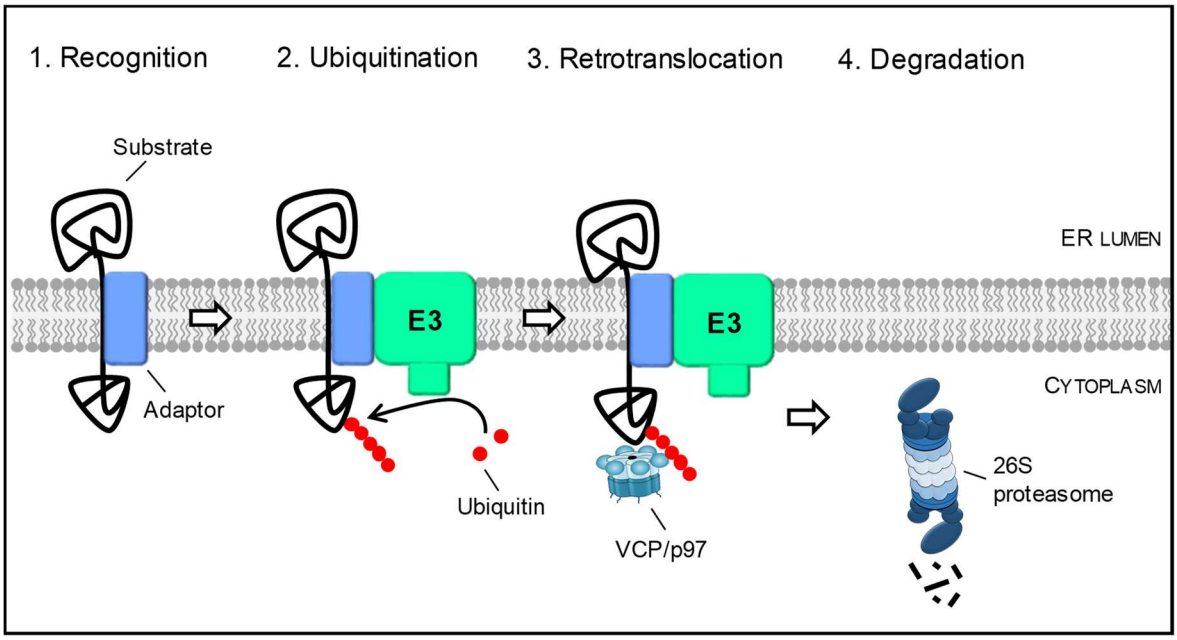


Figure 4: Key steps of ER-associated degradation (ERAD). The substrate is recognised by an adaptor protein based on a feature present in the transmembrane domain (as shown here), or at the luminal or cytoplasmic extremity. During the second step, an E3 ubiquitin ligase catalyses the addition of the polyubiquitin chain on the cytoplasmic end of the substrate. This feature is recognised by the AAA ATPase VCP/p97 which allows the extraction of the substrate from the ER membrane during the retrotranslocation. The channel allowing the retrotranslocation can be the E3 ligase itself, as it has been shown for Hrd1 in yeast (Baldridge and Rapoport, 2016). Finally, the substrate is proteolytically degraded by the 26S proteasome.

Although ERAD is often considered to be a mechanism for clearance of misfolded proteins, evidence has begun to accumulate that demonstrate its roles in the regulation of sterol biosynthesis and signalling. Indeed, the key enzyme of cholesterol biosynthesis, HMG-CoA reductase (HMGR), is degraded by ERAD in high sterol conditions (Song et al., 2005). The importance of ERAD in cell signalling is highlighted by Hrd1-dependent degradation of sonic hedgehog by the 26S proteasome (Chen et al., 2011). Finally, ERAD is also exploited by pathogens to affect the immune response. The viral protein US11 recruits the E3 ligase TMEM129 for degradation of MHC1 heavy chain, thereby preventing antigen presentation of the infected cells (van de Weijer et al., 2014).

Several members of the rhomboid-like superfamily have been linked to ERAD. Among the active proteases, RHBDL4 has been shown to cleave the pre-T cell receptor α subunit to allow its degradation by the proteasome. The involvement of RHBDL4 in ERAD is supported by its ability to bind VCP/p97, and to interact with ubiquitinated proteins via its ubiquitin-interacting motif (Fleig et al., 2012). Although it is an inactive member of the superfamily, UBAC2 shows similarities with RHBDL4 as it also presents a ubiquitin-binding domain and it binds to VCP/p97 adaptor UBXD8 (Christianson et al., 2011; Greenblatt et al., 2011). In addition, it has recently been demonstrated that UBAC2 is part of the complex with the central ERAD E3 ligase gp78 (Zhang et al., 2015). Finally, the most known inactive members of the superfamily for their participation in ERAD are derlins. Their role was first described in yeast, where there are two derlins: Der1 and Dfm1 (Knop et al., 1996; Stolz et al., 2010). Der1 is part of the Hrd1 complex and it is required for the retrotranslocation of luminal substrates during ERAD (Gauss et al., 2006; Mehnert et al., 2014; Stanley et al., 2011), whereas Dfm1 is required for the retrotranslocation during ERAD of the polytopic protein Hmg2 (Neal et al., 2018). Mammalian cells possess three Derlins, among which Derlin1 is best characterised for its role the retrotranslocation of the NHK mutant of the luminal protein α1-antitrypsin (Greenblatt et al., 2011) and for its role in ERAD complexes processing the degradation of MHC class I (Lilley and Ploegh, 2004; van de Weijer et al., 2014; Ye et al., 2004)

1.3.2.2. ER-phagy

ER-phagy constitutes an alternative pathway to ERAD for the degradation of ER transmembrane proteins. It relies on macro-autophagy (hereafter autophagy) components to target transmembrane proteins for degradation. Autophagy refers to the degradation of organelles and cytoplasmic constituents by the lysosome. During

autophagy, a membrane from the ER (called the phagophore) elongates to engulf cargoes that are targeted for degradation. It leads to the formation of a double membrane vesicle, called the autophagosome, which eventually fuses with the lysosome for the degradation of the cargoes.

Although the molecular mechanisms are not fully elucidated yet, several core components have been identified to play a role in autophagy (Figure 5). Among them, the kinase ULK1/2 is one of the most upstream components and it forms the ULK complex together with components such as FIP200. Upon various stimuli — such as amino acid starvation that releases mTORC inhibition — ULK1/2 activates the Beclin-1 complex, which contains the PI3K enzyme Vps34. The activity of the Beclin-1 complex leads to formation of PI3P on the phagophore to recruit the PI3P-interacting protein WIPI2. WIPI2 binds to the Atg8 conjugation system, of which Atg5 and Atg7 are core components. The Atg8 conjugation system catalyses the addition of phosphatidylethanolamine (PE) to Atg8s proteins, such as LC3. Accumulation of LC3-PE (called LC3-II) triggers extension of the phagophore. In addition, LC3-II is specifically recognised by cargo receptors that are targeted for autophagy degradation. After closure of the phagophore to form the autophagosome, the latter then fuses with a lysosome, which leads to degradation of the cargoes (Figure 5) (Dikic and Elazar, 2018; Fraser et al., 2017; Mizushima, 2018; Moon et al., 2018).

In addition to cytoplasmic cargoes, autophagy selectively targets different organelles for degradation. To be recognised by the machinery, an autophagy cargo presents specific receptors that can interact with Atg8s proteins, for example via the LC3-interacting region (LIR) (Dikic and Elazar, 2018). Such receptors have recently been identified for the ER, and these define ER-phagy (Figure 5). During this

process, specific subdomains of the ER are recognised by the autophagy machinery due to the presence of ER-phagy receptors. The latter can be divided into two structural categories: i) the intramembrane receptors with a reticulon-homology domain: RTN3 and FAM134B; and ii) the transmembrane receptors: Sec62 and CCPG1 (Stolz and Grumati, 2019).

Although the field is recent, two common themes already emerge regarding ER-phagy. First, the degradation of specific substrates has been reported for the intramembrane receptors. FAM134B sustains the degradation of alpha-1-antitrypsin mutants (Fregno et al., 2018) and of misfolded procollagens (Forrester et al., 2019). In the latter case, it has been shown that calnexin acts as an adaptor to allow recognition of luminal substrates by the receptor in the outer membrane of the ER. The second emerging theme is the importance of ER-phagy in response to increased stress in the ER. CCPG1 triggers degradation of ER subdomains upon treatment with ER stressors (Smith et al., 2018), whereas Sec62 acts after ER stress for the recovery of the organelle homeostasis (Fumagalli et al., 2016).

These data suggest that intramembrane ER-phagy receptors target specific substrates, whereas transmembrane receptors play a more global role in ER proteostasis, but further characterisation of the known receptors and identification of new ones will put this hypothesis to the test. Finally, the recent identification of the transmembrane receptor TEX264 gives an interesting insight into the potential structural requirement of ER-phagy receptors. TEX264 possesses a disordered cytoplasmic tail, which has been predicted in the other receptors (An et al., 2019; Chino et al., 2019). This raises the possibility that an unstructured cytoplasmic extremity is required to recruit the autophagy machinery.

Overall, ER-phagy has emerged as a novel route for the degradation of ER proteins. It relies on autophagy core components, such as the ULK and Beclin1 complexes, and the Atg8 conjugation system. ER-phagy receptors are central for the specificity of the different routes. Recognition of the substrates likely occurs via direct interaction with the receptor, or via an adaptor in the ER membrane.

As a conclusion, iRhoms destabilise EGFR ligands at the protein level in *Drosophila* and mammalian cells. Given the predominant ER localisation of iRhoms, two main degradation pathways might be involved. The first one is ERAD, which relies on the ubiquitination of the ER substrate that requires access to the cytoplasm to be degraded by the proteasome. The second one is ER-phagy, in which a specific receptor in the ER membrane recruits the autophagy machinery to target substrates to lysosomal degradation. Both degradation pathways therefore contribute to maintaining the proteostasis of the ER (De Leonibus et al., 2019; Forrester et al., 2019; Sun and Brodsky, 2019).

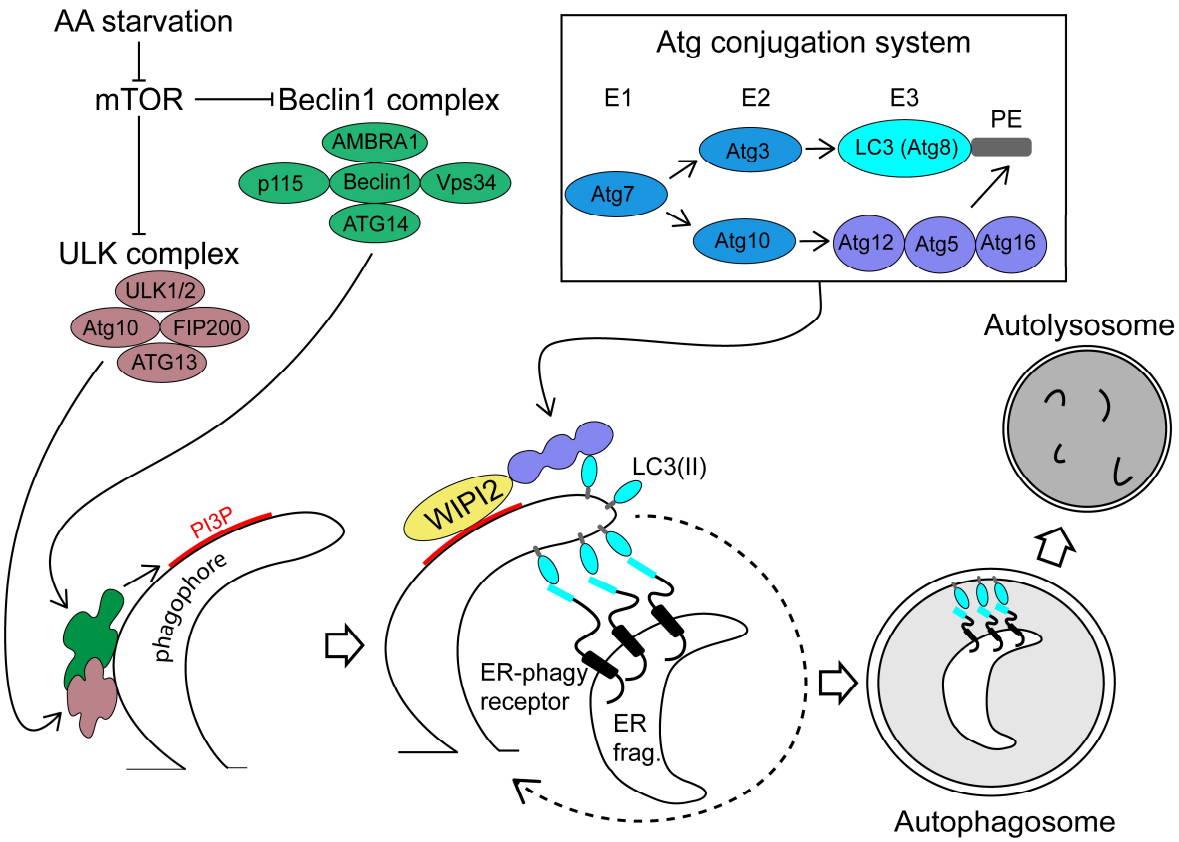


Figure 5: Key steps of ER-phagy. This schematic depicts the degradation of ER contents by recruitment of the autophagy machinery (ER-phagy). During initiation of the process, the autophagy machinery can be activated by numerous stimuli, notably by amino acid (AA) starvation relieving mTOR inhibition on the ULK complex (composed of ULK1/2, Atg10, FIP200 and ATG13). Activation of the Beclin1 complex (constituted of Beclin1, Vps34, ATG14 and AMBRA1) by the ULK complex allows the nucleation of the autophagic membrane (phagophore). The active Beclin-1 complex converts phosphatidylinositol into phosphatidylinositol-3-phosphate (PI3P). The next step is constituted by phagophore expansion and recognition of the cargo, which both rely on the conjugation to phosphatidylethanolamine (PE) of Atg8 proteins, such as LC3. Upon activation by Atg7 (E1-activating-like enzyme), the conjugation of Atg8 proteins to PE is mediated by Atg3 (E2-like enzyme), and this reaction is catalysed by the Atg12-Atg5-Atg16 complex formed in presence of Atg10. The Atg conjugation system is recruited to the phagophore in presence of PI3P-binding proteins, such as WIPI2, allowing the formation of LC3-II (LC3-PE) on the surface of the phagophore. LC3-II is recognised by ER-phagy receptors, to ensure the tethering of targeted ER fragments. Upon closure, the double-membrane vesicle constitutes the autophagosome, which fuses will the lysosome to ensure the degradation of the targeted ER contents.

1.4. Pathological importance of iRhoms and TACE

1.4.1. iRhoms and TACE in inflammation and immunity

TACE is a central regulator of numerous processes, including the inflammatory response due to its ability to release the primary inflammatory cytokine TNFα. Given the role of iRhom2 as a TACE cofactor in immune cells, iRhom2 plays a crucial role in the regulation of inflammation. Upon stimulation by the bacterial cell wall component lipopolysaccharide (LPS) to mimic bacterial infection, the release of TNFα by macrophages requires iRhom2 (Adrain et al., 2012; Grieve et al., 2017; McIlwain et al., 2012). This function relies on the role of iRhom2 in TACE maturation. The importance of iRhom2 for inflammation has already been shown for specific inflammatory diseases, such as rheumatoid arthritis (Issuree et al., 2013). Using a mouse model for this disease, the authors demonstrated that iRhom2 depletion drastically decreases the symptoms, and that this effect can be linked to the role of iRhoms as TACE cofactors.

The importance of iRhom2 phosphorylation for TACE activation has been demonstrated in iRhom2 KO macrophages. Expression of iRhom2 variants with mutated phosphorylation sites drastically reduces LPS-induced shedding of TNFα by TACE (Cavadas et al., 2017; Grieve et al., 2017). In addition binding of 14-3-3 proteins to iRhom2 was also demonstrated upon LPS stimulation (Grieve et al., 2017). As a result, the phosphorylation of the iRhom2 N-terminus and the recruitment of 14-3-3 proteins is a conserved mechanism in macrophages for the shedding of the primary inflammatory cytokine TNFα.

In addition to inflammation, iRhom2 plays a crucial role as a TACE cofactor during the immune response. First, iRhom2 is required for an effective immune response

to bacterial infection. This role has been shown for infection by *Listeria monocytogenes*, the agent of listeriosis. iRhom2 KO macrophages failed to produce TNFα in response to *Listeria* infection. In the infected iRhom2 KO mice, the bacterial titre was increased and their survival was drastically reduced in comparison to infected wild-type mice (McIlwain et al., 2012).

Finally, iRhom2 is also crucial for the immune response to viral infection due to its regulation of the innate immunity adaptors VISA and STING (Luo et al., 2016, 2017). VISA is determinant for the response to RNA virus, whereas STING triggers immune response to DNA virus. Upon RNA or DNA viral infection, iRhom2 KO mice show increase in the viral charge, leading to early lethality. iRhom2 is necessary to increase the stability of STING and VISA at the protein level. In the absence of iRhom2, the innate immune response triggered by STING and VISA are strongly decreased (Luo et al., 2016, 2017)

1.4.2. iRhoms and TACE in cancers

1.4.2.1. iRhom1 in cancer cells

The pathological importance of iRhoms is demonstrated not only by their involvement in inflammation and immunity, but also by their role in tumorigenesis. A few pieces of evidence have associated iRhom1 is with breast cancer (Yan et al., 2008; Zhou et al., 2014), colorectal cancer (Yuan et al., 2018), and head and neck squamous cell cancer (HNSCC) (Zou et al., 2009).

The importance of iRhom1 in cancer is first illustrated by the increase of its mRNA level in colorectal cancer (Yuan et al., 2018) and breast cancer (Yan et al., 2008; Zhou et al., 2014). In breast cancer iRhom1 level increases during cancer progression, and high iRhom1 levels correlate with increased metastasis number

and poor prognosis. Experiments in HNSCC cells also suggest an oncogenic involvement of iRhom1 but only under stimulation: iRhom1 knockdown only impairs cell migration upon stimulation of G protein-coupled receptor (GPCR) (Zou et al., 2009).

The malignancy potential of a cell can be determined by several assays, including focus formation and xenograft. The requirement of iRhom1 for tumorigenesis is suggested by experiments in HNSCC and breast cancers cells, in which iRhom1 knockdown decreases cell proliferation and xenograft growth (Yan et al., 2008). This result is supported by iRhom1 knockdown in colorectal cancer cells, which decreases cell migration, cell invasion, focus formation and in xenograft growth. The importance of iRhom1 in cancer is further illustrated by iRhom1 overexpression in these cells that is sufficient to increase their tumourigenic potential, including for tumour growth (Yuan et al., 2018). As a result, it would be interesting to combine the two approaches to validate the oncogenic role of iRhom1 by rescuing its expression in the knockdown background.

As a conclusion, these data support the involvement of iRhom1 in tumourigenesis, although no clear molecular mechanism for this role has been demonstrated. It would be interesting to determine the extent to which the importance of iRhom1 in cancer relies on its ability to regulate TACE activity.

1.4.2.2. iRhom2 in cancer cells

Unlike for iRhom1, mutations in iRhom2 has been shown to be causative for cancer formation. The most documented link between iRhom2 and cancer is the familial autosomal dominant cancer syndrome called tylosis with oesophageal cancer (TOC). TOC is a rare syndrome that has been identified in multiple families

around the world (Ellis et al., 2015). They all present a missense mutation in a small region of iRhom2 N-terminus: I186T (UK and US families), D188N (Finnish) , D188Y (African), P189L (German), or R197S (Chinese) (Brooke et al., 2014; Hennies et al., 1995; Mokoena et al., 2018; Qu et al., 2019; Saarinen et al., 2012). A feature of TOC syndrome is the development, at around seven years of age, of cutaneous features such as palmoplantar keratoderma, oral and oesophageal lesions and follicular keratosis. This is accompanied by a very high susceptibility to develop oesophageal squamous cell carcinoma from the mid-fifties onwards. Given the crucial importance of early detection of oesophageal dysplasia to improve the prognosis, screening programmes have been implemented for the concerned families (Ellis et al., 2015).

To determine the molecular mechanism leading to the syndrome, TOC keratinocytes from biopsies of the affected skin of tylotic patients from the UK have been isolated and immortalised (Blaydon et al., 2012). These cells show an increase in constitutive shedding of several TACE substrates, such as Areg, HB-EGF, IL-6, IL-8, TGFα and TNFR (Brooke et al., 2014; Maney et al., 2015). Experiments in iRhom1/2 DKO mouse embryonic fibroblasts, reconstituted with tylotic iRhom2 mutant protein, also show increased constitutive shedding of TGFα (Maney et al., 2015). Although the molecular mechanism leading to this upregulation is not understood, it is interesting to note that PMA-stimulated shedding of TNFα is also increased in TOC keratinocytes (Brooke et al., 2014). Overall, these results highlight the importance of TACE regulation by iRhom2.

To further understand the biological cause of TOC a mouse model expressing P189L has been generated. This mouse shows increased Areg level in the serum,

as well as defects in the skin and the fur, which are rescued by Areg deletion (Hosur et al., 2017). This evidence further supports the model that TOC represents a case of EGFR hyperactivation. Finally, although few experiments on TOC cultured cells directly investigate their malignancy potential, it has been shown that TOC keratinocytes present an increased migration rate (Blaydon et al., 2012). Further work will therefore be required to determine how tylotic mutations affect the ability of iRhom2 to regulate TACE-dependent shedding, and to determine its sufficiency for cell transformation and cancer formation *in vivo*.

1.4.2.3. TACE in cancers

As a major regulator of EGFR signalling, TACE has been implicated in numerous cancers. The first evidence of this role is the elevated expression of TACE in several tumour tissues (Mochizuki and Okada, 2007). More direct evidence of the oncogenic role of TACE has been shown for breast cancer (Giricz et al., 2013; Kenny and Bissell, 2007), colon cancer (Das et al., 2012) and non-small-cell lung carcinoma (NSCLC) (Sharma et al., 2016; Zhou et al., 2006). Silencing of TACE reduces cell proliferation and cell invasion of breast cancer cells (Kenny and Bissell, 2007; Xu and Derynck, 2010; Zheng et al., 2009). Finally, the importance of TACE for tumourigenesis has also been investigated for the cancers triggered by mutations in the Ras proto-oncogenes (see section 1.5.3).

1.5. Ras proto-oncogenes

1.5.1. Ras mutations

Ras genes are the first identified proto-oncogenes (Der et al., 1982; Parada et al., 1982; Santos et al., 1982; Taparowsky et al., 1982) and they are mutated in more than one fourth of all human cancers (Hobbs et al., 2016). Three Ras genes are present in human: KRas, HRas and NRas. Due to alternative splicing in the C-terminus, there a two isoforms for KRas, KRas4A and KRas4B, (Schubbert et al., 2007). Oncogenic mutations of Ras genes show a strong tissue-specificity: KRas mutations are prevalent in lung, pancreatic and colorectal cancers, whereas HRas is the main mutated Ras gene in bladder cancer, and NRas mutations are prevalent in melanoma. Overall, KRas is the most mutated Ras protein and its importance is well established in lung cancer (see section 1.5.3) (Hobbs et al., 2016; Schubbert et al., 2007).

Ras proteins are small GTPases that function as binary switches (Hobbs et al., 2016). They are activated upon binding to GTP, which is stimulated by guanine nucleotide exchange factors (GEFs). Binding to GTP triggers a conformational change in Ras, leading to recruitment of its effectors (Vetter and Wittinghofer, 2001). Ras is then slowly inactivated by intrinsic hydrolysis of GTP into GDP. This conversion is catalysed by the binding of Ras to GTPase-activating proteins (GAPs) (Hunter et al., 2015). An important regulation of this GDP/GTP cycle is the translocation of Ras to the plasma membrane induced by lipidation of their C-terminus. At the plasma membrane, Ras proteins are activated by GEFs to recruit their effectors (Simanshu et al., 2017).

Structurally, Ras proteins are composed of a highly conserved G domain, followed by a hypervariable region at the C-terminus (Figure 6). The G domain contains the P-loop, which binds to GTP, and two switches, which undergo conformational change upon GTP binding to regulate interaction with the effectors (Schubbert et al., 2007; Simanshu et al., 2017). The hypervariable C-terminal region accounts for most of the differences between Ras proteins (Figure 6). This region undergoes lipidations specific to each of the Ras proteins, which all participate in their translocation at the plasma membrane to be activated by GEFs (Hobbs et al., 2016; Schubbert et al., 2007).

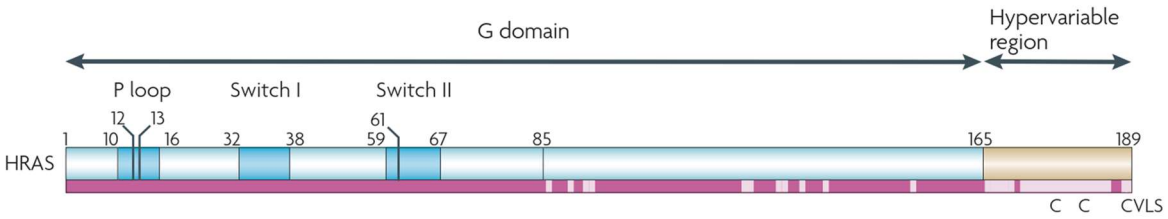


Figure 6: Structural organisation of the Ras proteins (adapted from (Schubbert et al., 2007)). Schematic representation of HRas, highlighting the conserved residues with KRas and HRas proteins in magenta. The G domain containing the GTP-binding P-loop and the two switches shows a high level of conservation, whereas the C-terminal hypervariable region presents more the variability with the other Ras proteins.

Most Ras mutations occur in the P-loop (especially at glycine 12) or in switch II (at glutamine 61). Among them, the best studied activating mutation is Ras-G12V, which leads to a loss of GAP sensitivity (Smith et al., 2013). As a result, Ras-G12V remains bound to GTP and it is constitutively active. Ras-G12V mutation therefore constitutes an activating, oncogenic mutation. Most mutations of glycine 12 are activating mutations due to the loss of GAP sensitivity (Simanshu et al., 2017). There is, however, a difference of intrinsic hydrolytic activity between these mutations. For example, whereas Ras-G12V has very low intrinsic hydrolysis and remains active, Ras-G12C has a much higher ability to convert GTP into GDP via

its intrinsic hydrolytic activity (Hunter et al., 2015). This finding suggests that Ras-G12C still relies on upstream effectors to be in an active conformation. This has recently been demonstrated, as EGFR activation increases the binding of KRas-G12C to GTP (discussed in section 5.1.3) (Patricelli et al., 2016). Finally, some mutations in other regions of Ras have been shown to be inactivating, such as for Ras-S17N. This mutation reduces the GTP affinity and therefore decreases Ras activity (Farnsworth and Feig, 1991; Feig and Cooper, 1988; Nassar et al., 2010).

To conclude, Ras mutants are some of the best characterised oncogenes in human cancers. Ras activation relies on binding to GTP, and this activation is lost when GTP is hydrolysed into GDP. Ras-G12 mutations reduce this hydrolysis, thereby leading to increased Ras activity. This allows Ras to activate pathways that are central for tumourigenesis, such as the Raf/MEK/ERK cascade.

1.5.2. Ras effectors and cell transformation

Upon activation, Ras proteins trigger diverse pathways for the regulation of cell proliferation, differentiation and survival by binding to their effectors. Among the more than 20 reported effectors of Ras, the best characterised are Raf, PI3K and RALGDS (Schubbert et al., 2007). The Raf/MEK/ERK cascade is one of the most important Ras effector pathways for cell proliferation of cancer cells, and it is central for Ras-induced cell transformation. (McCubrey et al., 2007). Preferential activation of an effector has been reported for the Ras proteins. For example, Raf is more potently activated by KRas-G12V than by HRas-G12V (Voice et al., 1999; Yan et al., 1998). Finally, mutation-specific activation has also been shown for KRas. For example, KRas-G12D leads to higher activation of the PI3K pathway than KRas-G12S or KRas-G12C (Ihle et al., 2012). Although further experiments are required

to draw a precise activation network of KRas-G12 mutations, these results already illustrate the specificity of KRas mutations on their effector pathways.

To activate the Raf/MEK/ERK cascade the active form of Ras (GTP-bound) recruits Raf proteins at the plasma membrane, where they dimerise to become active (Nussinov et al., 2019; Terrell and Morrison, 2019). The three Raf proteins (A-Raf, B-Raf and Raf-1) are serine/threonine kinases that activate the threonine/tyrosine kinases MEK1/2 by phosphorylation. Finally, phosphorylated MEK1/2 activate the serine/threonine kinases ERK1/2 (Cristea and Sage, 2016). The remarkable feature of this pathway is its upstream specificity, which results in the ability of active ERK1/2 to phosphorylate hundreds of substrates (Heigener et al., 2015). This leads to the regulation of numerous cell processes, including the induction of cell growth and proliferation that contribute to Ras-induced tumourigenesis (Roskoski, 2012).

Activation of effectors pathways (especially the Raf/MEK/ERK cascade) by oncogenic Ras results in the acquisition of malignant features by the cell. This process is called cell transformation (Hanahan and Weinberg, 2011; Speiseder et al., 2017). The characteristics of transformed cells are based on the observation of *in vitro*-transformed and tumour cells. This led to the identification of three main hallmarks of cell transformation: 1) The loss of cell-cell contact inhibition, thereby allowing the cells to grow as foci; 2) The loss of substrate requirement, which allows the cells to grow in anchorage-independent conditions; 3) The ability of the cells to form tumours upon injection into an immunocompromised mouse (Hanahan and Weinberg, 2011; Martinez et al., 2003). These hallmarks set the framework to assess whether expression of a Ras mutant is sufficient for cell transformation. In

addition, it also allows to test the requirement of Ras effectors in transformed cells, such as the lung cancer cell lines expressing KRas mutations.

1.5.3. Oncogenic KRas in lung cancer

The importance of oncogenic KRas has been extensively studied in lung cancer. Lung cancer represents the leading cause of cancer-related deaths (Siegel et al., 2017). It can be divided into two categories: i) small-cell lung cancer (SCLC), and ii) non-small cell lung cancer (NSCLC). NSCLC represents 85% of all lung cancers, and it encompasses several sub-categories, including the lung adenocarcinoma (LAC) (Cheung and Nguyen, 2015). KRas is the most mutated Ras gene in NSCLC, and oncogenic KRas is sufficient to induce tumorigenesis in the lung (Schubbert et al., 2007).

To study the role of oncogenic KRas in lung cancer, a mouse model with conditional expression of KRas-G12D has been created. Within a few months upon expression of KRas-G12D in the lungs, the mouse develops lung adenocarcinomas (DuPage et al., 2009; Jackson et al., 2001). This result highlights the sufficiency of oncogenic KRas in lung tumourigenesis, and the interest of using this mouse as a model to study LAC.

Another approach consists in focusing on the NSCLC cells, which can be grown using standard tissue culture techniques. One of the best studied NSCLC cell line is A549, which expresses oncogenic KRas-G12S (Gazdar et al., 2010). Using KRas shRNA it has been demonstrated that A549 cells require KRas for anchorage-independent growth, and for tumour formation upon injection in immunosuppressed mice (Scholl et al., 2009). This result therefore demonstrates that KRas is crucial for the transforming potential of A549. Interestingly, some data also support the

involvement of TACE in A549. For example, it has been shown that TACE siRNA reduced cell proliferation (Sharma et al., 2016), whereas a TACE/ADAM10 inhibitor decreases xenograft growth (Zhou et al., 2006) (also see section 5.1.2 for presentation of (Saad et al., 2019)). Given the requirement of iRhoms for the maturation and activation of TACE, it would be interesting to investigate whether iRhoms participate in KRas-induced tumourigenesis.

1.6. Aim of the projects

I have investigated the two main functions of iRhoms during my DPhil: 1) the regulation of TACE activity, and 2) the regulation of protein degradation. For the first project, it was recently demonstrated that the phosphorylation of iRhom2 is required for the activation of TACE at the plasma membrane. However, neither the role of iRhom1, not the pathological importance of the mechanism in an oncogenic context was understood. In chapter 3, first I will report the role of iRhom1 phosphorylation in supporting TACE activation. To investigate the oncogenic role of iRhoms in TACE activation, I will show the importance of the phosphorylation of iRhom1 and iRhom2 in KRas-induced substrate shedding by TACE. In section 5.1, I will discuss the implications of my findings for the study of KRas tumorigenesis, particularly in lung cancers.

The second project concerns the degradation of Myc-EGF driven by iRhoms. This function was demonstrated in *Drosophila* and in mammalian cells, but its molecular mechanism remained unknown. Chapter 4 will report that iRhom-driven degradation of Myc-EGF requires both the proteasome and lysosomes. For the latter, I will demonstrate the importance of substrate trafficking and the involvement of autophagy core components. At the end of the chapter I will present my attempts to develop a reliable method to study the role of endogenous iRhoms in Myc-EGF degradation. In section 5.2, I will present the potential reasons that hampered these attempts, and I will show how my findings integrate with the other proteostasis studies.

CHAPTER 2

Material and Methods

2. Material and methods

2.1. Molecular biology methods

2.1.1. Molecular cloning

2.1.1.1. Polymerase chain reaction (PCR)

Amplification of DNA fragments was performed by polymerase chain reaction (PCR) using Phusion High-Fidelity DNA polymerase (Thermo Fisher Scientific) in a 96-well thermal cycler (Applied Biosystems) according to the protocol described in Table 1. The primers used for PCR reactions (Table 2) were ordered from Sigma-Aldrich or Invitrogen. The PCR products were used to generate new vectors by DNA assembly (section 2.1.1.4).

Table 1: Phusion PCR protocol

PCR mix (250µl)		**PCR programme**		
150µl	Water	1x	95°C	1 min
50µl	5X Phusion HF buffer (Thermo Fisher Scientific)	35x	98°C	20 s
12.5µl	Dimethyl sulfoxide		55°C	30 s
5µl	dNTP mix (10mM) (Bioline)		72°C	30 s / kb
12.5µl	Forward primer (10µM)	1x	72°C	7 min
12.5µl	Reverse primer (10µM)	Hold	4°C	
2.5µl	Phusion polymerase (Thermo Fisher Scientific)			
5µl	Template DNA (250ng in total)			

Table 2: PCR primers

primer name	sequence
BS_74	GATCTGGGCGGCCGC
BS_75	CGCCCTTGCTCACCATCTTAACTGGCTCTGTCTGCCGTG
BS_76	ATGGTGAGCAAGGGCGAGG
BS_77	ACGGGCCCTCTAGACTACTTGTACAGCTCGTCCATGCCGA
BS_397	CGGTGCATCTGTCCTGCA
BS_400	GGTTTAAACGGGCCCTCTAG
BS_404	GCCTACGTAGCTTGCTCGCGAGTGTCTTGTACAGCTCGTC
BS_405	GCAAGCTACGTAGGCGTAGACGCATCTAGTCTAGAGGGCCC
BS_643	CTGAGTCGCCCGGGGGGGATCCATGGCCTCAGCTGACAAGAATG
BS_645	CTAGAGTCGCGGCCGCTCTACTCGAGTTAGCCGGCGTAATCCGG CAC

2.1.1.2. Restriction digest

Plasmid DNA was digested by endonucleases according to the protocol described in Table 3. The restriction digest was performed at 37°C for 4 h. The reaction buffer was selected according to the manufacturer's instructions. Following restriction digest, the DNA fragments were separated by agarose gel electrophoresis and purified as described in the section below (2.1.1.3).

Table 3: Restriction digest protocol

restriction digestion (15µl)	
1.5µl	10x Reaction Buffer (New England Biolabs)
0.15µl	Bovine serum albumin (New England Biolabs)
2µl	Vector DNA (2µg in total)
1µl each	Restriction enzyme(s) (New England Biolabs)
add up to 15µl	Water

2.1.1.3. Agarose gel electrophoresis and gel purification

To analyse the digested plasmid and the PCR products, DNA was separated on a 1% agarose gel of 1x Tris-Borate-EDTA (TBE) buffer (Sigma-Aldrich) containing SYBR safe (1:10'000 dilution; Invitrogen). DNA bands were isolated with a scalpel, and they were purified using PCR clean-up gel extraction kit (Macherey-Nagel) according to the manual instructions.

2.1.1.4. DNA assembly

Purified PCR products were ligated with digested DNA vectors using In-Fusion cloning (Park et al., 2015). This method requires homology of 15 bp between the DNA fragments to be ligated. The homology fragments were added by PCR using overhanging primers (Table 2). Digested vectors and purified PCR products were incubated for 20 minutes at 50°C with 5X In-fusion HD Enzyme Premix (Clontech) according to the protocol in Table 4.

Table 4: In-Fusion cloning

In-Fusion cloning (10µl)	
2µl	5X In-fusion HD Enzyme Premix (Clontech)
1µl	PCR product (50ng)
1µl	Vector DNA (50ng)
6µl	Water

The expression constructs generated by In-Fusion cloning are listed in Table 5, and the list of other used plasmids is described in Table 6

Table 5: Generated expression constructs

vector name	primers	target vector
3xMyc-mouse EGF-EGFP (green-EGF)	BS_74 + BS_75; BS_ 76 + BS_77	pCDNA3.1
3xMyc-mouse EGF-EGFP-RxR (ER-EGF)	BS_397 + BS_404; BS_405 + BS_400	pCDNA3.1
mouse iRhom2^{WT}-3xHA	BS_643 + BS_645	pHRSIN.blast
mouse iRhom2$^{site1-3}$-3xHA, which contains the following mutations: S58A, S60A, S83A, S85A, S87A, S357A, S359A, S360A, T361A	BS_643 + BS_645	pHRSIN.blast

Table 6: Other plasmids used

vector name	backbone	source
human iRhom1^{WT}-3xHA	pM6P.blast	Hongmei Xu
human iRhom1^{pDEAD}-3xHA, which contains the following mutations: S8A, S11A, S51A, S61A, S76A, T78A, T85A, S92A, T139A, S176A, T180A, T183A, S188A, T380A, S390A	pM6P.blast	Hongmei Xu
human iRhom1$^{site1-3}$-3xHA, which contains the following mutations: S51A, T75A, S76A, T78A, T80A, S390A	pM6P.blast	Hongmei Xu
human iRhom2^{WT}-3xHA	pLEX.puro	Colin Adrain
3xMyc-mouse EGF (Myc-EGF)	pCDNA3.1	Colin Adrain (Zettl et al., 2011)
mouse iRhom2^{WT}-3xHA	pEGFP-N1	Marius Lemberg
human iRhom1-3xHA	pEGFP-N1	Colin Adrain
lentiviral packaging plasmid	pCMV-delta8.91	Colin Adrain (Adrain et al., 2011)

lentiviral envelope plasmid	pMD-VSV-G	Colin Adrain (Adrain et al., 2011)
retroviral packaging plasmid	pCL-Eco	Imgenex

2.1.1.5. Transformation

Assembled plasmids from In-Fusion cloning (section 2.1.1.4) were transformed into Stellar competent *E. coli* (Clontech). To do so, 2 µl of ligated vector was added to 50 µl of competent bacteria. After 30 min of incubation on ice, the bacteria underwent heat shock at 42°C for 45 sec, followed by incubation on ice for 1 min. 500µl of room temperature SOC medium was added to the bacteria, which were then incubated at 37°C for 1 h. The bacteria were plated in Petri dishes containing LB agar supplemented with 30 µg/ml kanamycin or 100 µg/ml ampicillin, and incubated overnight at 37°C.

2.1.1.6. Plasmid preparation

For plasmid preparation the bacteria transformed with the plasmid of interest were grown in 4 ml LB supplemented with the corresponding antibiotics in a shaker overnight at 37°C. The suspension cultures were then pelleted by centrifugation (4500 x g, 10 min). The QIAprep Spin Miniprep kit (Qiagen) was used to isolate DNA from bacteria according the manufacturer's instructions.

2.1.1.7. Sequencing

Generated DNA constructs and PCR fragments of isolated genomic DNA were sequenced using the Sanger Sequencing Service from Source BioScience. The self-designed sequencing primers are presented in Table 7.

Table 7: Designed sequencing primers

primer name	sequence	target
BS_32	CTTATCGAAATTAATACGACTC	pCDNA3.1
BS_59	CAAATATAGCAGTGGATCCAATAG	mouse EGF cDNA
BS_60	GAAGATGTCAATGAATGTGCCACTC	mouse EGF cDNA
BS_61	GACGTAGGGATGTCTCCACGGATTG	mouse EGF cDNA
BS_62	GACTGCTGAGTGTCAGTGTCTGAAAG	mouse EGF cDNA
BS_63	GACCCAACAGCAGCAGCGGGGCAGC	mouse EGF cDNA
BS_367	GAAGGAAGGTCCGCTGGATTGAGGGC	pHRSIN
BS_368	GGCATTAAAGCAGCGTATCCAC	pHRSIN
BS_373	AGATGCCCAAGATTGTGG	mouse iRhom2 cDNA
BS_389	GAAGCCATAGAGCCCACCGCATCC	pCDNA3.1
BS_397	CGGTGCATCTGTCCTGCA	mouse EGF cDNA

2.1.2. mRNA isolation and quantitative PCR

RNA was extracted from HEK293T cells using the RNeasy kit (Qiagen) according to the manufacturer's instructions. For DNase treatment, on-column digestion was performed using RNase-Free DNase Set (Qiagen) according to the manufacturer's instructions. The concentration of RNA was determined using a Nanodrop spectrophotometer (Thermo Fischer Scientific). 2 µg of RNA were reverse transcribed using the Superscript VILO kit (Invitrogen) according to the protocol in Table 8. Following 1:10 dilution, the cDNA was used with TaqMan Gene Expression Master Mix (Applied Biosystems) for quantitative PCR (qPCR) according to the protocol in Table 9. Using Fast Optical 96-Well Reaction plates (Applied Biosystems), the qPCR was performed in a StepOnePlus system (Applied Biosystems) using the settings described in Table 9. The TaqMan probes used for qPCR are described in Table 10. Gene expression was normalised to

Glyceraldehyde 3-phosphate dehydrogenase (GAPDH) and analysed using the StepOne software (Applied Biosystems).

Table 8: Reverse transcription

reverse transcription (10µl)	
2µl	SuperScript VILO MasterMix
5µl	RNA (2µg in total)
3µl	RNase-free water

Table 9: qPCR protocol

TaqMan PCR mix (10µl)		**PCR programme**			
1.5µl	cDNA (diluted 1:10)	1x		95°C	20 s
5µl	2X TaqMan Gene Expression Master Mix	1x		95°C	20 s
0.5µl	20X TaqMan probe	40x	[	95°C	1 s
3µl	Water		[	60°C	20 s

Table 10: TaqMan probes for qPCR

target gene	**product number**	**company**
Human RHBDF1	Hs01102745_m1	Thermo Fisher Scientific
Human RHBDF2	Hs00226277_m1	Thermo Fisher Scientific
Human TMEM115	Hs00183656_m1	Thermo Fisher Scientific
Human GAPDH	Hs02758991_g1	Thermo Fisher Scientific
Mouse EGF	Mm00438696_m1	Thermo Fisher Scientific

2.1.3. Isolation of genomic DNA

Cells were pelleted at 800 x g for 5 min, and DNA extraction was performed using a DNA extraction mix prepared from the Rapid Extract PCR Kit (PCR Biosystems)

(Table 11). Following 1:10 dilution and centrifugation at 13'000 x g for 1 min, the supernatant was used for PCR, as described in section 2.1.1.1 (where 1 µl of supernatant is used in place of the 250 ng of template DNA), and analysed by agarose gel electrophoresis (section 2.1.1.3).

Table 11: DNA extraction

DNA extraction mix (50µl)	
10µl	5x PCRBIO Rapid Extract Buffer A
5µl	10x PCRBIO Rapid Extract Buffer B
35µl	water

2.1.4. CRISPR/Cas9 constructs

CRISPR/Cas9 is a method of efficient, targeted genome editing that can be applied in many organisms (Doudna and Charpentier, 2014; Jinek et al., 2012). The system is composed of Cas9 endonuclease from *Streptococcus pyogenes*, and of a guide RNA (gRNA) which directs Cas9 to a specific genomic sequence. The gRNA specifically recognises 20 bp of genomic sequence, which must be followed by a 3 bp protospacer adjacent motif (PAM). Upon recognition of the sequence, Cas9 introduces double-strand breaks (DSBs) via its two nuclease domains: RuvC and HNH. The DSBs are either repaired by error-prone non-homologous end joining (NHEJ) or by homologous recombination. To further increase the specificity of the system, the Cas9 D10A nickase (Cas9n) can be used. Due to the presence of an inactivating mutation in the nuclease domain RuvC, this Cas9n only cleaves the opposite DNA strand, thereby generating single-strand breaks (called nicks). To generate insertions and deletions, two Cas9n-guide RNAs are used to target opposite DNA strands with a distance of 100 bp at most. The specificity of this

method is based on the required recognition of two close DNA sequences to trigger genomic modifications (Sander and Joung, 2014).

To generate iRhom1/2 double-knock out (DKO) cells, D10A S. *pyogenes* Cas9n and identified gRNAs were expressed from the vector pSpCas9(BB) 2A-Puro V2.0 (pX462 V2.0). The genomic sequences expressing the start codon and TMD1 of iRhoms were targeted to prevent expression of potential transcripts with residual functionality. For gRNA design, target sequences with a low chance of off targets were selected using online tools (http://crispr.mit.edu; http://www.sanger.ac.uk/htgt/wge). The sequences of the gRNAs that were cloned into pX462 V2.0 are described in Table 12.

Table 12: CRISPR/Cas9 gRNA sequences

target region	paired gRNA sequences	targeted protein feature
Human RHDBF1, exon 3	GGAACCATGAGTGAGGCCCC GGGTGGCTTCTTGCGCTGCC	start codon of iRhom1
Human RHDBF1, exon 10	AGCCGTGTGCATCTATGGCC CCGTCTCATGCTGCGAGAAC	TMD1 of iRhom1
Human RHDBF2, exon 2	GCAGAGCCGGAAGCCACCCC GGGTCTCTTTCTCGGGTGGC	start codon of iRhom2
Human RHDBF2, exon 9	AAACTCGTCCATGTCATCATCACC ACGGGTGCGATGCCATACGC	TMD1 of iRhom2

2.2. Cell biology methods

2.2.1. Cell lines and culture

Mouse embryonic fibroblast (MEF), human embryonic kidney 293T (HEK293T) and human non-small-cell lung cancer (NSCLC) A549 cells were cultured in DMEM (Sigma-Aldrich) supplemented with 10% fetal bovine serum (FBS) and 2 mM L-

Glutamine (Gibco). Using trypsinisation (TrypLE Select, Gibco) cells were split twice a week.

Table 13: generated cell lines

cell line	strategy and details
MEF DKO + iRhom1^{WT}	retroviral transduction
MEF DKO + iRhom1$^{site1-3}$	retroviral transduction
MEF DKO + iRhom1^{pDead}	retroviral transduction
HEK DKO + iRhom2^{WT}	lentiviral transduction
HEK DKO + iRhom2$^{site1-3}$	lentiviral transduction
HEK DKO + iRhom1^{WT}	lentiviral transduction
HEK iRhom1/2 DKO	CRISPR/Cas9; RHBDF1 targeted in exons 3 and 10, RHBDF2 targeted in exons 2 and 9
A549 iRhom1/2 DKO	CRISPR/Cas9; RHBDF1 targeted in exon 10, RHBDF2 targeted in exon 9

2.2.2. DNA transfection

For transient transfections of MEF and HEK293T, cells were seeded 24 h before transfection at ~20% cell confluency. They were transfected using non-liposomal transfection reagent FuGENE HD (Promega). FuGENE HD was added to OptiMEM reduced serum medium (Gibco) and incubated for 5 min before adding the DNA. Table 14 indicates the volume of the transfection mixes used in different plate sizes. Following 20 min of incubation at room temperature, the transfection mix was added to the cells. For transient transfections of A549, the reagent Lipofectamine 2000 (Thermo Fisher Scientific) was used instead of FuGENE HD due to its higher efficiency in transfecting A549 cells. Lipofectamine 2000 transfection of A549 cells in 24-well plates was performed with the transfection mix indicated in Table 15. To perform CRISPR/Cas9 knockout electroporation was performed to further increase

the transfection efficiency in A549 cells. For electroporation of A549 cells, 100 µl aliquots of 7.5 x 10^5 cells were transfected using the Neon Transfection System (Invitrogen) according to the manufacturers instructions. The following settings were used: 1230 volts, pulse width = 30 seconds and pulse number = 2. After electroporation, the cells were seeded in 6-well plates containing 2 ml of medium and incubated at 37°C for 24 h.

Table 14: Transfection mixes for MEF and HEK293T cells

plate size	FuGENE HD	DNA	total volume
6-well	4µl	0.5-1µg	100µl
12-well	2µl	0.3-0.8µg	50µl
24-well	0.4µl	0.05-0.2µg	20µl

Table 15: Transfection mix for A549 cells

plate size	Lipofectamine 2000	DNA	total volume
24-well	1µl	0.03µg	100µl

2.2.3. siRNA transfection

For knockdown experiments, HEK293T cells were seeded at ~10% confluency 24 h before transfection in 6-well plate. Using Lipofectamine RNAiMAX (Thermo Fisher Scientific) cells were transfected with siRNA according to the following protocol: per well in a 6-well plate, 4 µl Lipofectamine RNAiMAX were mixed with 100 µl OptiMEM reduced serum medium (Gibco) and 7µl siRNA (20µM) (Table 16). Following 15 min of incubation at room temperature, the reaction mix was added to the cells in 6-well plates. After 24 h a second siRNA transfection was performed in fresh medium, as described above. DNA transfection described in section 2.2.2 was

performed in fresh medium 48 h after the first siRNA transfection. The cells were collected for western blot and qPCR 72 h after the first transfection.

Table 16: siRNA for knockdown

siRNA name	manufacturer
non-targeting control (scramble)	Thermo Fischer Scientific (12935113)
Beclin1 siGENOME SMARTpool siRNA	Dharmacon (A-010552-14-0005)
CCPG1 siGENOME SMARTpool siRNA	Dharmacon (M-013998-01-0005)
FIP200 siGENOME SMARTpool siRNA	Dharmacon (M-021117-01-0005)
ATG7 siGENOME SMARTpool siRNA	Dharmacon (M-020112-01-0005)
STING siGENOME SMARTpool siRNA	Dharmacon (M-024333-00-0005)
iRhom1 siGENOME SMARTpool siRNA	Dharmacon (M-015651-01-0005)
iRhom2 siGENOME SMARTpool siRNA	Dharmacon (M-015783-01-0005)
iRhom1 stealth siRNA	Thermo Fisher Scientific (HSS148857)
iRhom2 stealth siRNA	Thermo Fisher Scientific (HSS148859)
TMEM115 stealth siRNA	Thermo Fisher Scientific (HSS117142)

2.2.4. Lentiviral transduction

HEK293T and MEF stable cell lines were generated respectively by lentiviral and retroviral transductions. The transfection mixes were performed as described in Table 17 and incubated at room temperature for 15 min, before being added to the cells. After 24 h, the transfection medium was replaced with 2 ml of fresh medium. The medium containing viruses was collected after 48 h and filtered through a 45 µm filter (Sartorius). The multiplicity of infection (MOI) was adjusted by either diluting the filtered medium with fresh medium at 1:1 ratio (high MOI), or 1:4 ratio (low MOI). The total volume was supplemented with 10µg/ml polybrene (Millipore) and used to transduce HEK293T or MEF cells growing at ~50% cell confluency in a 6-well plate.

48 h after transduction the cells were selected in medium supplemented with 10 µg/ml blasticidin S (Gibco) for at least 24 h. The generated cell lines are described in Table 13.

Table 17: Transfection mixes for lentiviral and retroviral transductions

	HEK293T	**MEF**
Expression vector	1µg pHRSIN (lentiviral)	0.5µg pM6P (retroviral)
Transfection reagent	6µl Polyethylenimine	4.5µl FuGENE HD
Packaging vector(s)	0.7µg pCMV-delta8.91 0.3µg pMD-VSV-G	0.5µg pCL-Eco
OptiMEM reduced serum medium	250µl	200µl

2.2.5. CRISPR/Cas9 knockout

To generate iRhom1/2 DKO cell lines, HEK293T cells were transfected with 250 ng of each of the eight pX462 V2.0 plasmids containing the gRNAs described in Table 12, and A549 cells were electroporated with 3.75 µg of each of the four pX462 V2.0 plasmids containing the gRNAs targeting the TMD1 of RHBDF1 and RHBDF2 (Table 12). 48 h after transfection the cells were selected with 1 µg/ml puromycin (Gibco) for 48 h. The cells were seeded at low density in 15 cm dishes and in 96-well plates for the selection of clonal cell lines. The cell lines were analysed by genomic extraction and PCR of the targeted loci, by western blot with concanavalin A enrichment and by alkaline phosphatase assay to detect loss of iRhom/TACE activity.

2.3. Biochemical methods

2.3.1. Cell lysis

Cells washed once with ice-cold PBS were lysed in Triton X-100 lysis buffer (1% Triton X-100, 50 mM Tris-HCl (pH 7.5), 150 mM NaCl) containing EDTA-free protease inhibitor mix (Roche) and 10 mM 1,10 Phenanthroline for 20 min at 4°C. Upon centrifugation at 13'000 rpm at 4°C for 15 min, the supernatants were transferred into fresh tubes.

2.3.2. Bicinchoninic acid (BCA) assay

The determination of protein concentration by the Pierce BCA assay kit (Thermo Scientific) is based on two sequential reactions: i) the reduction of Cu^{2+} into Cu^{+} by the peptides bonds of the proteins in an alkaline environment; ii) the reaction of the BCA reagent with Cu^{+} to form a complex that absorbs at 562 nm. To measure the protein concentration in the cell lysates, 200 µl of BCA mix was added to each well of a 96-well plate containing 10 µl of 1:10 diluted cell lysate according to the manufacturer's instructions. In parallel, serial dilutions of BSA standard (2 mg/ml, Thermo Scientific) were performed. After 20 min of incubation at 37°C the 562 nm absorbance of the samples was measured using a plate reader (SpectraMax M3, Molecular Devices).

2.3.3. Co-immunoprecipitation

Anti-HA magnetic beads (Thermo Scientific) were washed three times with Triton X-100 lysis buffer before being added to cell lysates to be incubated at 4°C for 5 h with over-head rotation. The beads were then washed five times with Triton X-100 lysis buffer, followed by elution of the proteins in 2x LDS buffer (Invitrogen) supplemented with 50 mM DTT for 15 min at 65°C.

2.3.4. Concanavalin A enrichment

To enrich for N-glycosylated proteins, sepharose coupled with the lectin concanavalin A (Sigma-Aldrich) was used. Cell lysates were incubated with concanavalin A sepharose at 4°C for 3 h with over-head rotation. The beads were centrifuged at 2000 x g for 5 min and washed three times with Triton X-100 lysis buffer. The proteins were eluted in 2x LDS containing 50% sucrose and 50 mM DTT at 65°C for 15 min.

2.3.5. Deglycosylation assay

Proteins in the cell lysate were denatured using Glycoprotein Denaturing Buffer (New England Biolabs) at 65°C for 15 min. 15 µl of the denatured cell lysate were incubated with 1µl peptide *N*-glycosidase F (PNGase, New England Biolabs), 1 µl endoglycosidase H (endo H, New England Biolabs), or left untreated at 37°C for 2 h according to the manufacturers instructions. After incubation with 4x LDS buffer at 65°C for 15 min, the samples were analysed by sodium dodecyl sulphate-polyacrylamide gel electrophoresis (SDS-PAGE) and western blot.

2.3.6. SDS-PAGE and western blot

Using SDS-PAGE, proteins were separated on 4-12% Bis-Tris NuPAGE gradient gels (Invitrogen) using MOPS SDS running buffer (50 mM MOPS, 1 mM EDTA, 50 mM Tris, 0.1% SDS) at 150 V for 2 h. Following activation of the polyvinylidene difluoride (PVDF) membrane (Millipore) with methanol, proteins were wet-transferred from gels to PVDF membranes in transfer buffer (25 mM Bis-Tris, 25 mM Bicine, 1 mM EDTA, 20% methanol) at 100 V for 105 min. The membranes were blocked in 5% milk-TBST (10 mM Tris-HCL (pH 7.5), 150 mM NaCl, 0.05% Tween 20, 5% dry milk powder) at room temperature for 1 h, followed by incubation

with the primary antibody in milk-TBST (see Table 18 for dilution ratios) overnight at 4°C. To increase the detection of 14-3-3 and Beclin-1, the incubation time of the primary antibody was prolonged by 72 h. The membranes were washed five times with TBST (10 mM Tris-HCL (pH 7.5), 150 mM NaCl, 0.05% Tween 20) at room temperature. Incubation of the membrane with diluted secondary antibody in milk-TBST (Table 18) was performed at room temperature for 1 h. After five washes with TBST at room temperature, the membranes were incubated with enhanced chemiluminescence (ECL) reagent (GE Healthcare) for antibody detection. X-ray films (Thermo Scientific) or high sensitivity films (Amersham Hyperfilm ECL, GE Healthcare) were exposed to ECL-treated membranes in a dark room, before being developed with a SRX-101A medical film processor (Konica).

Table 18: Antibodies for western blot

antibody	dilution	manufacturer
primary antibody		
anti-HA-HRP, rat monoclonal	1:2'000	Roche (12013819001)
anti-β-actin-HRP, mouse monoclonal	1:6'000	Sigma-Aldrich (A3854)
anti-TACE, rabbit polyclonal	1:1'000	Abcam (ab39162)
anti-pan14-3-3, rabbit polyclonal	1:500	Cell Signaling Technology (8312)
anti-GFP, chicken polyclonal	1:4'000	Abcam (ab13970)
anti-Myc, goat polyclonal	1:4'000	Abcam (ab9132)
anti-FIP200, monoclonal rabbit	1:1'000	New England Biolabs (12436S)
anti-Beclin-1, monoclonal rabbit	1:1'000	Cell Signaling Technology (D40C5)
anti-ATG7, monoclonal rabbit	1:1'000	Cell Signaling Technology (D12B11)
anti-TMEM115, polyclonal rabbit	1:500	Sigma-Aldrich (HPA015497)
secondary antibody		
anti-goat-HRP, mouse monoclonal	1:10'000	Santa Cruz (sc-2354)
anti-rabbit-HRP, goat polyclonal	1:5'000	Cell Signaling Technology (7074)
anti-chicken-HRP, bovine polyclonal	1:10'000	Santa Cruz Biotechnology (sc2497)

2.3.7. Alkaline phosphatase assay

To measure TACE activity, cells were transfected with alkaline phosphatase (AP)-conjugated substrates of TACE or the related protease ADAM10, and the AP activity in the supernatant and in cell lysates was assessed using a colorimetric assay. The different cell lines were seeded as follow: 3 x 10^4 HEK293T cells were seeded in poly-(L)-lysine (PLL)-coated 24-well plate, 3 x 10^4 MEF cells and 8 x 10^4 A549 were seeded in uncoated 24-well plates. After 24 h the cells were transfected with AP-conjugated TGFα, Areg, IL6R or EGF (received from Prof Carl Blobel) and with Ras constructs as described in section 2.2.2. For constitutive shedding, the medium was replaced 28 h after transfection with 300µl colourless OptiMEM reduced serum medium (Gibco), which was collected after 16 h. For stimulated shedding, the medium was replaced 48 h after transfection with 300µl colourless OptiMEM reduced serum medium (Gibco) supplemented with phorbol 12-myristate 13-acetate (PMA) and incubated at 37°C for 30 min. After the indicated times, the supernatants were collected, and the cells were lysed in Triton X-100 lysis buffer supplemented with protease inhibitor cocktail (Roche) and diluted 1 in 10. 100 µl of the supernatant and the diluted lysates were incubated with 100 µl AP substrate p-nitrophenyl phosphate (pNPP) (Thermo Scientific) at 37°C, until the yellow colour was visible. To measure the 405 nm absorbance a plate reader was used. The percentage of released AP was calculated by dividing the AP signal in the supernatant by the sum of the AP signal in the cell lysate and in the supernatant. Unless specified otherwise, three biological replicates were performed in each experiment, which were used to calculate the mean of released AP signal. For statistical analysis, an unpaired two-tailed student t-test was performed using Prism 7 (GraphPad).

2.3.8. Immunofluorescence staining and confocal microscopy

3 x 10^4 HEK293T cells were seeded in 6-well plates containing poly-D-lysine (PDL) pre-coated glass coverslips (Neuvitro) and transfected as described in section 2.2.2. After 48 h the cells were washed with PBS and fixed with 4% paraformaldehyde (Electron Microscopy Sciences) diluted in PBS at room temperature for 20 min. After three washes with PBS, the cells were permeabilised with 0.5% Triton X-100 (in PBS) for 20 min. After one wash with PBS, the cells were incubated overnight at 4°C with a selected primary antibody (Table 19) diluted in blocking buffer (3% Bovine Serum Albumin (BSA), 50mM Tris pH 7.5). The cells were washed three times with 0.5% Triton X-100 before incubation with the corresponding secondary antibody (Table 19) diluted in blocking buffer at room temperature for 1 h. After one wash with PBS, the coverslips were incubated in PBS supplemented with DAPI for 5 min, before a final wash with PBS. The coverslips were mounted in Fluoromount-G (eBioscience) and analysed by inverted FV1000 confocal system (Olympus).

Table 19: Antibodies for immunofluorescence

antibody	dilution	catalogue number
primary antibody		
anti-GFP, rabbit polyclonal	1:800	Invitrogen (A-6455)
Phalloidin Alexa Fluor 568	1:500	Invitrogen (A-12380)
anti-BAP31, mouse monoclonal	1:1’000	Alexis Biochemicals (804-601-c100)
secondary antibody		
anti-mouse Alexa Fluor 568, donkey polyclonal	1:500	Invitrogen (A-10037)
anti-rabbit Alexa Fluor 488, donkey polyclonal	1:500	Invitrogen (A-21206)

CHAPTER 3

Regulation of TACE activity

3. Regulation of TACE activity

3.1. Introduction

One of the central regulatory events for intercellular signalling is the stimulated release of extracellular signals at the plasma membrane. Many growth factors and cytokines are transmembrane-containing proteins that are cleaved from the plasma membrane, in a process called shedding. As a central shedding enzyme, TACE (for TNFα-converting enzyme, also known as ADAM17) is responsible for the release of dozens of substrates, including TNFα, EGFR ligands and IL6R (Zunke and Rose-John, 2017). As a result, TACE plays a pivotal role in the regulation of inflammation, cell proliferation and cancer formation. TACE is a type I transmembrane protein that is synthesised as an inactive zymogen, due to its inhibitory pro-domain at the N-terminus (Zunke and Rose-John, 2017). To become active, TACE requires iRhoms to reach the Golgi, where furin cleavage removes the inhibitory prodomain, in a process termed TACE maturation (Adrain and Freeman, 2012; Christova et al., 2013; McIlwain et al., 2012). Although the requirement of iRhoms for TACE maturation has been known for several years, how TACE is activated at the plasma membrane is unclear. Pharmacological stimuli such as phorbol 12-myristate 13-acetate (PMA) can stimulate TACE shedding via PKC activation (Doedens et al., 2003; Rovida et al., 2001). However, the precise molecular mechanism by which pharmacological and physiological stimuli activate TACE remains to be understood. Given the importance of EGFR dysregulation in cancers and the cases in which TACE has been associated with tumorigenesis, it is particularly important to understand how TACE receives the activation signals.

3.2. Results

3.2.1. The stimulated activation of TACE requires iRhom phosphorylation

The main project of my DPhil concerns the role of iRhoms in the regulation of TACE activity. Our lab and others have established that iRhoms are necessary for TACE maturation (Adrain and Freeman, 2012; Christova et al., 2013; McIlwain et al., 2012). However, how TACE is activated upon stimuli such as PMA is less well studied. It was recently discovered that PMA induces ERK-dependent phosphorylation of the iRhom2 N-terminus (Cavadas et al., 2017; Grieve et al., 2017). To investigate the importance of this phosphorylation, both sets of authors mutated all the potential phosphorylation sites in mouse iRhom2 (Figure 7) to alanines, which cannot be phosphorylated, to design a mutant called iRhom2^{pDEAD}. iRhom1/2 double knock-out (DKO) cells were then rescued with iRhom2^{WT}, or iRhom2^{pDEAD}. It was found that DKO-iRhom2^{WT}, but not DKO-iRhom2^{pDEAD}, can support PMA-induced shedding. This demonstrated the requirement of iRhom2 phosphorylation residues for stimulated TACE activity. These phosphorylation residues can be divided into three main sites (Figure 7), which each participate in PMA-induced shedding (Grieve et al., 2017). Concerning the molecular mechanism, iRhom2 phosphorylation leads to its interaction with phospho-binding proteins 14-3-3, and this interaction is sufficient to induce TACE activity (also see section 1.2.3) (Cavadas et al., 2017; Grieve et al., 2017). As a conclusion, phosphorylation of iRhom2 and binding to 14-3-3 are required for stimulus-induced activation of TACE.

Given the importance of iRhom2 phosphorylation for TNFα release by macrophages (Grieve et al., 2017), I decided to investigate whether regulation by phosphorylation is conserved in iRhom1. iRhom1 shows a much broader expression than iRhom2 (Christova et al., 2013; Li et al., 2015), and iRhom1 upregulation has

been observed in colorectal and breast cancer cells (section 1.4.2.1). As a result, understanding the importance of iRhom1 regulation is particularly important from a pathological and physiological point-of-view.

To investigate the role of the phosphorylation of iRhom1, I needed a system depleted of both iRhoms given the functional redundancy between iRhoms. Although iRhom1/2 DKO mice display perinatal lethality (Christova et al., 2013; Li et al., 2015), DKO mouse embryonic fibroblasts (MEFs) can be isolated for cell biological use and analysis. These cells show a loss of TACE maturation and therefore have no TACE activity (Christova et al., 2013; Li et al., 2015). To assess the requirement of iRhom1 phospho-sites, I have reconstituted them with different HA-tagged iRhom1 constructs: i) iRhom1^{WT}; ii) iRhom1$^{site1-3}$ (in which the conserved residues of mouse iRhom2$^{sites1-3}$ in iRhom1 are mutated to alanines); iii) iRhom1^{pDEAD} (in which all putative phosphorylation sites are mutated) (list of the mutations in section 2.1.1.4). Stable expression of the variant has been achieved by using retroviral vector pM6P and infecting the cells with either a high multiplicity of infection (MOI) or a low MOI. To be able to compare the ability of each iRhom1 variant to support TACE activation, I first needed to check that they are similarly expressed. To do so, I performed a western blot of the stable cell lines, which shows three cell lines in which iRhom1 constructs are expressed at a similar level (Figure 8). This observation, conditional on the repetition of this experiment, indicates that the ability of iRhom1 constructs to mediate TACE activity is comparable.

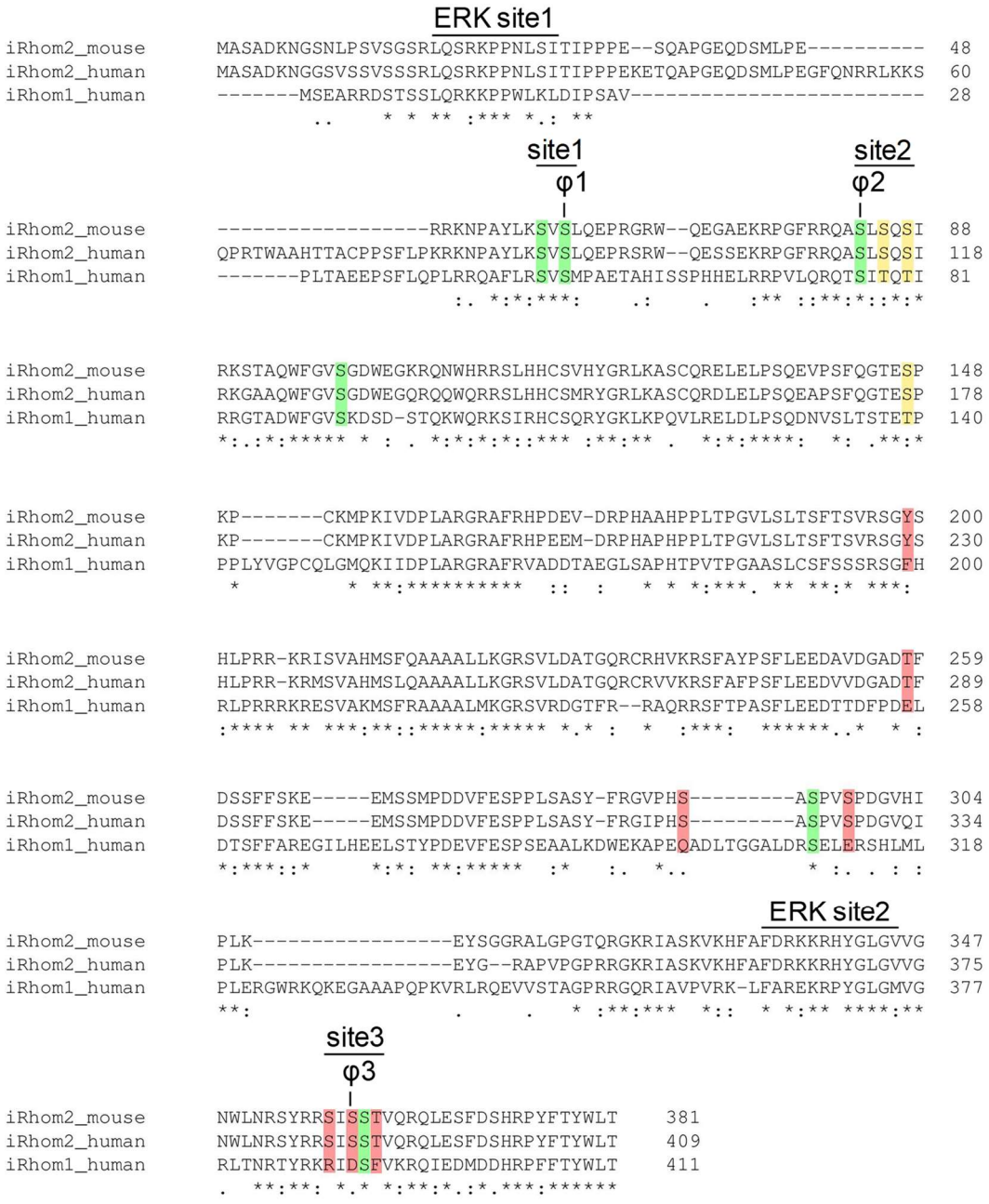


Figure 7: Alignment of N-terminus of mouse iRhom2, human iRhom2 and human iRhom1. The conservation of the phosphorylation residues identified in mouse iRhom2 (Cavadas et al., 2017; Grieve et al., 2017) is indicated as follow: total conservation (identical amino acid) in green, partial conservation (serine-threonine conversion) in yellow, and absence of conservation in red. The three main phosphorylation sites identified in mouse iRhom2 (Grieve et al., 2017) are indicated, as well as the predicted ERK docking sites and 14-3-3 binding sites (denoted by φ) (Cavadas et al., 2017). The alignment was performed with Clustal Omega using the following notation: an asterisk (*) for fully conserved residue, a colon (:) for residues with similar properties and a period (.) for residues with weakly similar properties.

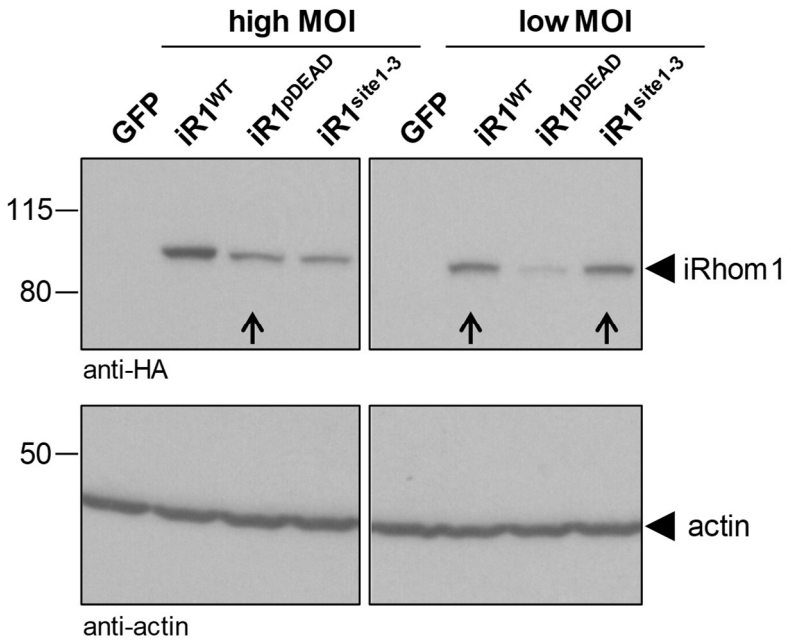


Figure 8: Stable expression of iRhom1 variants in iRhom1/2 DKO MEFs. Western blot of DKO MEFs stably expressing GFP as control, or HA-tagged human iRhom1^{WT}, iRhom1^{pDEAD} or iRhom1$^{site1-3}$ after anti-HA and anti-actin staining. The retroviral transduction was performed at either high multiplicity of infection (MOI) or low MOI. The arrows identify the selected cell lines for their similar level of iRhom1 expression. These data come from a single western blot in which only the cell lines of interest are represented.

To measure TACE-dependent shedding, I used the alkaline phosphatase (AP) assay, which is a quantitative readout. The rationale of the AP assay is to fuse AP to the luminal end of a TACE ligand, such as if it is cleaved, it leads to accumulation of AP in the supernatant (Figure 9). The abundance of released AP in the extracellular medium is assessed by adding the AP substrate pNPP (p-Nitrophenyl phosphate), which is converted into a yellow product, pNP (paranitrophenol) that can be detected using a plate reader for 405nm absorbance (Figure 9). The release percentage of the AP-tagged ligand is calculated by dividing the shed AP signal to the total amount of AP (in the cell and in the supernatant). To measure TACE-dependent shedding, AP-Areg and AP-TGFα were used to optimise the induction fold induced by pharmacological stimulation. As a negative control I used AP-EGF,

which is shed in a PMA-independent manner by ADAM10, and not by TACE (Sahin et al., 2004).

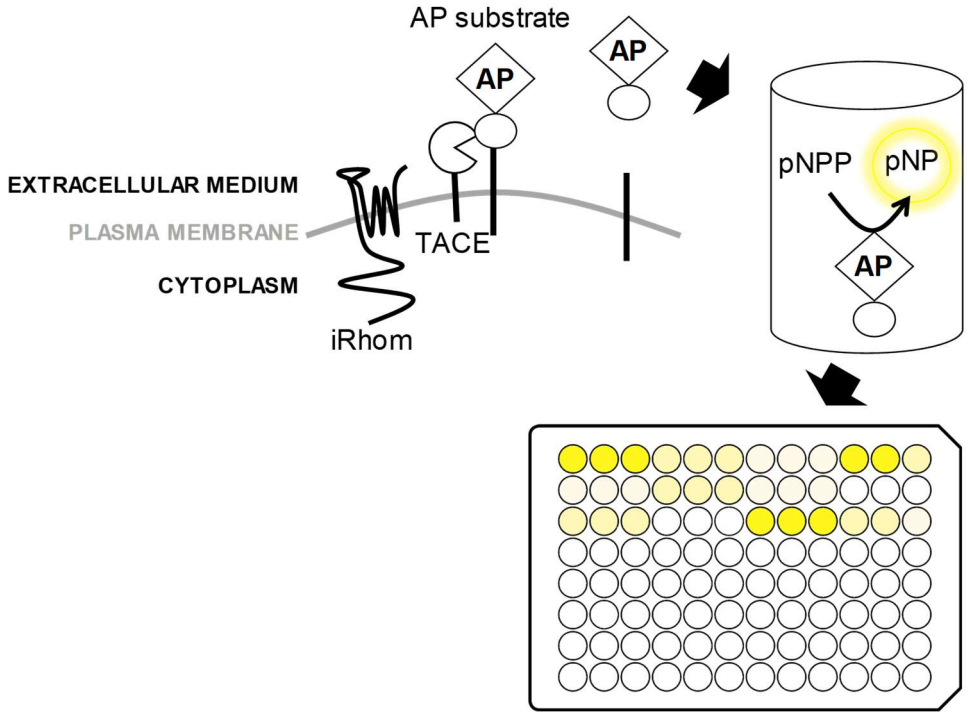


Figure 9: Schematic representation of the alkaline phosphatase (AP) assay. To measure TACE activity, AP-fused substrates of TACE and ADAM10 are transfected in the cell. In the presence of iRhoms, TACE is activated at the plasma membrane and proteolytically cleaves the substrates, releasing AP in the extracellular medium. AP activity in the extracellular medium and in cell lysate is detected by conversion of the AP substrate pNPP (p-Nitrophenyl phosphate) into the yellow product pNP (paranitrophenol). The yellow absorbance (405 nm) is measured in the 96-well plate using a plate reader.

The release percentage for AP-TGFα in DKO-iRhom1^{WT} cells shows an increase in TACE shedding upon PMA stimulation compared to the control condition (Figure 10). These results demonstrate for the first time that iRhom1 mediates PMA-induced activation of TACE, as it has been shown for iRhom2 (Grieve et al., 2017). As a control for the specific effect of PMA on TACE, experiments were also performed with AP-EGF (Figure 10), which is shed by ADAM10. The fact that PMA induces AP-TGFα shedding, but not AP-EGF shedding, demonstrates that this stimulus is

specific to TACE, and not to ADAM10. Concerning the importance of iRhom1 phosphorylation upon TACE activation, DKO-iRhom1$^{site1-3}$ and DKO-iRhom1^{pDEAD} displayed a significant decrease in PMA-induced shedding of TGFα compared to DKO-iRhom1^{WT} (Figure 10). PMA-induced stimulation of TACE therefore requires the three main sites of phosphorylation in iRhom1, but additional sites contribute to the event.

As a conclusion, I have shown that PMA stimulated shedding is supported by iRhom1, in which three sites of phosphorylation are required. These results demonstrate that the molecular mechanism of TACE activation by PMA is conserved between iRhom1 and iRhom2. Given the broader expression pattern of iRhom1 and its importance in tumour formation, it would be interesting to investigate the requirement of iRhom1 phosphorylation in these contexts.

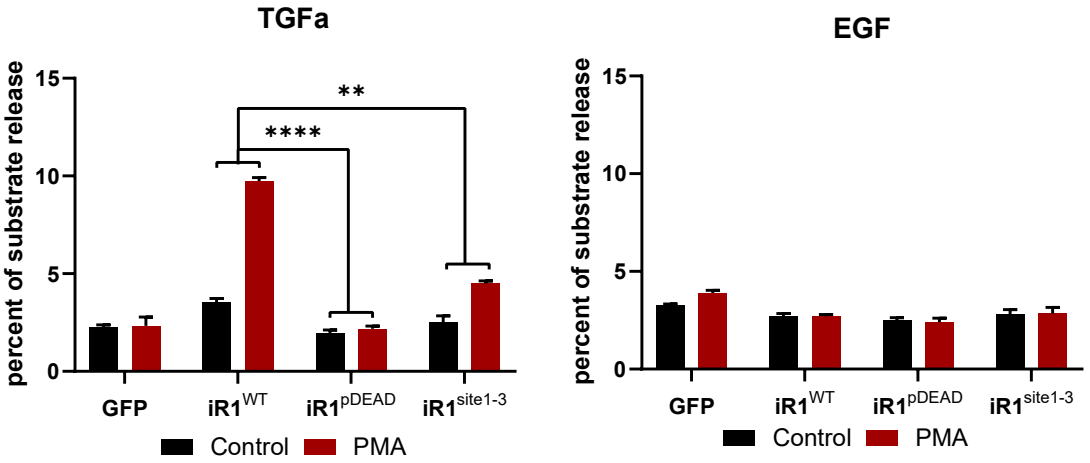


Figure 10: The phosphorylation sites in iRhom1 are required for PMA-induced shedding by TACE. DKO MEFs transduced with GFP or different versions of iRhom1 (described in Figure 8) were transfected with alkaline-phosphatase(AP)-tagged transforming growth factor (TGFα) or epidermal growth factor (EGF), before stimulation with 300 nM PMA during 30 min. Values represent the percentage of AP substrate release (released AP/total AP). The experiment was performed in biological triplicates. The bars indicate the mean value and the error bars represent the standard deviation. The statistical analysis of AP-TGFα has been performed on the induction fold (AP substrate release for PMA treated / AP substrate release for untreated) on n = 3 using unpaired two-tailed student t-tests; ns = p value > 0.05; * = p value < 0.05; ** = p value < 0.01; *** = p value < 0.001; **** = p value < 0.0001.

3.2.2. Generating HEK293T iRhom1/2 DKO to study Ras-induced shedding DKO

I have demonstrated that the mechanism for induced release of cytokines and growth factors by TACE is conserved between iRhom1 and iRhom2. As a follow up, I wanted to focus on the pathological importance of this mechanism. Although we have established the importance of iRhom2 phosphorylation for macrophage responses to bacterial infection (Grieve et al., 2017), the role of phosphorylation of either iRhom in other contexts remains unexplored.

To investigate novel pathological contexts of iRhom phosphorylation, I needed to explore the consequences of perturbing iRhom function in specific ways. To do this, I required an easily transfectable system, which can be reconstituted with iRhom constructs before transfection. I chose HEK293T (shortened as HEK), a widely employed cell line that had used with success in the lab, and I performed CRISPR/Cas9 gene editing to create double-knockout (DKO) cells. To do this, I designed guide RNAs (gRNAs) against RHBDF1 (encoding iRhom1) and RHBDF2 (encoding iRhom2). In addition to targeting the start codon, I targeted the first transmembrane domain (TMD1) of both iRhoms to disrupt the rhomboid fold, thereby preventing any potential residual activity of a transcript that could initiate from an alternative start codon. gRNAs were designed against exon 2 (containing the start codon) and exon 9 (encoding TMD1) of RHBDF1 (Figure 11), and exon 3 (containing the start codon) and exon 10 (encoding TMD1) of RHBDF2 (Figure 11, see section 2.1.4 for gRNA sequences). The gRNAs were integrated into the Cas9n plasmid, which was transfected into HEK cells. After clonal selection I performed genomic extraction and PCR of the target genes in 22 clones, which led to identification of iRhom1 and iRhom2 KO cells, and of an iRhom1/2 DKO cell line. In

this HEK DKO cell line, there is a 3.4 kbp deletion in RHBDF1 that encompasses ATG and TMD1 (Figure 11), and there is a 43 bp deletion in exon 10 of RHBDF2 (Figure 11), which generates a premature stop codon (see Figure 35 in Appendix for sequence reads).

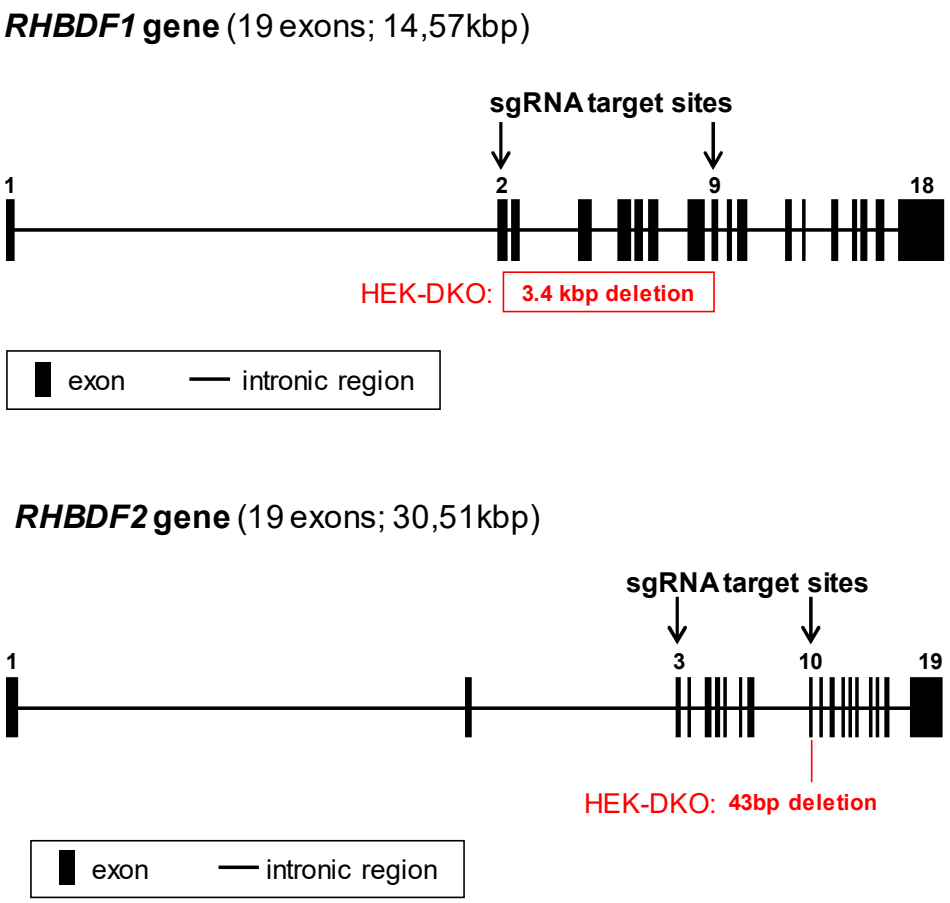


Figure 11: CRISPR/Cas9 strategy for double knock-out (DKO) of RHBDF1 and RHBDF2 in HEK293T. Maps of RHBDF1 and RHBDF2 based on the Ensembl browser (Yates et al., 2016), in which the target exons of gRNAs are indicated. In red are the deletions identified in HEK DKO cells (see Figure 35 in Appendix for the sequences reads).

To validate the iRhom1/2 DKO HEK cell line, I investigated iRhom function by assaying TACE maturation. To do so, I used Concanavalin A beads to enrich for N-glycosylated proteins, which includes TACE. Although the level of immature TACE remains unchanged in HEK DKO, these cells show a loss of mature TACE (Figure 12A), similar to that found in DKO MEFs (Christova et al., 2013; Li et al., 2015). Therefore, TACE maturation is abrogated in HEK DKO cells, which demonstrates the loss of iRhom function. Finally, I validated the loss of iRhom activity by assessing PMA-induced shedding in HEK DKO cells. In a preliminary experiment, PMA stimulates AP-Areg shedding in HEK WT, whereas HEK DKO show unstimulated AP-Areg shedding (Figure 12B). This defect in TACE activity in HEK DKO is similar to that observed for DKO MEFs (Christova et al., 2013; Li et al., 2015). The specific effect of PMA on TACE was confirmed by using AP-EGF, which is shed by ADAM10 (Figure 12B). As a conclusion, our lab now has a validated HEK cell line in which expression of both RHBDF1 and RHBDF2 has been abolished by CRISPR/Cas9 gene editing. This HEK DKO cell line represents a valuable resource to study the functions of iRhoms and it has already been used to characterise the requirement of FRMD8 in iRhom2 stability (Künzel et al., 2018).

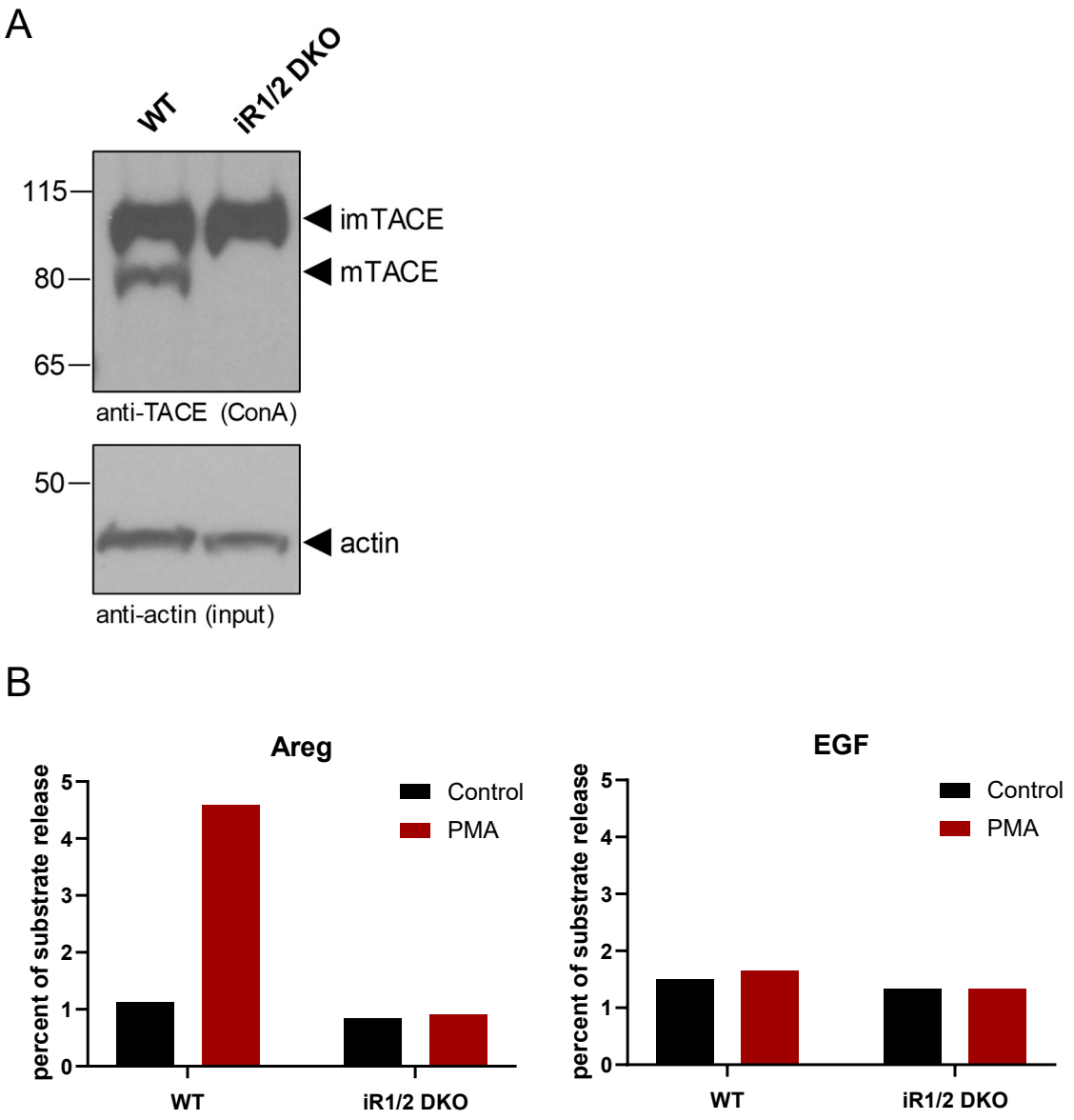


Figure 12: TACE maturation and activity are abrogated in HEK DKO cells. A) Cell lysates of HEK WT or iRhom1/2 DKO cells were enriched for glycosylated proteins using concanavalin A (ConA) sepharose to enhance anti-TACE staining. The upper band indicates immature TACE (imTACE) and the lower band indicates mature TACE (mTACE). Cell lysate from the input was used for anti-actin staining. **B)** HEK WT or DKO were transfected with AP-Areg or AP-EGF and they were stimulated with 200 nM PMA for 30 min. Values represent the percentage of AP substrate release (released AP/total AP). The data of the shedding assays represent a single experiment.

3.2.3. Oncogenic Ras induces shedding in an iRhom2-dependent manner

Upregulation of EGFR signalling is a hallmark of human cancers (Ciardiello and Tortora, 2008; Kenny and Bissell, 2007; Wilson et al., 2009). TACE is a major regulator of EGFR signalling and itself has been shown to be important for tumourigenesis (Das et al., 2012; Giricz et al., 2013; Kenny and Bissell, 2007; Schmidt et al., 2018; Zheng et al., 2012). Finally, both iRhoms have been associated to tumourigenesis. iRhom2 regulates TACE and it is also itself directly linked to cancer development, as point mutations in iRhom2 N-terminus are associated with tylosis with oesophageal cancer syndrome (TOC), a rare familial cancer syndrome (Blaydon et al., 2012; Brooke et al., 2014; Mokoena et al., 2018; Saarinen et al., 2012).

To support my aim of studying iRhoms beyond inflammation and because of the potential links described above, I decided to explore the importance of iRhoms in cancer. I have focused on Ras proteins, which are the most frequently mutated proto-oncogenes in human cancers (Fernández-Medarde and Santos, 2011; Haigis, 2017). The interest of Ras proteins relies in their ability to activate ERK1/2 (Schubbert et al., 2007; Simanshu et al., 2017), the kinases participating in iRhom phosphorylation upon PMA stimulation (Cavadas et al., 2017; Grieve et al., 2017). Finally, the focus on Ras proteins is supported by the involvement of TACE in Ras-induced tumourigenesis (Ardito et al., 2012; Baumgart et al., 2010). We therefore hypothesised that Ras proteins would induce TACE activity by triggering the phosphorylation of iRhoms.

To assess if Ras has an effect on TACE shedding in an iRhom-dependent manner, I required a means to upregulate Ras activity in my cell system. Ras

proteins are small GTPases that are regulated by a GDP/GTP cycle: they are activated upon binding to GTP stimulated by guanine nucleotide exchange factors (GEFs), and can be subsequently inactivated through GTP hydrolysis to GDP catalysed by GTPase-activating proteins (GAPs). Oncogenic Ras mutants, such as G12V, abolishes sensitivity to GAPs, thereby leading to constitutive activity. Whereas the Ras S17N mutant reduces GTP binding, thereby has a loss of enzymatic activity. K-Ras, H-Ras and N-Ras constitute the canonical members of the Ras family, in which the effect of G12V and S17N mutations is conserved (Hunter et al., 2015; Ostrem and Shokat, 2016). GTP bound Ras can bind numerous effectors to regulate cell proliferation and differentiation. One of the best characterised effector pathways of Ras is Raf-MEK-ERK, resulting in the activation of ERK, which then phosphorylates targets to regulate cell proliferation and cell cycle progression (Schubbert et al., 2007).

To investigate the importance of iRhoms in Ras-induced tumourigenesis, I first assessed whether Ras induces TACE activity by using oncogenic (constitutively active) or Ras S17N. Before transfecting Ras constructs in iRhom1/2 DKO HEK, I needed to reconstitute these cells with iRhoms. I first focused on iRhom2 reconstituted cells, for which I checked the rescue of iRhom function. While HEK DKO cells are unresponsive to PMA, HEK DKO cells reconstituted with iRhom2^{WT} vector (DKO-iRhom2^{WT} cells) show PMA-induced shedding of TGFα (Figure 13). The ADAM10 substrate AP-EGF was used as a negative control for PMA stimulation (Figure 13). As a conclusion, DKO-iRhom2^{WT} cells display restored iRhom function in TACE activity. As HEK DKO cells are easily transfectable, I now have a system to test the different Ras constructs.

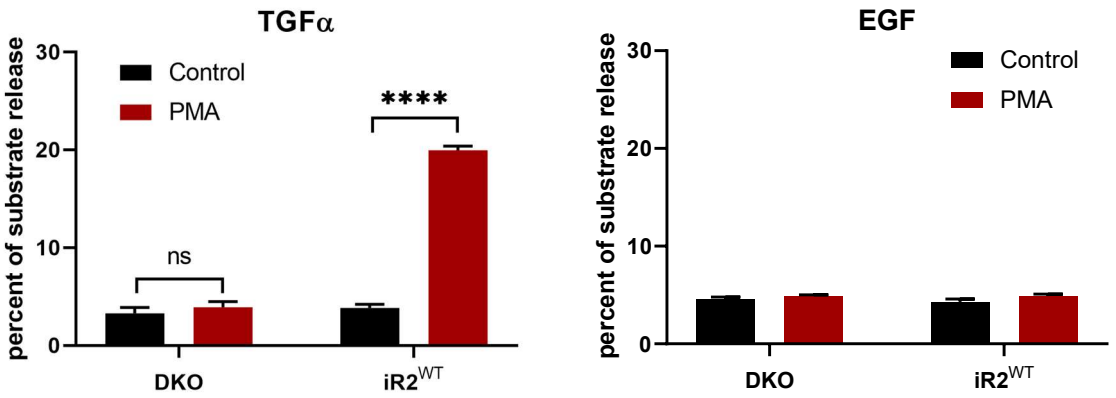


Figure 13: Stable expression of iRhom2^{WT} supports stimulated TACE activity. HEK DKO and HEK DKO-iRhom2^{WT} were transfected with AP-tagged TGFα or EGF and stimulated with 300 nM PMA for 30 min. The data are shown as described in Figure 10. Each experiment was performed in biological triplicates. The statistical analysis of AP-TGFα has been performed on n = 3 using unpaired two-tailed student t-tests; ns = p value > 0.05; * = p value < 0.05; ** = p value < 0.01; *** = p value < 0.001; **** = p value < 0.0001.

To test the effect of Ras activity on TACE shedding, HEK DKO and DKO-iRhom2^{WT} cells were transfected with KRas G12V or S17N and with the AP substrate. After 36 hours the medium was changed for colourless OptiMEM in which the release of AP substrates was allowed for 16 hours. This constitutes a difference with PMA-induced shedding, where the medium is collected 30 minutes after stimulation by PMA. Finally, the abundance of AP substrate in the medium and the lysate is measured as described in section 3.2.1 to determine the percentage of shed substrate.

Expression of KRas G12V leads to a significant increase in TGFα shedding compared to KRas S17N in DKO-iRhom2^{WT} cells (Figure 14A). KRas G12V specifically activates TACE, but not ADAM10, as evidenced by the absence of increase for AP-EGF shedding (Figure 14A). This is one of the first pieces of evidence that Ras activity stimulates TACE shedding. The requirement for iRhom2 in KRas-induced shedding is evidenced by the lack of response in HEK DKO (Figure

14A). This raises the question on whether iRhom2 is only required for TACE maturation, or also to receive the Ras-induced stimulation for TACE activation at the plasma membrane (see below).

To assess if the activity of another Ras protein also induces shedding, I transfected HRas G12V or S17N in DKO-iRhom2^{WT} cells. AP-TGFα shedding, but not AP-EGF shedding, is induced by oncogenic HRas (Figure 14B), which further demonstrates that Ras activity, more generally, is sufficient to stimulate TACE. However, as the induction of TACE-dependent shedding with KRas was greater than with HRas, I focussed on KRas for the rest of the project.

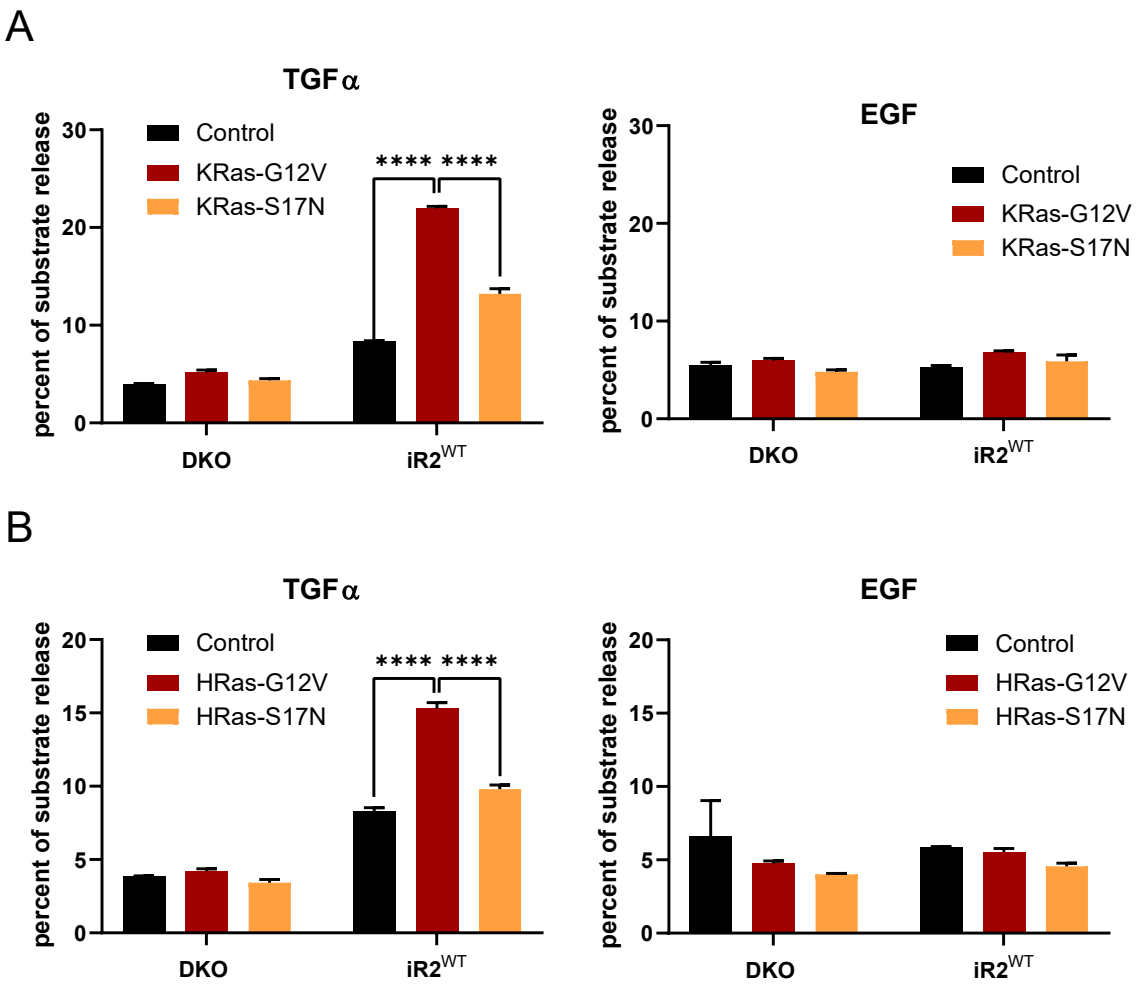


Figure 14: Oncogenic Ras proteins induce TACE activity in presence of iRhom2^{WT}. A) HEK DKO and HEK DKO-iRhom2^{WT} transfected with KRas-G12V or KRas-S17N, and with AP-tagged TGFα or EGF. **B)** The experiment was performed as described above, where HRas-G12V or HRas-S17N were transfected instead of the KRas constructs. In both experiments, the values represent the percentage of AP substrate release (released AP/total AP). The data are shown as described in Figure 10. The statistical analysis of AP-TGFα has been performed on n = 3 using unpaired two-tailed student t-tests; ns = p value > 0.05; * = p value < 0.05; ** = p value < 0.01; *** = p value < 0.001; **** = p value < 0.0001.

Having shown that iRhom2 can mediate Ras-induced TACE activity, I then tested whether iRhom1 has a similar function. To investigate whether KRas-induced shedding of TACE ligands is regulated by iRhom1, HEK DKO cells were reconstituted with iRhom1^{WT}. These cells have mature TACE, which supports AP-TGFα shedding induced by PMA (Figure 15). To control the specific effect of PMA on TACE, the experiment has been repeated with AP-EGF (Figure 15). These results show that DKO-iRhom1^{WT} cells show restored TACE sheddase activity. Surprisingly, in presence of iRhom1, KRas G12V does not further increase TGFα shedding compared to KRas S17N (Figure 16). As a control, the experiment was also performed with AP-EGF that is shed by ADAM10 cells (Figure 16). These results demonstrate that oncogenic KRas cannot induce TACE shedding in presence of iRhom1 only. This result highlights the unexpected specificity of KRas stimulation, which is only sustained by iRhom2, whereas PMA stimulation occurs in presence of both iRhom1 and iRhom2.

In conclusion, oncogenic Ras activates TACE-dependent shedding in the presence of iRhom2, but not of iRhom1. This result indicates that although iRhom1 is sufficient for pharmacological activation of TACE, it is not sufficient for Ras-induced shedding. It therefore suggests that iRhom2 is important for regulation of TACE activity at the plasma membrane upon specific stimulation by oncogenic Ras. Overall, this unexpected differential requirement shifts the focus toward a specific stimulation of iRhom2 by oncogenic Ras. Ras-induced shedding therefore represents a novel iRhom-dependent mechanism for release of EGFR ligands in an oncogenic context.

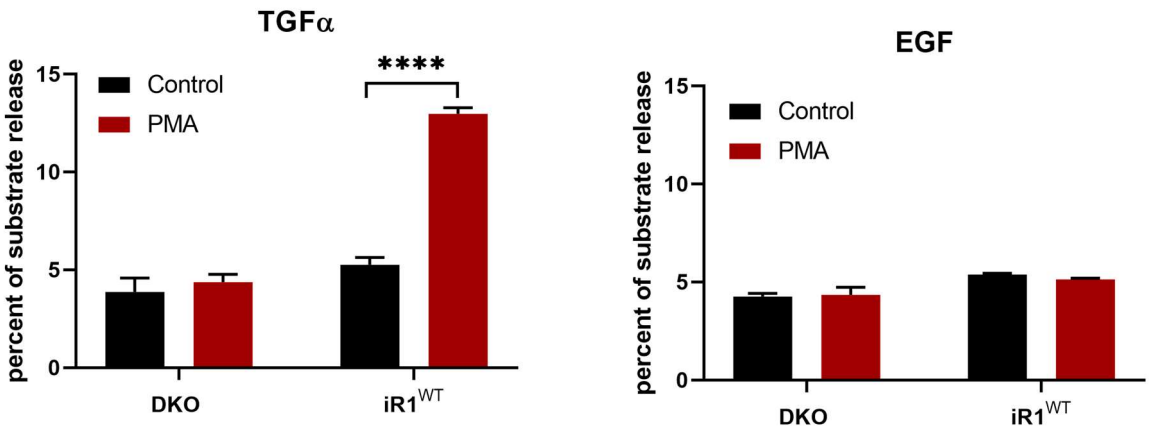


Figure 15: Stable expression of iRhom1^{WT} supports stimulated TACE activity in HEK DKO. HEK DKO and HEK DKO-iRhom1^{WT} were transfected with AP-tagged TGFα or EGF and stimulated with 300 nM PMA for 30 min. The data are shown as described in Figure 10. Each experiment was performed in biological triplicates. The statistical analysis of AP-TGFα has been performed on n = 3 using unpaired two-tailed student t-tests; ns = p value > 0.05; * = p value < 0.05; ** = p value < 0.01; *** = p value < 0.001; **** = p value < 0.0001.

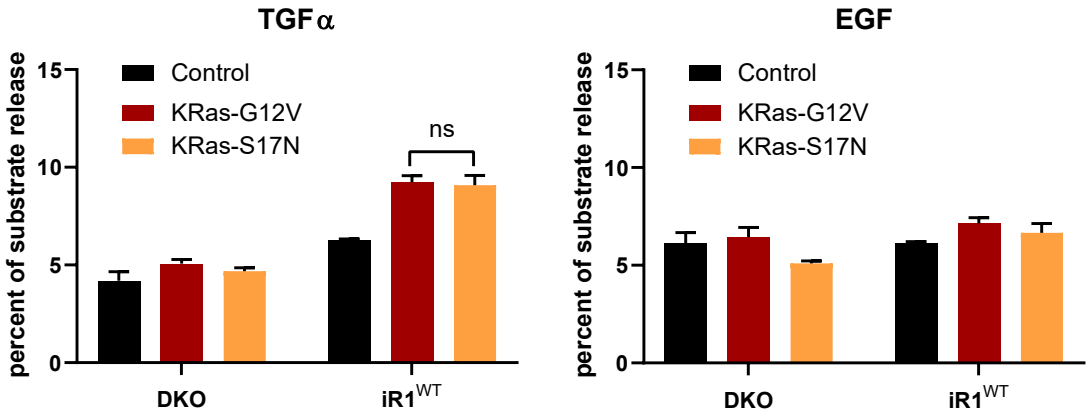


Figure 16: Stable expression of iRhom1^{WT} is not sufficient for KRas-induced shedding by TACE. HEK DKO and HEK DKO-iRhom1^{WT} transfected with KRas-G12V or KRas-S17N, and with AP-tagged TGFα or EGF. The data are shown as described in Figure 10. Each experiment was performed in biological triplicates. The statistical analysis of AP-TGFα has been performed on n = 3 using unpaired two-tailed student t-tests; ns = p value > 0.05; * = p value < 0.05; ** = p value < 0.01; *** = p value < 0.001; **** = p value < 0.0001.

3.2.4. Oncogenic Ras induces iRhom2 phosphorylation, which is required for shedding and 14-3-3 binding

As described in the previous section, iRhom2 is required for KRas-induced shedding of TACE ligands. This function could be due to either the role of iRhoms in TACE maturation, or in TACE activity at the plasma membrane, or in both. To determine how oncogenic KRas activates TACE-dependent shedding, I focused on iRhom2 phosphorylation. KRas acts upstream of ERK (Schubbert et al., 2007; Simanshu et al., 2017), which we have shown to be required for phosphorylation and 14-3-3 recruitment to iRhom2 N-terminus (Grieve et al., 2017). To assess the role of iRhom2 phosphorylation in KRas-induced shedding, I performed three transductions to reconstitute iRhom1/2 DKO HEK with either iRhom2^{WT} or iRhom2$^{site1\text{-}3}$ (in which the three main phosphorylation sites are mutated to alanines; list of the mutations in section 2.1.1.4). iRhom2 expression was checked, and the selected variants were expressed at comparable levels (Figure 18). As described above, oncogenic KRas was found to promote TACE shedding in cells expressing iRhom2^{WT}, but this was defective in cells expressing iRhom2$^{site1\text{-}3}$ (Figure 17). In the case of PMA stimulation, additional phosphorylation residues to the three main sites of phosphorylation in iRhom2 participate in stimulated TACE-dependent shedding of TACE ligands (Grieve et al., 2017). I am therefore currently assessing whether Ras-induced shedding of TACE ligands also depends on these additional residues by performing the experiment with cells expressing iRhom2^{pDEAD}, in which all possible sites are mutated. Overall, my current result demonstrates that the three main sites of phosphorylation in iRhom2 participate in KRas-induced shedding of TACE substrates.

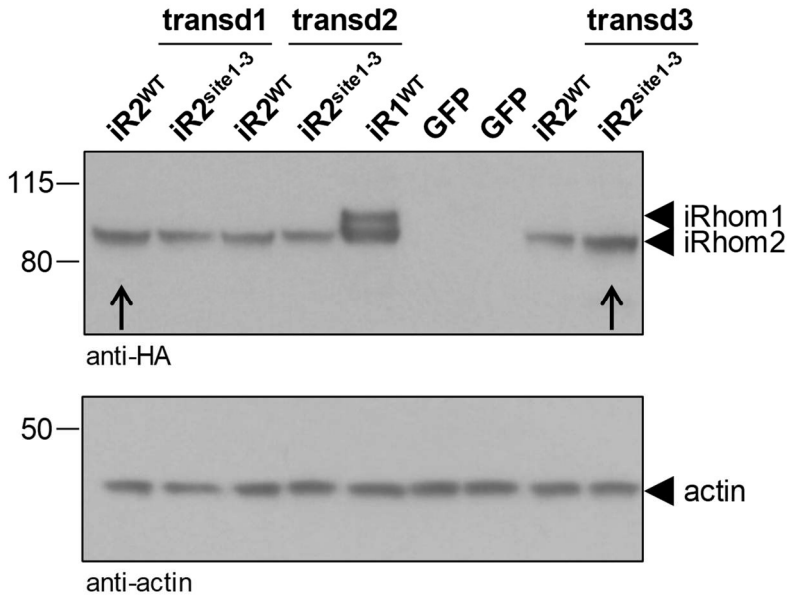


Figure 18: Stable expression of iRhom2 variants in DKO HEK cells. Western blot of HEK DKO stably expressing GFP (control), or HA-tagged human iRhom2^{WT}, iRhom2$^{site1-3}$ or iRhom1^{WT} after anti-HA and anti-actin staining. The retroviral transduction was performed in three experiments (transd1, transd2 and transd3). The arrows identify the selected cell lines for their similar level of expression.

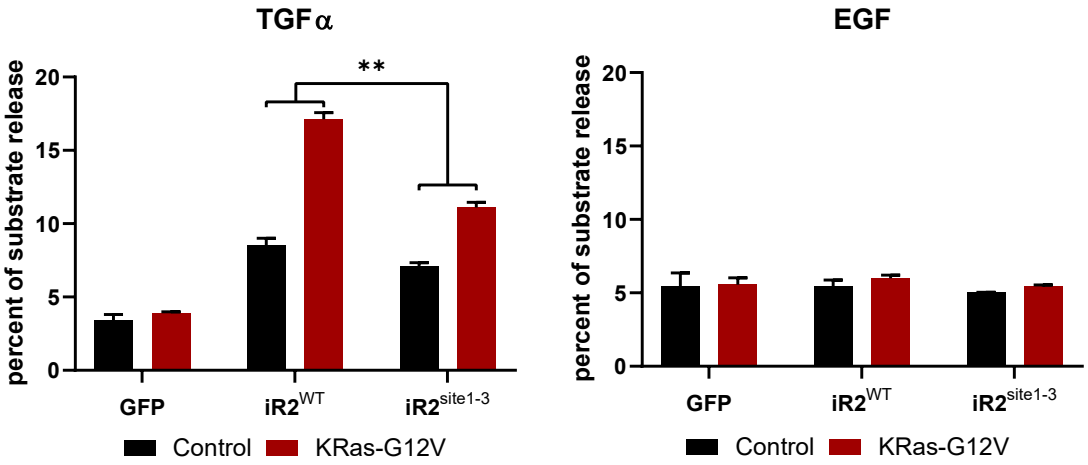


Figure 17: The three phosphorylation sites of iRhom2^{WT} participate in KRas-induced shedding by TACE. HEK DKO-iRhom2^{WT} and HEK DKO-iRhom2$^{site1-3}$ were transfected with KRas-G12V, and with AP-tagged TGFα or EGF. In both experiments, the values represent the percentage of AP substrate release (released AP/total AP). The data are shown as described in Figure 10. The statistical analysis of AP-TGFα has been performed on the induction fold (AP substrate release for PMA treated / AP substrate release for untreated) on n = 3 using unpaired two-tailed student t-tests; ns = p value > 0.05; * = p value < 0.05; ** = p value < 0.01; *** = p value < 0.001; **** = p value < 0.0001.

To assess the function of Ras-induced phosphorylation of iRhom2, I focused on the recruitment 14-3-3 proteins, which bind to phosphorylated iRhom2 upon PMA stimulation (Grieve et al., 2017). To do so, I transfected HEK DKO or DKO-iRhom2^{WT} cells with either KRas G12V or S17N. Western blots of iRhom2 immunoprecipitations show that 14-3-3 binding was induced by KRas G12V, but not by KRas S17N (Figure 19, lane 4 and 6). DKO cells were used as a negative control for the HA pulldown, and PMA was used as a positive control for 14-3-3 binding to iRhom2^{WT} (Figure 19). This result demonstrates that oncogenic KRas is sufficient to induce recruitment of 14-3-3 to iRhom2. As this recruitment is sufficient to increase TACE activity (Cavadas et al., 2017; Grieve et al., 2017), this result suggests that KRas induces shedding by recruiting 14-3-3 proteins to the phosphorylation sites of iRhom2 N-terminus. To put this hypothesis to the test, I am currently assessing if 14-3-3 binding by oncogenic KRas is abolished in DKO-iRhom2^{pDEAD} reconstituted cells. As a conclusion, oncogenic KRas leads to recruitment of 14-3-3 proteins to iRhom2, which is a marker of phosphorylation, and oncogenic KRas requires iRhom2 phosphorylation to induce TACE activity.

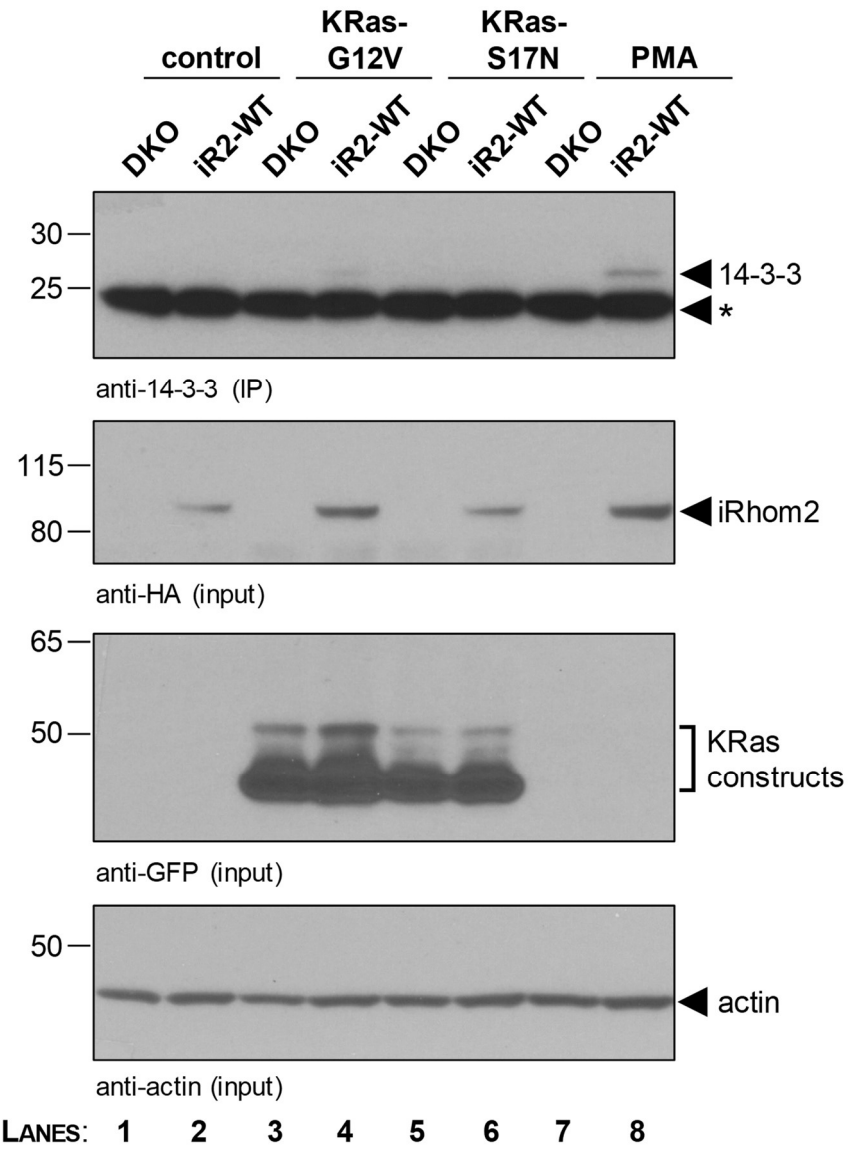


Figure 19: 14-3-3 proteins are recruited to iRhom2^{WT} by oncogenic KRas. Western blot of HEK DKO or HEK DKO-iRhom2^{WT} transfected with KRas-G12V or KRas-S17N, or treated with 300 nM PMA for 30 min, were subjected to anti-HA immunoprecipitation (IP), anti-HA, anti-GFP and anti-actin staining. An asterisk (*) indicates the non-specific band detected by anti-pan14-3-3 antibody. Lane numbers have been added for clarity. One representative western blot out of two independent experiments is shown.

3.3. Discussion and future plans

I have uncovered a novel mechanism by which activated Ras can trigger the release of EGFR ligands through activating TACE. This requires N-terminal phosphorylation of iRhom2, and is driven by 14-3-3 binding to iRhom2. Simultaneously with my work, Saad et al. also reported the role of TACE in mediating Ras stimulation of TACE activity, although they did not reveal the requirement for iRhom2 in this process (Saad et al., 2019). These results add to the perception that iRhom2 can be considered to be a regulatory subunit of TACE. Not only in the already-reported case of PMA stimulated TACE activity, but now also when Ras stimulates TACE, the cytoplasmic domain of iRhom2 transduces the signal from the stimulating pathway to TACE. Interestingly, KRas-induced shedding exhibits specificity towards iRhom2 (discussed in section 5.1.1).

KRas more than HRas activates iRhom2 for TACE-dependent shedding. Experiments support the fact that KRas more potently activates the Raf/MEK/ERK cascade than HRas (section 1.5.2). As a result, my results further demonstrate the importance of ERK phosphorylation of the N-terminus of iRhom2 for activation of TACE. Targeting this Ras-induced phosphorylation of iRhom2 represents a potential novel target for drug design (discussed in section 5.1). This strategy could have a large impact, especially given that KRas is the most frequently mutated Ras proteins in human cancers (Fernández-Medarde and Santos, 2011; Hobbs et al., 2016).

To determine the *in vivo* relevance of iRhom2/TACE function in mediating the effects of oncogenic KRas, I am now assessing the role of iRhom in cell transformation (described in section 1.5.2). The requirement of iRhoms for tumour

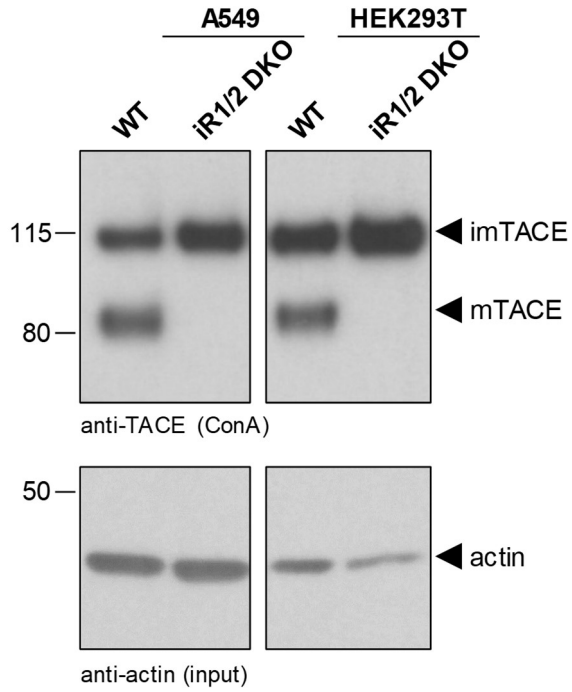
formation *in vivo* will be assessed by performing xenografts (see below). In the meantime, I am designing experiments to be done in tissue culture. Using stable cell lines expressing oncogenic KRas, I will study the requirement of iRhoms for anchorage-independent growth by performing spheroid formation assays and 3D-growth assays. As a result, I will be able to assess the importance of iRhoms in the acquisition of several malignant features of Ras-induced transformation.

The study published during the course of this project has shown the requirement of TACE for KRas-induced tumour formation was published (Saad et al., 2019). Using a mouse expressing $KRas^{G12D}$ in the lung, the authors show that TACE expression is the determinant of tumour formation in this organ. Genetic removal of TACE expression in the non-small cell lung cancer (NSCLC) cell lines A549, which express $KRas^{G12S}$, strongly decreases their ability for xenograft growth. In mice and in NSCLC cell lines, expression of oncogenic KRas is correlated with an increase of TACE phosphorylation in p38-dependent manner. Saad et al. concluded that TACE expression is required for tumour formation both in cell lines and in a mouse model (Saad et al., 2019). Clearly, some interesting questions arise from this publication concerning the molecular mechanism by which oncogenic KRas activates TACE (discussed in section 5.1). To address these questions and to place my findings into a more physiological context, I am focusing my future efforts on the A549 cell line used by Saad et al. to assess the importance of iRhoms for tumour formation.

To determine the role of iRhoms in KRas-induced cancer, the expression of RHBDF1 and RHBDF2 had to be deleted in A549 cells. During the past few months, I performed CRISPR/Cas9 gene editing to create iRhom1/2 DKO A549 cells by using the gRNAs validated in HEK cells (section 0). Several clonal cell lines were

obtained, and their genomic extracted DNA was analysed, which led to the identification of a DKO cell line. As for HEK DKO, the loss of iRhom activity was first determined by analysis of TACE maturation using concanavalin A enrichment. A549 DKO shows a loss of mature TACE (Figure 20A). This result is very similar to the profile of TACE maturation in HEK DKO, used as controls in this experiment (Figure 20A). To validate A549 DKO for the loss of iRhom activity, their ability to support PMA-stimulated shedding of IL6R by TACE was assessed. Whereas PMA induces IL6R shedding in A549 WT, A549 DKO show unstimulated IL6R shedding (Figure 20B). The shedding of AP-EGF was used as a control to assess the specificity of PMA stimulation (Figure 20B). Together, these results confirm the loss of iRhom activity in A549 DKO.

A



B

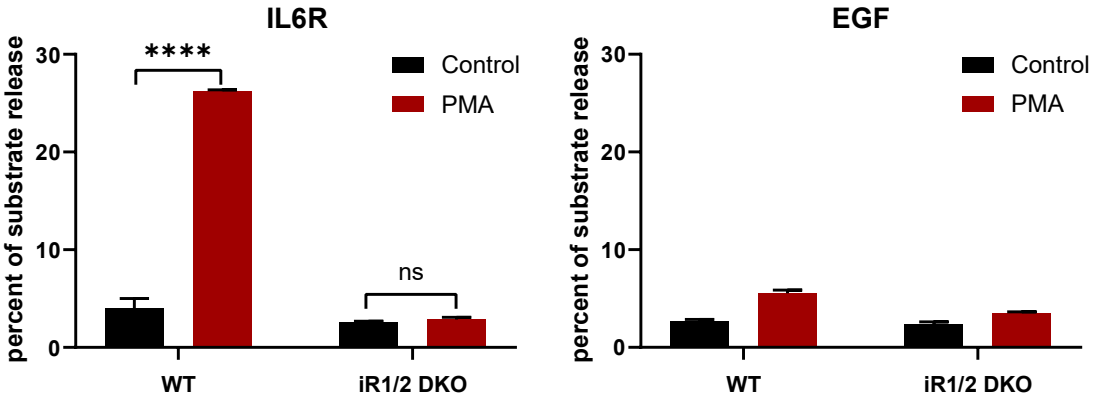


Figure 20: TACE maturation and activity are abrogated in A549 iRhom1/2 double knock-out (DKO) cells. A) Cell lysates of A549 and HEK WT or DKO were enriched for glycosylated proteins using concanavalin A (ConA) sepharose to enhance anti-TACE staining. Cell lysate from the input was used for anti-actin staining. One representative western blot out of three independent experiments is shown. **B)** WT or DKO A549 cells transfected with AP-IL6R or AP-EGF were stimulated with 300 nM PMA for 30 min. The data are shown as described in Figure 10. The shedding experiments were performed in triplicates (n = 3). The statistical analysis of AP-IL6R has been performed on n = 3 using unpaired two-tailed student t-tests; ns = p value > 0.05; * = p value < 0.05; ** = p value < 0.01; *** = p value < 0.001; **** = p value < 0.0001.

To determine the requirement of iRhoms in KRas-driven tumourigenesis we investigated the ability of A549-DKO cells to form tumours upon injection into immunodeficient mice. The xenograft of A549-DKO and A549-WT cells were performed by the group of Prof. Anderson Ryan (Oncology department, University of Oxford) as described in (Saad et al., 2019). In contrast to the tumour growth observed for A549-WT, A549-DKO xenografts failed to grow and remained at a similar volume until the end of the experiment (Figure 21). This result demonstrates for the first time the requirement of iRhoms for xenograft growth of lung cancer cells. It also represents the basis to investigate the oncogenic importance of iRhom2 phosphorylation for KRas-induced shedding. To do so, I am reconstituting A549-DKO cells with different iRhom2 constructs that will be used to perform xenografts. This approach will thus demonstrate the contribution of iRhom2 phosphorylation for KRas-induced tumourigenesis.

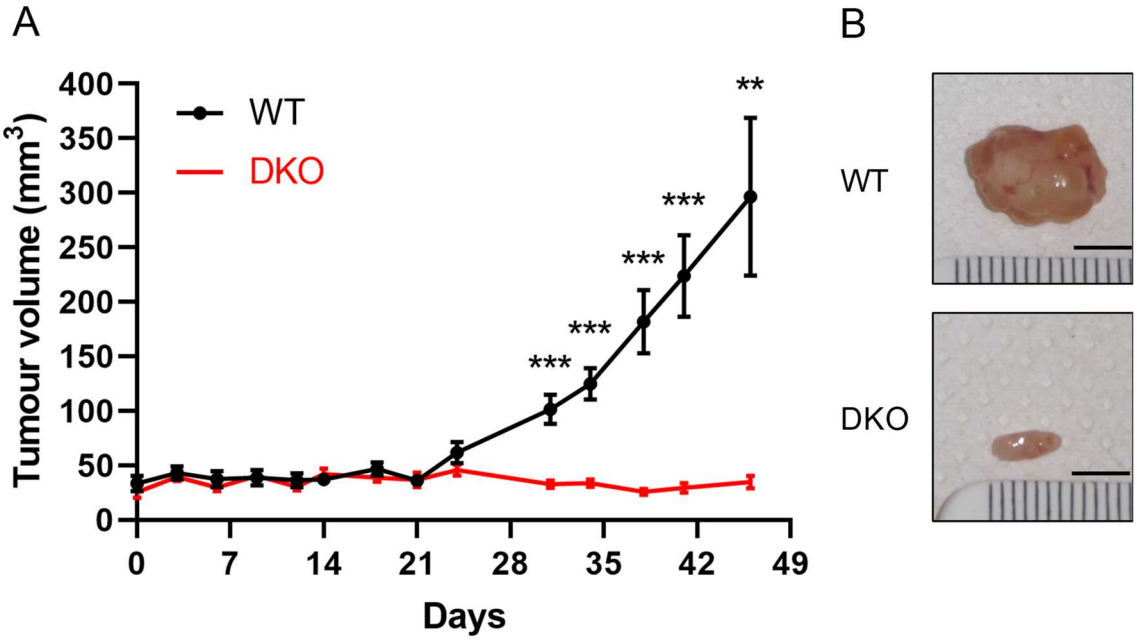


Figure 21: Xenograft growth is abrogated in A549-DKO cells. A549-WT and A549-DKO cells were injected in NOD *scid* gamma (NSG) mice as described in (Saad et al., 2019). **A)** The tumour volume was measured starting seven days post-injection until it reached 400 mm3. The data represent the mean of individual injection into six mice per condition, and the error bars indicate the standard error of the mean. The statistical analysis has been performed on n = 6 using unpaired two-tailed student t-tests; * = p value < 0.05; ** = p value < 0.01; *** = p value < 0.001; **** = p value < 0.0001. **B)** Representative images of tumours extracted at the end of the experiment. The scale bars indicate 5 mm. The xenograft assay has been performed by the group of Prof. Anderson Ryan (Oncology department, University of Oxford).

CHAPTER 4

iRhom-driven degradation of EGFR ligands

4. iRhom-driven degradation of EGFR ligands

4.1. Introduction

Although the role of iRhoms in TACE activity has been its most studied function, it has also been reported to have other roles (see section 1.3.1). The earliest report about iRhom function was in *Drosophila*, where it was found to participate in the degradation of EGF ligands by a process that resembled endoplasmic reticulum (ER)-associated degradation (ERAD) (Zettl et al., 2011).

The endoplasmic reticulum (ER) is an essential organelle for biosynthesis of transmembrane proteins. As a safeguard, ER protein quality control ensures proper folding of these proteins. Misfolded proteins in the ER undergo degradation by two main mechanisms: autophagy and ERAD. It has recently been discovered that some ER proteins act as receptors for autophagy of the ER, in a process named ER-phagy, allowing lysosomal degradation of ER contents (Smith and Wilkinson, 2017; Stolz and Grumati, 2019). The second route of ER protein degradation is via ERAD. During this process, the substrate is first recognised, before being ubiquitinated by an E3 ubiquitin ligase, such as Hrd1 or gp78. This allows the substrate to be retrotranslocated from the ER into the cytosol by the AAA ATPase VCP/p97. Finally, the substrate is recognised and degraded by the 26S proteasome. Although ERAD is mostly considered as a degradation pathway for misfolded proteins, recent findings demonstrate the presence of some regulatory ERAD routes, which target specific, functional proteins for degradation to regulate signalling pathways (Ruggiano et al., 2014).

Several members of the rhomboid-like superfamily have been linked to ERAD. Among the active proteases, RHBDL4 has been shown to cleave the pre-T cell

receptor α subunit to allow its degradation by the proteasome. The involvement of RHBDL4 in ERAD is supported by its ability to bind VCP/p97, and to interact with ubiquitinated proteins via its ubiquitin-interacting motif (Fleig et al., 2012). Inactive members of the rhomboid-like superfamily have been shown to participate in ERAD. Derlins are among the most cited examples, as they interact with the central ERAD E3 ligase Hrd1 (Lemberg and Adrain, 2016). Finally, iRhoms constitute one of the best characterised examples of the involvement of rhomboid-like superfamily members in protein degradation.

Our lab discovered that iRhoms are negative regulators of the EGFR pathway, acting by triggering degradation of EGFR ligands (Zettl et al., 2011). In *Drosophila*, iRhom KO shows a sleep-like phenotype, similar as that observed for activation of EGFR signalling (Foltenyi et al., 2007). In addition, genetic interactions demonstrate that EGFR signalling is under the negative regulation of iRhom and of the ERAD components EDEM2 and Hrd1 (Zettl et al., 2011). This inhibitory role is further illustrated by the decrease the level of EGFR ligands upon expression of *Drosophila* iRhom.

The ability to decrease EGFR ligands is conserved for mammalian iRhoms. This mechanism appears specific to EGFR ligands, and it is not supported by other polytopic transmembrane proteins (RHBDL2-SA, Unc93b). As EGF level is rescued by proteasomal inhibitors in presence of iRhoms, this supports the hypothesis that iRhoms trigger an ERAD-like process (Zettl et al., 2011). Overall, these findings demonstrate that iRhoms trigger degradation of EGFR ligands both in *Drosophila* and in mammalian cells. However, the precise molecular mechanism of this degradation is unclear.

4.2. Results

4.2.1. iRhoms reduce Myc-EGF level in a dose-dependent manner

To investigate the molecular mechanism of iRhom-driven degradation, I started my project by validating previous results and establishing an experimental system in HEK cells, which can be easily transfected. Previous work in the lab has shown that degradation of EGF triggered by iRhoms is conserved in human cells. Interestingly, this process is not dependent on the glycosylation of the substrate, and it does not require the main ERAD E3 ligases Hrd1 and gp78 (Dr Iqbal Dulloo, unpublished data).

To assess iRhom-driven degradation in HEK cells, we decided to use Myc-EGF as a reporter for this degradation pathway and to assess its level upon over-expressions of iRhoms, as it has been performed in COS7 cells (Zettl et al., 2011). In HEK cells, I co-expressed Myc-tagged EGF with increasing amounts of HA-tagged iRhom2^{WT}. After cell lysis, I performed a western blot in which I blotted with anti-Myc, anti-HA and anti-βactin. Increasing amounts of iRhom2^{WT} led to decreasing levels in Myc-EGF (Figure 22). These data indicate that expression of iRhom2 leads to decrease of Myc-EGF in a dose-dependent manner. This result is consistent with previous experiments in *Drosophila* and mammalian cells ((Zettl et al., 2011); Dr Iqbal Dulloo, unpublished data) and it demonstrated that HEK cells can be used as a system to identify the molecular mechanism of iRhom-driven degradation.

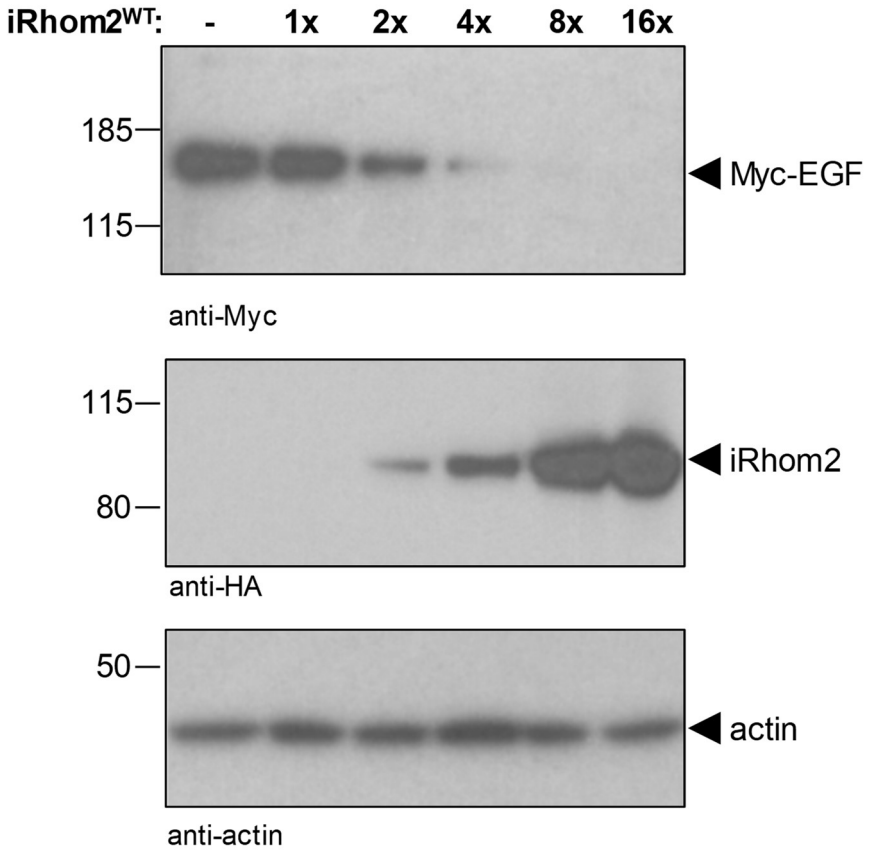


Figure 22: Ectopic expression of iRhom2^{WT} leads to dose-dependent decrease of Myc-EGF. Western blot of HEK cell lysates transfected with 250 ng of Myc-EGF and increasing doses of human iRhom2^{WT} (1x = 50 ng) after anti-Myc, anti-HA and anti-actin staining.

4.2.2. iRhom-driven degradation is rescued by proteasomal and lysosomal inhibitors

To investigate the molecular mechanism of iRhom-driven degradation of EGF, I wanted to assess which degradation machinery is required. There are two main cellular degradation machineries: the proteasome and the lysosome. I first focused on the proteasome, as two lines of evidence supported the hypothesis that iRhom-driven degradation of EGF is an ERAD-like pathway: i) genetic interactions in Drosophila suggested the involvement of ERAD components (Zettl et al., 2011), ii) the involvement of VCP/p97 and of the proteasome has been supported by

experiments in mammalian cells ((Zettl et al., 2011); Dr Iqbal Dulloo, unpublished data).

I first assessed whether iRhom1^{WT} decreases Myc-EGF level, as it is the case for iRhom2^{WT}. To do so, HEK cells were transfected with Myc-EGF and iRhom1^{WT}. Expression of iRhom1^{WT} strongly reduces Myc-EGF signal (Figure 23), demonstrating that iRhom1 also reduces Myc-EGF level. As a result, the ability to Myc-EGF is conserved between iRhom1 and iRhom2.

To assess the requirement of the proteasomal activity, I expressed Myc-EGF and iRhom1^{WT} in presence of the proteasomal inhibitor MG132 (Figure 23). Low level expression of iRhom1 led to potent EGF degradation, which was further increased upon higher expression of iRhom1 (Figure 23). This demonstrated that the dose-dependent degradation observed with iRhom2 can be reproduced with iRhom1. The decrease in Myc-EGF levels upon iRhom1 expression was strongly rescued by MG132 (Figure 23). This result indicates that the proteasome is involved in iRhom-driven degradation of Myc-EGF. Interestingly, there was also a mild increase of Myc-EGF upon MG132 treatment in absence of overexpressed iRhom1 (Figure 23). As this experiment was performed in a wild-type background, we interpreted that this modest stabilisation was due to inhibition of degradation by endogenous iRhoms.

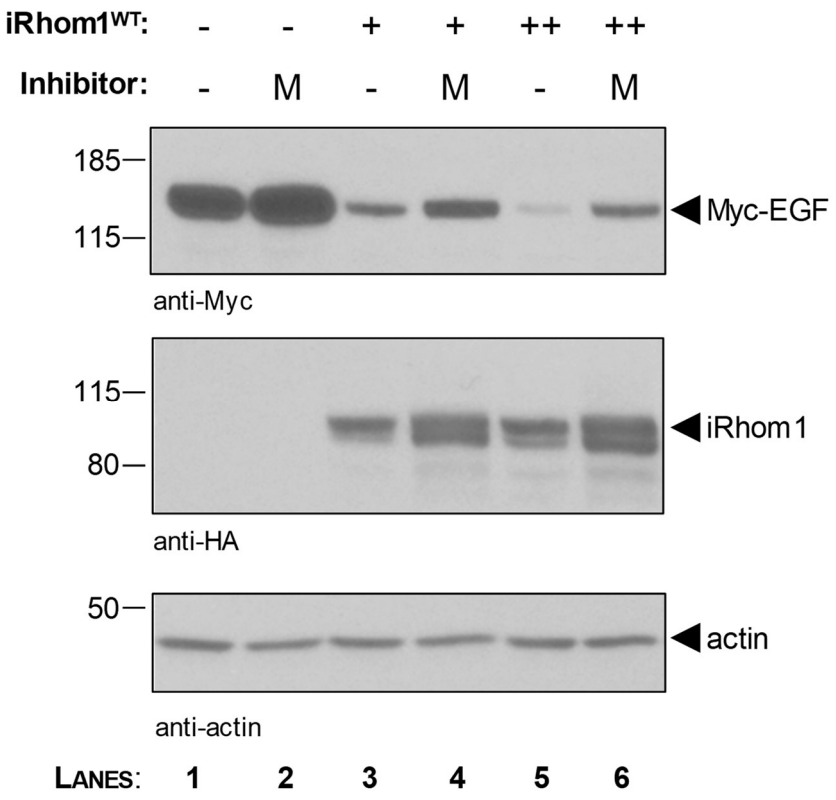


Figure 23: Assessing the participation of the proteasome in iRhom-driven degradation. Western blot of HEK cell lysates transfected with 250 ng of Myc-EGF and 50 ng (+) or 100 ng (++) of HA-tagged iRhom1^{WT}. 28 h after transfection the cells were treated with 10 µM of proteasomal inhibitor MG132 (M) for 18 h before being lysed for western blot. The membranes were subjected to anti-Myc, anti-HA and anti-actin staining.

Although MG132 treatment rescued iRhom-driven degradation of Myc-EGF (Figure 23), the rescued level remains lower than in absence of iRhom1^{WT} (Figure 23). This partial rescue could be explained either by the inhibition of the proteasomal activity being only partial, or by the involvement of another degradation pathway. To test the latter hypothesis, I assessed the role of lysosomal degradation in iRhom-driven degradation of Myc-EGF (Figure 24, lanes 5-8). As in the previous experiment, iRhom1^{WT} led to a clear decrease of Myc-EGF level (Figure 24, lane 6). Interestingly, this degradation was strongly rescued by the lysosomal inhibitor bafilomycin A1 (Figure 24, lane 8). This result consitutes the first evidence that the lysosome is involved in iRhom-driven degradation of Myc-EGF.

To directly compare the respective effect of the proteasomal and the lysosomal inhibitors, I repeated the experiments alongside one another (Figure 24, lanes 1-4). As observed in Figure 23, the proteasomal inhibitor led to a partial rescue of iRhom-driven degradation (Figure 24, lane 4). Interestingly, comparision of the two inhibitors showed that the lysosomal inhibitor more strongly rescued Myc-EGF than the proteasomal inhibitor (Figure 24, lanes 4 and 8). Of note, bafilomycin A1 potently increases Myc-EGF level in absence of transfected iRhom1^{WT}, more strongly than MG132 (Figure 24, lanes 3 and 7). This suggests that degradation of Myc-EGF by endogenous iRhoms is more contributed to by the lysosome than by the proteasome. Overall, these results raise the question of whether the proteasome and the lysosome cooperate in degradation of Myc-EGF. Unfortunately, co-treatment of cells with MG132 and bafilomycin was toxic for the cells (data not shown), so a conclusion for this could not be made. To summarise, my results confirm earlier data that iRhoms trigger the degradation of EGF; and uncovers a previoulsy unappreciated role for the lysosome in iRhom-driven degradation of EGF. In addition to the novelty of this finding, the higher rescue by lysosomal than by proteasomal inhibitor decided me to focus my future efforts on the pathway by which iRhoms induce lysosomal degradation of Myc-EGF.

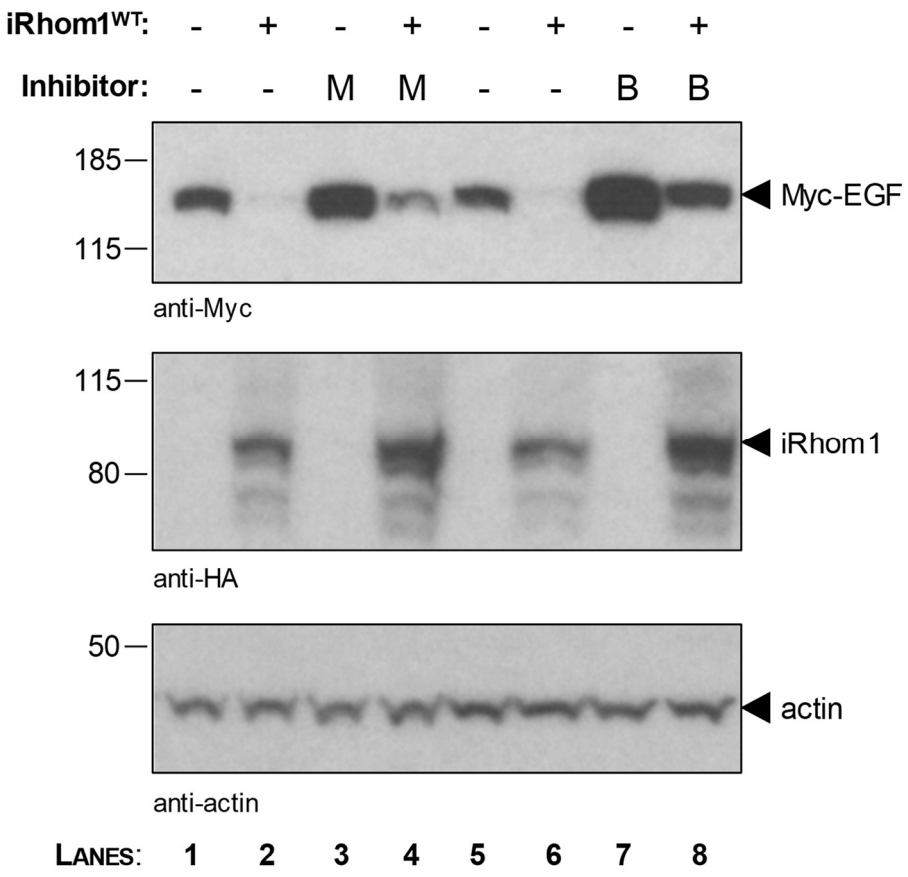


Figure 24: Predominant participation of the lysosome in iRhom-driven degradation. Western blot of HEK cell lysates transfected with 250 ng of Myc-EGF and 100 ng of HA-tagged iRhom1^{WT}. 28 h after transfection the cells were treated either with 10 µM of proteasomal inhibitor MG132 (M), or with 100 nM of lysosomal inhibitor bafilomycin A1 (B) for 18 h. For both experiments, the membranes were subjected to anti-Myc, anti-HA and anti-actin staining.

4.2.3. iRhoms drive degradation of Myc-EGF from the ER in a Beclin 1-dependent manner

As the lysosomal route described in section 4.2.2 consistutes a novel Myc-EGF degradation pathway, we decided to investigate the starting point of this mechanism. We first wanted to distinguish between the two main routes leading to lysosomal degradation: i) degradation from the ER by an autophagy-like process, and ii) degradation from the plasma membrane by an endocytosis-dependent process. One of the main differences between the two routes is the fact that the substrate traffics to the plasma membrane in the case of endocytosis, whereas it is directly sent from the ER for autophagic degradation. As a result, understanding whether iRhom-driven degradation of Myc-EGF requires trafficking through the secretory pathway would provide information on the degradation route that iRhoms trigger. I used two strategies to investigate this: I tracked glycosylation of Myc-EGF, and I engineered an ER-retained mutant of Myc-EGF that was unable to traffic through the secretory pathway.

Deglycosylation assays can be used to assess whether a protein has trafficked through the trans-Golgi network (TGN). As EGF contains N-glycosylation (Dempsey et al., 1997), this can be used to indicate whether it has passed through the TGN. During N-glycosylation, proteins in the ER are glycosylated with high mannose glycan (Figure 25A). Upon trafficking to the TGN, the glycan is processed into a complex glycan by oligosaccharide-modifying enzymes (Stanley et al., 2009). The deglycosylation assay relies on the ability of endoglycosidase H (Endo H) to remove high mannose glycans, but not complex glycans (Figure 25A) (Medzihradszky, 2005). As a result, an ER-resident protein remains Endo H-sensitive, whereas a plasma membrane protein that has trafficked through the TGN is Endo H-resistant.

To identify the extent of N-glycosylation of a protein, the enzyme peptide *N*-glycosidase F (PNGase F) is used to remove most N-glycans (Figure 25A) (Medzihradszky, 2005).

To assess the glycosylation status of rescued Myc-EGF, I performed a deglycosylation assay on the pool of Myc-EGF sent to lysosomal degradation upon expression of iRhom1^{WT} but rescued by bafilomycin A1 (Figure 25B). The first three lanes of the western blot show that in absence of iRhom1^{WT} transfection, Myc-EGF is Endo H-resistant: the Myc-EGF band after Endo H treatment migrates at a similar molecular weight to the sample without treatment (Figure 25B, lanes 1 and 2), whereas PNGase F treatment leads to a downward shift (Figure 25B, lane 3). The Endo H resistance of Myc-EGF in absence of transfected iRhom1^{WT} supports the conclusion that it has trafficked through the TGN. Interestingly, the pool of bafilomycin-rescued Myc-EGF shows a different pattern: the Myc-EGF band after Endo H treatment migrates at the same molecular weight as the PNGase deglycosylated sample (Figure 25B, lanes 11-12). The Endo H enzyme was able to cleave the N-glycans of this bafilomycin-rescued pool of Myc-EGF. This indicates that, in the presence of iRhom1^{WT}, Myc-EGF has trafficked to the lysosome directly from the ER, without transport through the TGN. This is the first evidence that iRhom-driven lysosomal degradation of EGF involves direct transport from the ER to the lysosome.

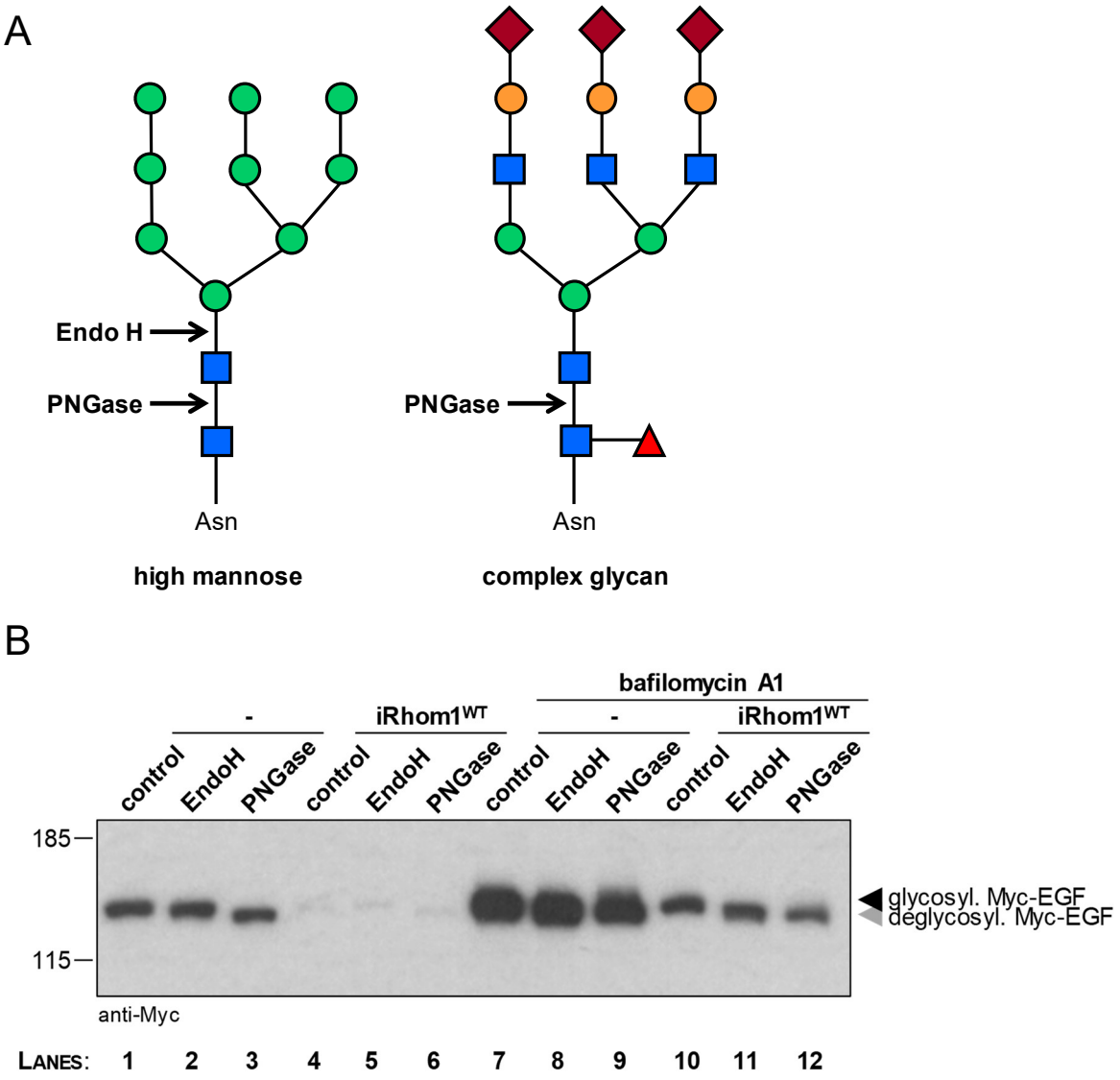


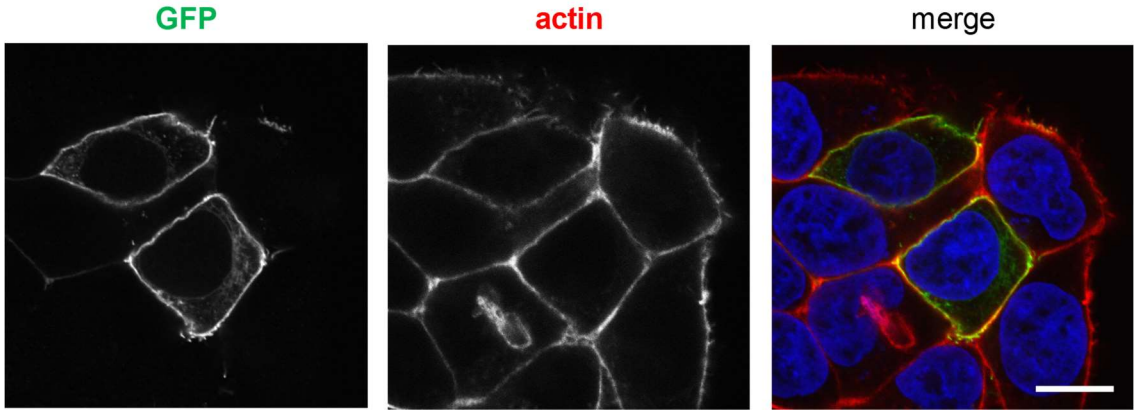
Figure 25: Bafilomycin-rescued pool of iRhom-driven degraded Myc-EGF is endo H sensitive. A) Schematic representation of different N-glycosylation and their sensitivity to endoglycosidase H (Endo H) and peptide N-glycosidase F (PNGase F) based on (Stanley et al., 2009). **B)** Western Blot of HEK cell lysates described in Figure 24 were denatured and treated with endo H or PNGase. The membrane was subjected to anti-Myc staining. Lane numbers have been added for clarity. One representative western blot out of two independent experiments is shown.

The localisation of Myc-EGF in the absence of iRhom1^{WT} transfection can already be partially inferred from its glycosylation status. The deglycosylation assay demonstrated that, in absence of iRhom1^{WT}, Myc-EGF does not act as an ER-resident protein, since it contains glycans that have been modified in the TGN (Figure 25B). To determine the precise localisation of this Myc-EGF pool, I added the fluorescent EGFP tag at the C-terminus of Myc-EGF to create Myc-EGF-EGFP (hereinafter referred to as green-EGF) (Figure 26A). I immunolabelled fixed cells expressing green-EGF, which shows that green-EGF extensively colocalises with cortical actin (Figure 26B). This result demonstrates that green-EGF targets the plasma membrane, consistent with my deglycosylation assay and as previously reported (Adrain et al., 2011; Rousselet et al., 2011). Finally, I checked whether addition of the EGFP tag altered the ability of iRhoms to induce degradation of green-EGF. A comparison of the expression of either green-EGF or Myc-EGF showed a similar degradation pattern triggered by iRhom1^{WT} (Figure 26C). As this experiment was performed before the focus on lysosomal degradation, the proteasomal inhibitor MG132 was used. Overall, these results indicate that, in absence of transfected iRhom1^{WT}, a pool of green-EGF localises at the plasma membrane. Upon expression of iRhom1^{WT}, however, green-EGF is still degraded in a similar fashion as Myc-EGF.

A


• Myc-EGF:
EGF
1255
• green-EGF:
EGF
EGFP
1494
• ER-EGF:
EGF
EGFP
1506
RxR

B


GFP
actin
merge

C

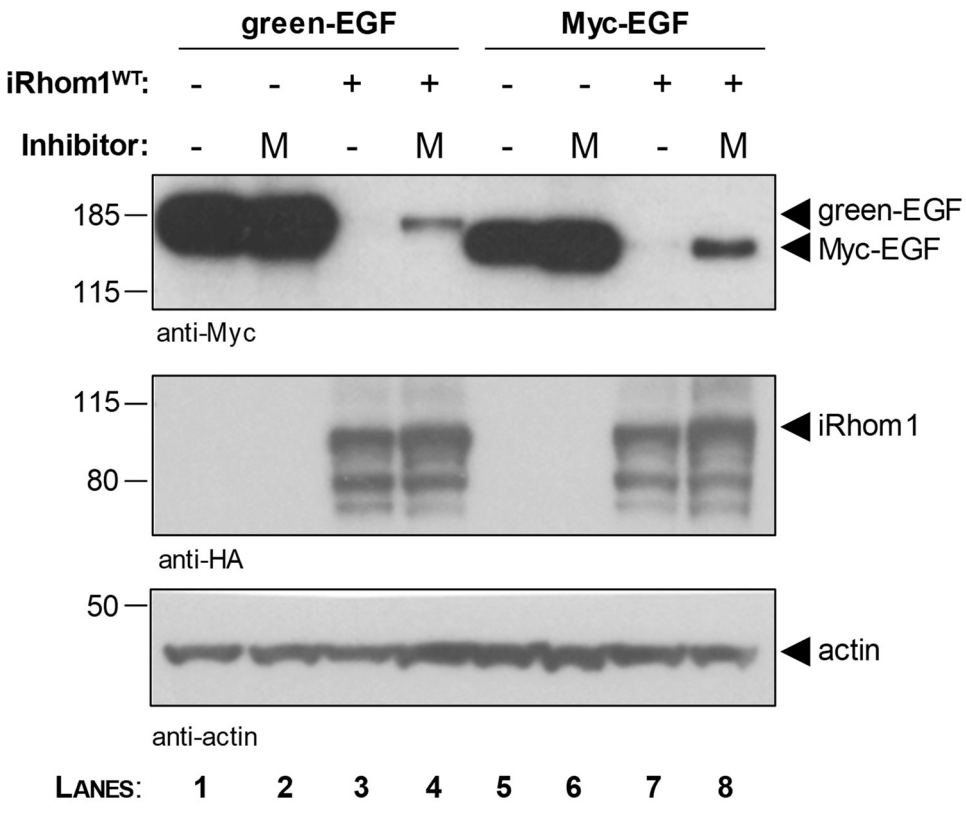

green-EGF
Myc-EGF
iRhom1WT: - - + + - - + +
Inhibitor: - M - M - M - M
185
115
green-EGF
Myc-EGF
anti-Myc
115
80
iRhom1
anti-HA
50
actin
anti-actin
LANES: 1 2 3 4 5 6 7 8

Figure 26: Green-EGF shows similar iRhom-driven degradation to Myc-EGF A) Schematic representation of Myc-EGF, green-EGF and ER-EGF plasmids, in which each purple diamond represents the Myc tag and the number on the right is the length of the protein in amino acids. **B)** Immunofluorescence microscopy of HEK cells transfected with green-EGF and stained with anti-GFP (green) and anti-actin (red) and DAPI for DNA (blue). The white scale bar represents 10µm. **C)** Western blot of HEK cells transfected with 750 ng green-EGF and Myc-EGF, and with 250 ng iRhom1^{WT}(+). 28 h after transfection the cells were treated with 10 µM of proteasomal inhibitor MG132 (M) for 18 h. The membrane was subjected to anti-Myc, anti-HA and anti-actin staining.

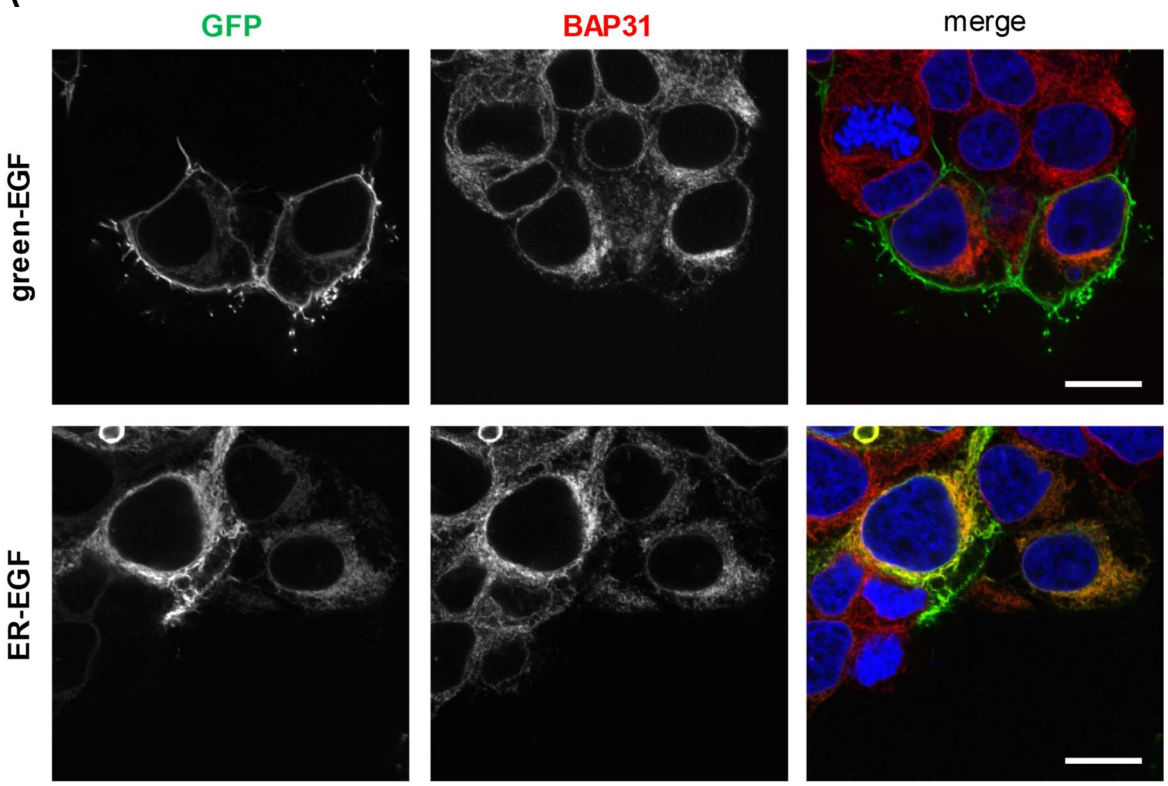
To create a pool of green-EGF that is uniquely sensitive to iRhom-driven degradation, an ER-retention motif was added to the C-terminus of green-EGF. As green-EGF is a type-I transmembrane protein with its C-terminus in the cytoplasm, the ER retention motifs RXR or KKXX can be used (rather than KDEL, which works in the ER lumen) (Ellgaard and Helenius, 2003). The amino acids surrounding RXR and KKXX lead to efficient ER retention of GFP tagged proteins (Zerangue et al., 2001). As KLRRRRT is one of the most efficient ER retention signals (Zerangue et al., 2001), it was added at the C-terminus of green-EGF to form ER-retained green-EGF (hereinafter referred to as ER-EGF) (Figure 26A). To assess the localisation of ER-EGF, I immunolabelled cells expressing green-EGF or ER-EGF. Green-EGF showed a predominant plasma membrane localisation (as in Figure 26B), whereas only a small pool colocalised with the ER marker BAP31 (Figure 27A). Conversely, ER-EGF extensively colocalised with BAP31 (Figure 27A). These results demonstrate that addition of the ER-retention signal is sufficient to retain ER-EGF in the ER.

To determine whether iRhom1 can target ER-EGF to degradation, ER-EGF was co-expressed with iRhom1^{WT}. ER-EGF level was strongly reduced in the presence of iRhom1^{WT} (Figure 27B, lane 2), similar to that shown for green-EGF (Figure 26C).

As a conclusion, iRhom1 induced degradation of an ER-retained client, which further supports my finding that iRhoms drive degradation of ER-localised clients. In addition, we also had developed a unique tool to isolate the effect of iRhom-driven degradation in the ER.

To investigate the role of the lysosome in ER-EGF degradation we tested whether the degradation was sensitive to bafilomycin A1. The lysosomal inhibitor efficiently rescued iRhom-driven degradation of ER-EGF (Figure 27B, lane 4). Interestingly, bafilomycin treatment also induced a stabilisation of iRhom1^{WT} (Figure 27B, lane 4). As a control, treatment with MG132 did not lead to a detectable rescue of ER-EGF degradation (Figure 27B, lane 6). These results represent the second evidence that iRhom-driven lysosomal degradation stems from the ER. Together with the deglycosylation assay, my results demonstrate that iRhoms target proteins from the ER to lysosomal degradation, thereby suggesting that iRhoms act in an autophagy-like process that originates in the ER.

A


GFP
BAP31
merge
green-EGF
ER-EGF

B

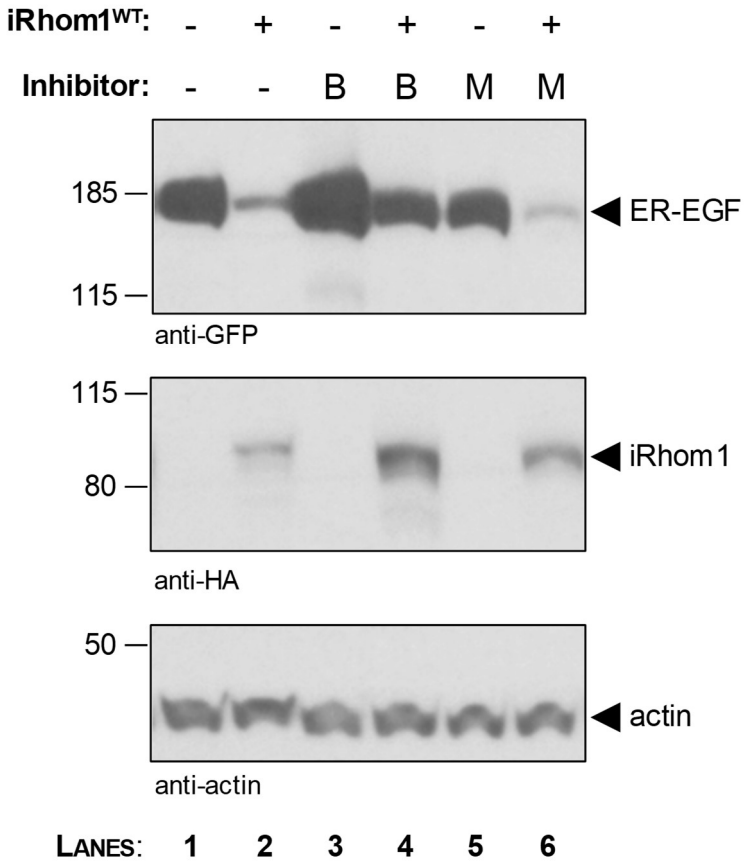

iRhom1WT: - + - + - +
Inhibitor: - - B B M M
185
115
ER-EGF
anti-GFP
115
80
iRhom1
anti-HA
50
actin
anti-actin
LANES: 1 2 3 4 5 6

Figure 27: ER-EGF undergoes iRhom-driven lysosomal degradation. A) Immuno-fluorescence microscopy of HEK cells transfected with green-EGF or ER-EGF and stained with anti-GFP (green) and anti-BAP31 (red) and DAPI for DNA (blue). The white scale bar represents 10µm. **B)** Western blot of HEK lysates transfected with 500 ng of ER-EGF and 200 ng of iRhom1^{WT}(+). 28 h after transfection the cells were treated either with 10 µM of proteasomal inhibitor MG132 (M), or with 100 nM of lysosomal inhibitor bafilomycin A1 (B) for 18 h. The membrane was subjected to anti-GFP, anti-HA and anti-actin staining.

To investigate the mechanism by which EGF was driven by iRhom1 to degradation by an autophagy-like mechanism, I tested whether core autophagy machinery was needed. Autophagy initiation requires the phosphorylation of ULK complex, which activates the Beclin-1 complex that produces PI3P on the phagophore. The phagophore elongation and closure into an autophagosome is ensured by the Atg8 conjugation system, which catalyses the formation of LC3-PE (see section 1.3.2.2). Among the core autophagy components, I investigated the requirement of Beclin-1, FIP200 (ULK complex) and Atg7 (Atg8 conjugation system) for Myc-EGF stability. Interestingly, Beclin-1 siRNA leads to a similar stabilisation of Myc-EGF as that observed for iRhom2 siRNA (Figure 28) (see section 4.2.4 for analysis of iRhom knockdown). The efficiency of Beclin-1 knockdown was demonstrated by its decrease at the protein level (Figure 28). Of note, knockdown of the ER-phagy receptor CCPG1 (Figure 28) did not affect Myc-EGF level either (Figure 29). To determine whether Beclin-1 acts in the same pathway as iRhoms, I assessed its requirement for degradation of Myc-EGF in presence of iRhom1^{WT}. Interestingly, knockdown of Beclin-1 rescues, albeit only partially, the decrease of Myc-EGF by iRhom1^{WT} (Figure 29, lane 8). Overall, these results indicate that Beclin-1 is a required component of Myc-EGF degradation and that it participates in iRhom-driven degradation.

To investigate the involvement of other autophagy components in Myc-EGF stability, I focused on FIP200 and Atg7. Surprisingly, siRNA of neither of them increases Myc-EGF level, although the protein level of FIP200 and Atg7 was strongly reduced upon siRNA (Figure 28 and Figure 29). Overall, these results demonstrate that Beclin-1 is a component of iRhom-driven degradation of Myc-EGF but imply that other core autophagy machinery does not participate. Further experiments are required to determine whether Beclin-1 is the only autophagy component to be involved in this pathway.

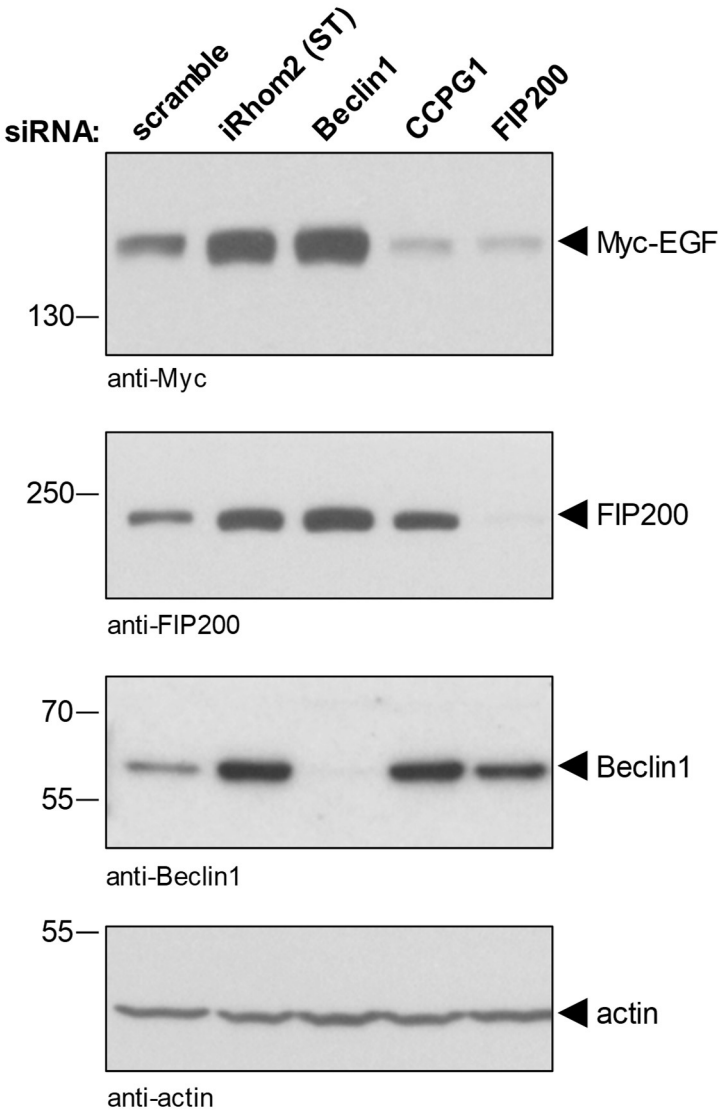


Figure 28: Beclin-1 knockdown stabilises Myc-EGF. Western blot of HEK cell lysates transfected with Myc-EGF. The cells had been transfected with siRNAs targeting iRhom2, Beclin-1, CCPG1, FIP200, or with non-targeting siRNA (scramble). All used targeting siRNAs are SmartPool siRNAs, except for the STealth siRNA (ST) targeting iRhom2. The membrane was subjected to anti-Myc, anti-FIP200, anti-Beclin-1 anti-actin staining.

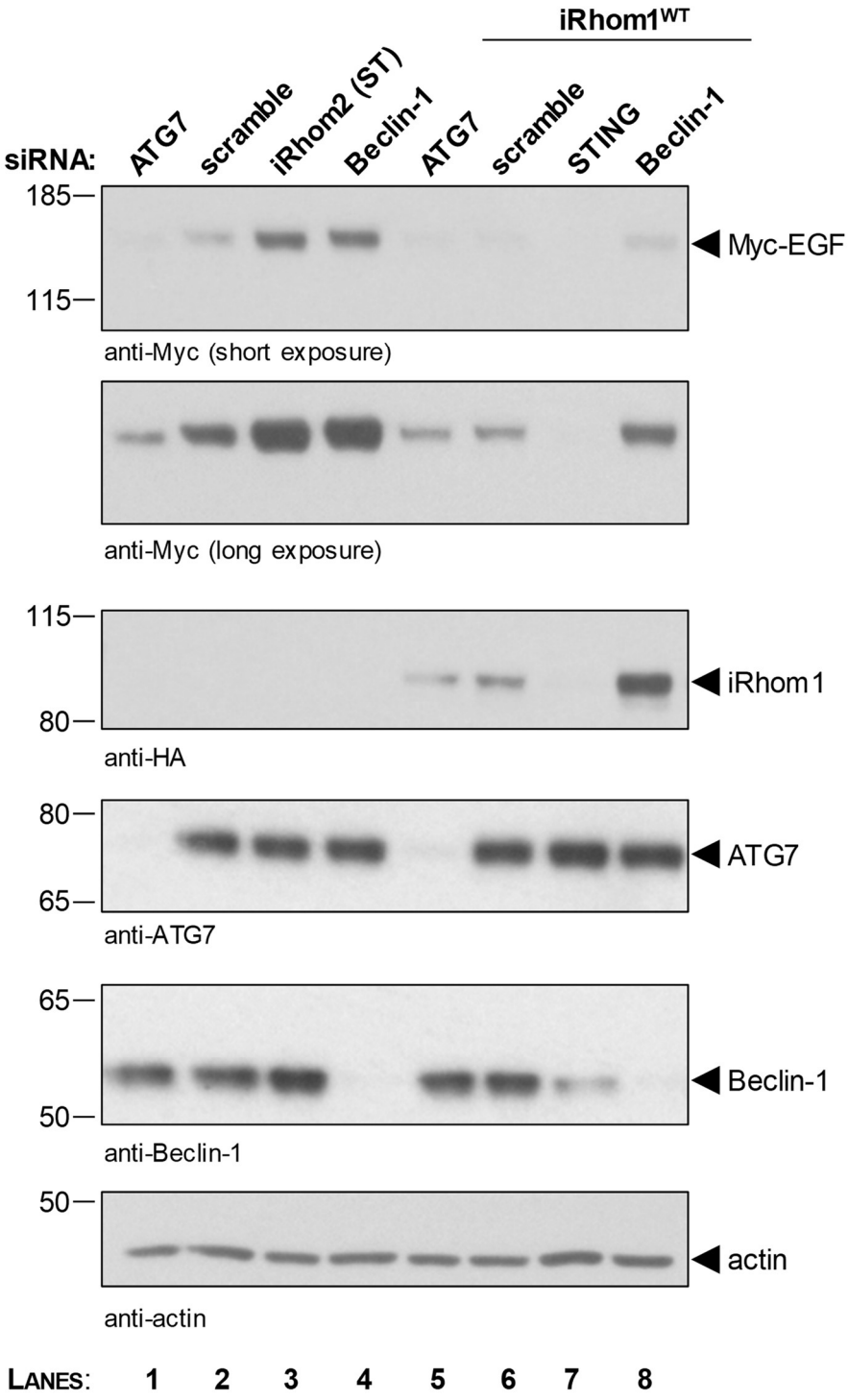


Figure 29: Beclin-1 knockdown increases Myc-EGF stability even in presence of iRhom1^{WT}. Western blot of HEK cell lysates transfected with 250 ng Myc-EGF and 40 ng iRhom1^{WT} where indicated. The cells had been transfected with siRNAs targeting ATG7, iRhom2, Beclin-1, STING, or with non-targeting siRNA (scramble). All used targeting siRNAs are SmartPool siRNAs, except for the STealth siRNA (ST) targeting iRhom2. The membrane was subjected to anti-Myc, anti-HA, anti-ATG7, anti-Beclin-1 anti-actin staining. A long and a short exposure of anti-Myc staining are shown for comparison.

4.2.4. Systems to study the role of endogenous iRhoms in Myc-EGF degradation

To investigate the required components of iRhom-driven lysosomal degradation, I decided to develop two loss-of-function assays. The first was a genetic knock-out (KO) of iRhoms, and the second was a set of depletion experiments using small interfering RNA (siRNA). I first focused on iRhoms as positive controls to determine the extent of Myc-EGF stabilisation in absence of degradation triggered by endogenous iRhoms.

iRhom1/2 DKO HEK cells were designed and validated for absence of iRhom activity in TACE maturation as described in section 0. To assess the role of endogenous iRhoms on Myc-EGF stability, HEK WT and DKO cells were transfected with Myc-EGF. As this experiment was performed before the focus on lysosomal degradation, the proteasomal inhibitor MG132 was used alongside bafilomycin A1. The levels of Myc-EGF were similar in HEK WT and DKO, irrespective of MG132 or bafilomycin A1 treatment (Figure 30). This result was very surprising as it indicated that Myc-EGF is not stabilised is absence of endogenous iRhoms, but that it still undergoes protein degradation. This suggests that HEK cells either present an iRhom-independent degradation mechanism, or that HEK DKO underwent adaptation to compensate for the loss of iRhoms by upregulating compensatory mechanisms (discussed in section 5.2.4) Therefore, I decided to first investigate whether acute loss of iRhom function led to Myc-EGF stabilisation.

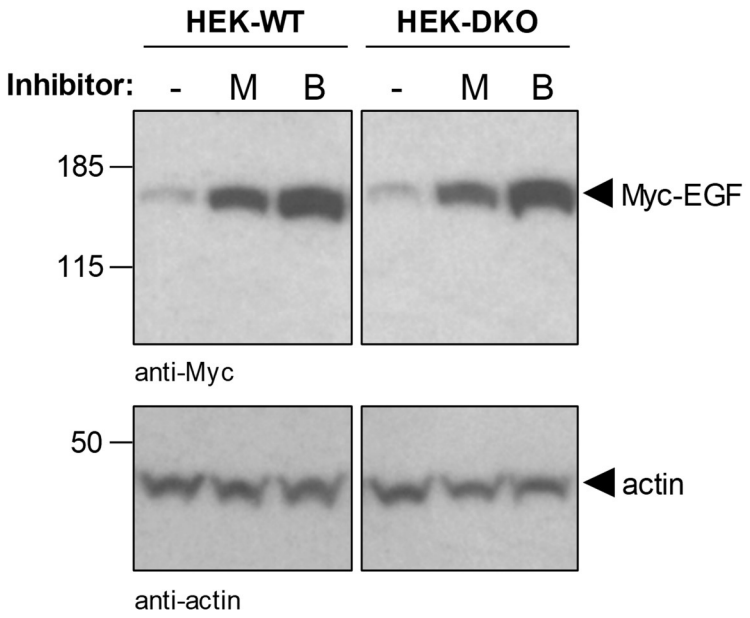


Figure 30: Myc-EGF shows comparable stability in HEK WT and HEK iRhom1/2 DKO cells. Western blot of HEK WT or DKO cell lysates transfected with 250 ng of Myc-EGF treated either with 10 µM of proteasomal inhibitor MG132 (M), or with 100 nM of lysosomal inhibitor bafilomycin A1 (B) for 18 h. The membrane was subjected to anti-Myc and anti-actin staining. One representative western blot out of two independent experiments is shown.

To investigate the effect of iRhom knockdown on Myc-EGF stability, HEK cells were treated with iRhom1 or iRhom2 siRNA twice over the course of 48 hours, before being transfected with Myc-EGF for 24 hours. The cells were then collected, lysed and their protein content was analysed by western blot. Alongside, mRNA was converted by a reverse transcriptase before quantitative PCR (qPCR). The siRNA used were either a SmartPool of three siRNAs (SP) or individual STealth siRNA (ST). Consistent with most previous results, but contradicting the HEK DKO cells described above, I found that siRNAs against iRhom1 or iRhom2 led to a strong increase in Myc-EGF level compared to scrambled siRNA (Figure 31A). As the ST siRNAs provided the strongest Myc-EGF stabilisation, I used ST siRNA in all subsequent experiments. The efficiency of the ST siRNAs was assessed by qPCR,

which showed a decrease of less than 30% of iRhom1 mRNA for iRhom1 siRNA, whereas iRhom2 siRNA led to a strong decrease in iRhom2 mRNA (Figure 31B). Although the mild decrease of iRhom1 mRNA was sufficient to stabilise Myc-EGF protein, I decided to focus on iRhom2 ST siRNA as it provided the most efficient depletion according to mRNA levels. As a control for a general effect of the depletion of transmembrane ER proteins, I assayed whether knockdown of the ER protein CCPG1 affected the Myc-EGF level. Depletion of CCPG1 did not affect the level of Myc-EGF (Figure 28). As a conclusion, in contrast to what happens in iRhom1/2 DKO cells, knockdown of either iRhom1 or iRhom2 results in a strong increase of Myc-EGF, which supports the hypothesis that endogenous iRhoms participate in Myc-EGF degradation.

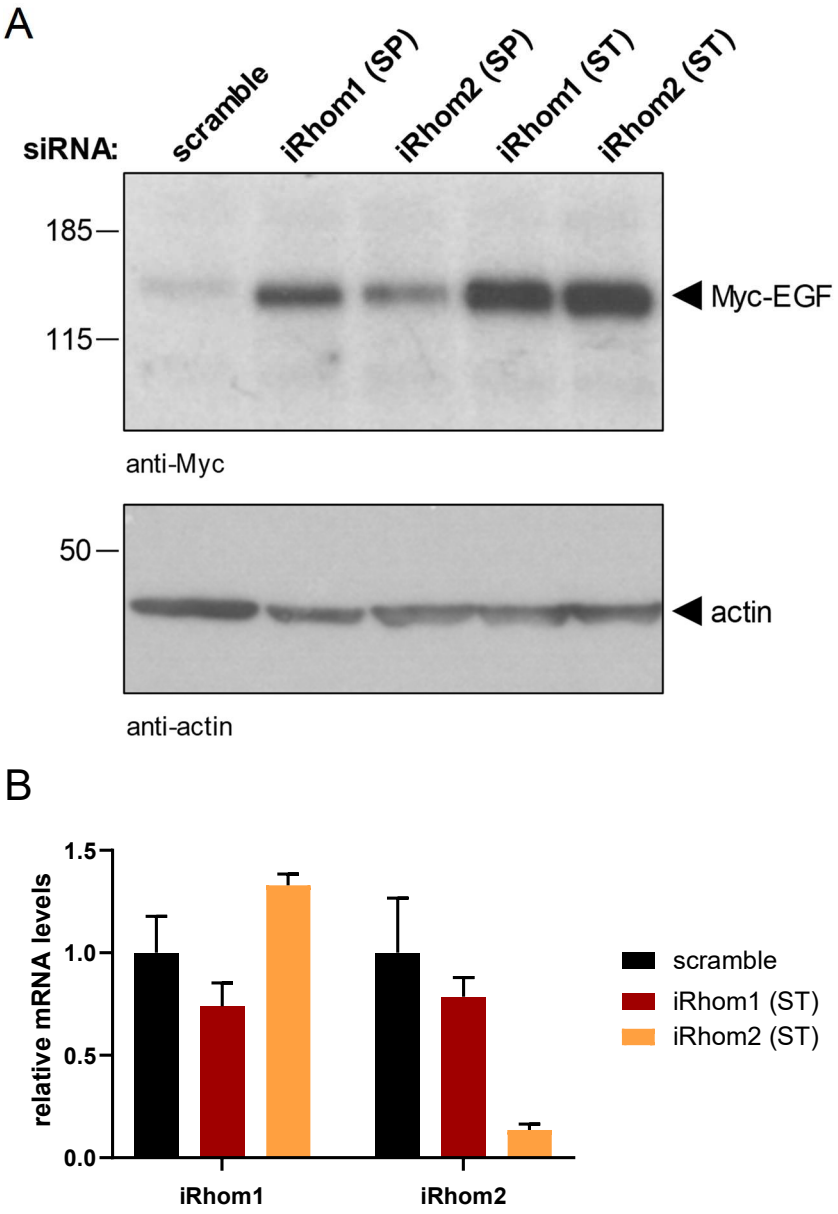


Figure 31: iRhom siRNA increases Myc-EGF level. A) Western blot of HEK cell lysates transfected Myc-EGF, and with non-targeting siRNA (scramble), SmartPool siRNA (SP) or individual STealth siRNA (ST) targeting iRhom1 or iRhom2. Before SDS-PAGE separation, the protein concentration was assessed by BCA assay and 15µg of protein was loaded per condition. The membrane was subjected to anti-Myc and anti-actin staining. **B)** mRNA levels of iRhom1 and iRhom2 relative to GAPDH levels were determined by quantitative PCR.

To investigate more rigorously the role of endogenous iRhoms, I first assessed whether iRhom siRNA increases Myc-EGF at the protein level, as expected if iRhom affects Myc-EGF protein stability as opposed to gene expression. To do so, I performed a cycloheximide (CHX) chase to determine the stability of Myc-EGF. iRhom2 siRNA was performed as described before, and its efficiency at mRNA level was confirmed by qPCR (Figure 32B). Before cell collection, protein translation was abrogated by treatment by CHX for up to five hours. By blocking protein synthesis, the stability of the existing Myc-EGF protein can be unambiguously measured. Surprisingly, although iRhom2 siRNA led to an increase in Myc-EGF level at the beginning of the CHX chase, this protein pool exhibited rapid turnover (Figure 32A). From a comparison of Myc-EGF stability under scrambled siRNA (Figure 32A, long exposure of anti-Myc staining) or under iRhom2 siRNA treatment (Figure 32A, short exposure of anti-Myc staining), it was apparent that Myc-EGF decreases at a similar rate in both conditions. As a result, the increased level under iRhom2 knockdown is not due to a defect in protein degradation. Moreover, the increased level of Myc-EGF appeared to be due to an increase in the expression of the protein. This result was very surprising as it suggested that iRhom2 siRNA has an effect prior to regulation of protein stability.

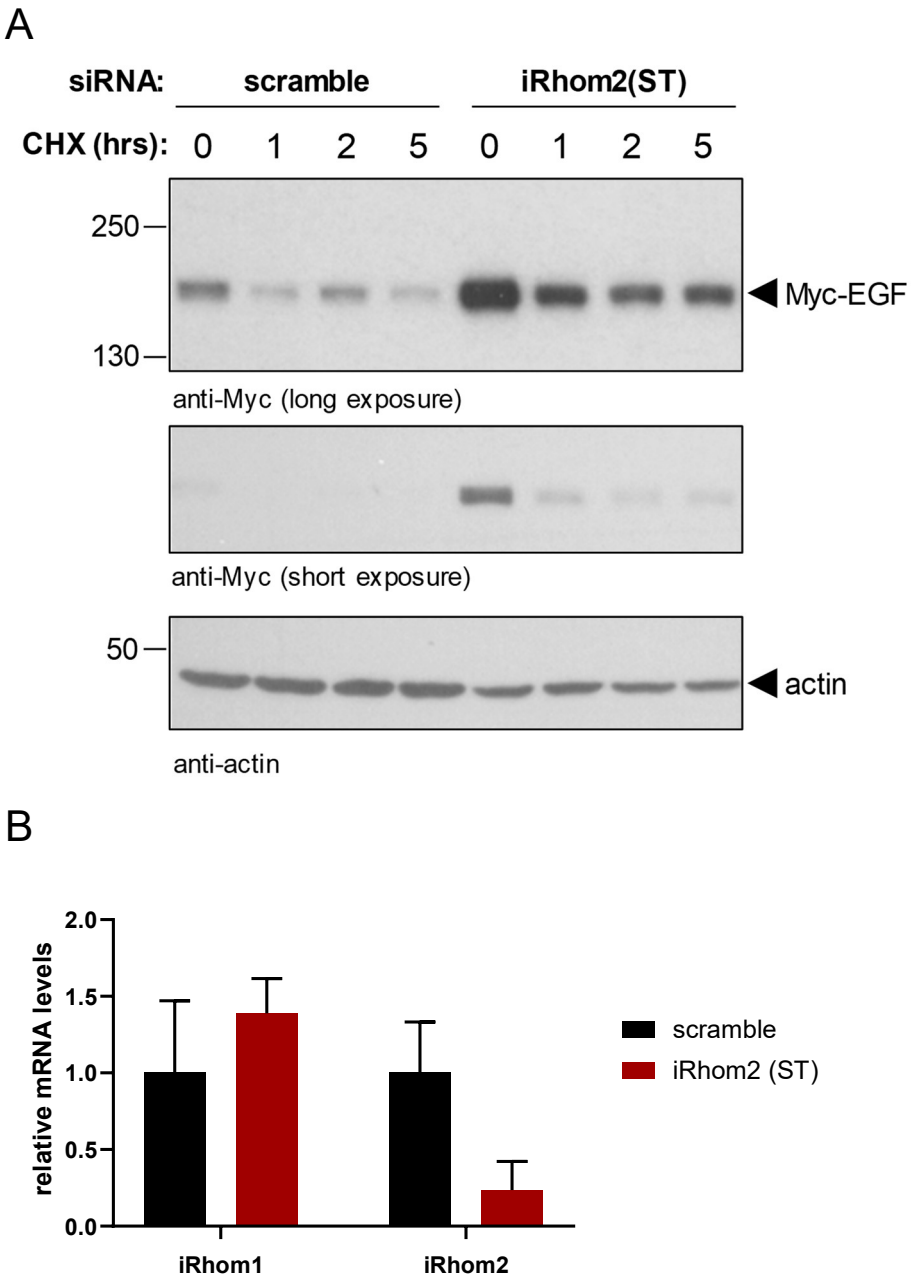


Figure 32: iRhom2 siRNA increases Myc-EGF protein level, but not its protein stability. **A)** HEK were transfected with individual STealth siRNA (ST) targeting iRhom2 or non-targeting siRNA (scramble). 48 h after the first siRNA transfection the cells were transfected with Myc-EGF for 24 h, and then treated with 50 µg/ml cycloheximide (CHX) for up to 5 h. The membrane was subjected to anti-Myc and anti-actin staining. Two exposures of anti-Myc staining are shown for comparison of the protein stability. **B)** mRNA levels of iRhom1 and iRhom2 relative to GAPDH levels were determined by quantitative PCR. One representative western blot and qPCR out of two independent experiments is shown

Zettl et al. have demonstrated that the decrease of Myc-EGF level upon iRhom1^{WT} expression is not due to an effect at the mRNA or cDNA level (Zettl et al., 2011). To determine if iRhom2 siRNA affected Myc-EGF at the mRNA or DNA level, I performed iRhom2 knockdown followed by Myc-EGF transfection, as previously described. TMEM115 siRNA was used to control if Myc-EGF is affected by the knockdown of another inactive member of the rhomboid-like superfamily. Myc-EGF protein level was strongly increased by iRhom2 siRNA, but not by TMEM115 siRNA (Figure 33A). The efficiency of both siRNAs was confirmed by qPCR (Figure 33B, left panels). To assess the effect of iRhom2 siRNA on Myc-EGF mRNA or cDNA level, qPCR using a mouse EGF probe was performed (Figure 33C). As this probe is specific to the mouse sequence, it does not recognise endogenous human EGF of HEK cells, but it binds to transfected Myc-tagged mouse EGF. However, as the cDNA sequence of mouse EGF was transfected, the mouse EGF probe recognises both the mRNA and the transfected plasmid. As a result, the qPCR signal represents the combined abundance of the mRNA and cDNA of transfected Myc-EGF.

To assess the extent of transfected Myc-EGF, the reference sample was attributed to the untransfected cells (Figure 33C). Upon Myc-EGF transfection, the signal increases by more than 5000 folds (Figure 33C). This result represents the transfected signal in absence of specific knockdown. TMEM115 siRNA shows a modest increase compared to scramble siRNA (Figure 33C). Surprisingly, iRhom2 siRNA dramatically increased the mouse EGF signal (Figure 33C). This result could be due to an increase in mRNA level, in cDNA level, or in both.

To determine the contribution of transfected Myc-EGF cDNA to the qPCR signal, a deoxyribonuclease (DNase) treatment prior to reverse transcription was

performed. For each siRNA condition, the qPCR signal was reduced between five and ten folds by the DNase (Figure 33C). Therefore, Myc-EGF cDNA contributed most of the qPCR signal. To control the effect of DNase treatment on mRNA, DNase treatment was also performed prior to the qPCR of endogenous iRhom2 and TMEM115. The DNase treatment does not affect the mRNA measurement, as the level of iRhom2 and TMEM115 with or without DNase are similar (Figure 33B). The relative contribution of Myc-EGF cDNA to the qPCR signal can be inferred from the difference between untreated and DNase-treated conditions. This DNase-sensitive signal is strongly increased by iRhom2 siRNA compared to scramble and TMEM115 siRNAs (Figure 33C). As a result, there is a massive increase of transfected cDNA in iRhom2 knockdown cells. Although it could be suggested that iRhom2 affects the transfection efficiency, it appears more likely that the increased Myc-EGF transfection is due to an effect of iRhom2 siRNA independent from its role on endogenous iRhom2, which could be further investigated (see below for the discussion). As a conclusion neither HEK DKO cells, nor siRNA can be used as a loss-of-function system to investigate iRhom-driven degradation protein.

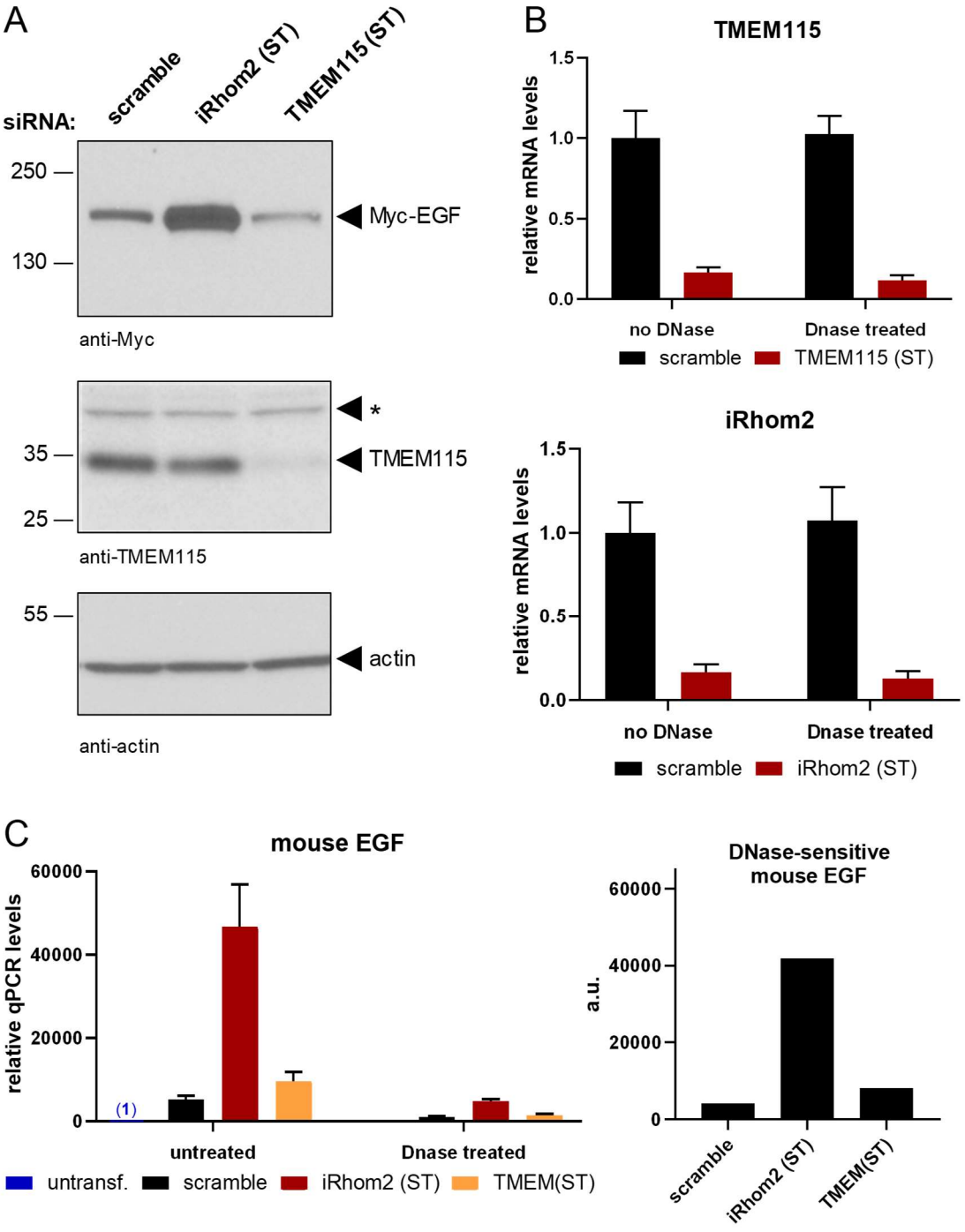

A
siRNA:
scramble
iRhom2 (ST)
TMEM115 (ST)
250
130
Myc-EGF
anti-Myc
35
25
*
TMEM115
anti-TMEM115
55
actin
anti-actin
B
TMEM115
relative mRNA levels
1.5
1.0
0.5
0.0
no DNase
Dnase treated
scramble
TMEM115 (ST)
iRhom2
relative mRNA levels
1.5
1.0
0.5
0.0
no DNase
Dnase treated
scramble
iRhom2 (ST)
C
mouse EGF
relative qPCR levels
60000
40000
20000
0
(1)
untreated
Dnase treated
untransf.
scramble
iRhom2 (ST)
TMEM(ST)
DNase-sensitive mouse EGF
a.u.
60000
40000
20000
0
scramble
iRhom2 (ST)
TMEM(ST)

Figure 33: iRhom2 siRNA increases Myc-EGF cDNA. A) HEK cells were transfected with individual STealth siRNA (ST) targeting iRhom2 or TMEM115 or non-targeting siRNA (control). 48 h after the first siRNA transfection the cells were transfected with Myc-EGF for 24 h. The membrane was subjected to anti-Myc, anti-TMEM115 and anti-actin staining. An asterisk (*) indicates the non-specific band detected by anti-TMEM115 antibody. **B)** mRNA levels of iRhom2 and TMEM115 relative to GAPDH levels were determined by quantitative PCR. On-column DNase treatment was performed prior to reverse transcription. **C)** qPCR levels using a TaqMan probe targeting the cDNA and mRNA level of transfected Myc-EGF. The qPCR levels were normalised to GAPDH levels. DNase treatment was performed as described above. The DNase-sensitive qPCR signal (untreated qPCR level - DNase-treated qPCR level) is shown in the right graph. One representative western blot and qPCR graph out of two independent experiments are shown.

4.3. Discussion

To sum up my findings on iRhom-driven degradation of Myc-EGF, experiments with overexpressed iRhoms show that Myc-EGF undergoes dose-dependent degradation. This process involves both degradation machineries, as proteasomal and lysosomal inhibitors partially rescued Myc-EGF in presence of iRhom1^{WT}. Focusing on the lysosomal degradation allowed me to determine that the degradation stems from the ER, according to two complementary results. First, bafilomycin-rescued Myc-EGF presents a glycosylation signature of an ER-resident protein. Second, iRhom1^{WT} drives lysosomal degradation of ER-resident Myc-EGF. As a conclusion, experiments with iRhom1^{WT} indicate the potential relevance of the lysosome for Myc-EGF degradation via an autophagy-like process. It would be interesting to investigate whether this mechanism also concerns endogenous substrates, such as EGFR ligands.

To assess whether Myc-EGF undergoes an ER-phagy process driven by iRhoms I have focused on Beclin-1, which is an autophagy core component. Knockdown of Beclin-1 increases Myc-EGF level, even in presence of iRhom1^{WT}. Although the technical problem encountered with iRhom2 siRNA highlights the importance of validating the increased Myc-EGF stability in Beclin1 KO cell line, this result suggests that Beclin-1 is part of the molecular machinery triggered by iRhoms for Myc-EGF degradation. If this hypothesis was validated, the question about whether Beclin-1 is required as part of an autophagy route would remain (addressed in section for 5.2). Upon characterisation of this lysosomal degradation route, it would be interesting to determine its relationship with proteasomal degradation, as it has been done for other proteins undergoing dual degradation (see section 5.2.2)

Given these findings, the natural follow-up was to investigate other required components of iRhom-driven degradation. For this to work, removal of iRhoms is the most important control, as it indicates the screening window for degradation. Unfortunately, Myc-EGF is not stabilised in iRhom1/2 DKO HEK. In addition, whereas iRhom2 siRNA increases Myc-EGF level, qPCR shows that there is already an increase in Myc-EGF cDNA. Of note, the effect of iRhom2 siRNA on cDNA seems distinct from the ability of transfected iRhom1^{WT} to reduce Myc-EGF level, as the expression of iRhom1^{WT} has been shown not to influence Myc-EGF at the cDNA or mRNA level (Zettl et al., 2011). Overall, neither the HEK DKO cells, nor the knockdown assay can be used to validate the involvement of endogenous iRhoms in Myc-EGF degradation.

It could be suggested that investigating the results in DKO or knockdown cells would be an interesting follow up for the project. Indeed, it is possible that there is a compensatory mechanism in HEK DKO that counters Myc-EGF stabilisation (discussed in section 5.2). Concerning iRhom2 siRNA, investigating whether the increase of Myc-EGF levels are caused by unspecific effects of iRhom2 siRNA would drive the project outside the focus on protein degradation. I have therefore decided not to continue this project further, but to focus instead on the project about TACE regulation (section 3) as it was producing promising and exciting results. Of note, a positive outcome of studying iRhom-driven degradation has been the production of HEK DKO which allowed me to contribute to a publication in the lab (Künzel et al., 2018).

CHAPTER 5

Discussion

5. Discussion

5.1. Regulation of TACE activity

TACE is the central regulator of numerous signalling pathways including EGFR signalling. Our lab and Colin Adrain's lab have recently discovered that the phosphorylation of iRhom2 is required for stimulated activity of TACE at the plasma membrane (Cavadas et al., 2017; Grieve et al., 2017). In this project I have uncovered the role of iRhom1 in the activation of TACE. Reconstitution of iRhom1/2 double KO (DKO) cells with iRhom1^{WT} rescues TACE-dependent shedding stimulated by PMA. This result demonstrates that iRhom1 is sufficient to support TACE activation. To investigate the molecular mechanism, I have focused the phosphorylation of the N-terminus of iRhom1. Mutation of the putative phosphorylation sites in iRhom1 abolished PMA-induced shedding by TACE. This result demonstrates the requirement of the phosphorylation sites of iRhom1 for TACE activation. Overall, the results support a model that TACE activation by pharmacological stimuli requires phosphorylation of iRhom1. As this model is similar to the role of iRhom2 in TACE activation (Cavadas et al., 2017; Grieve et al., 2017), my results support the presence of a conserved mechanism between iRhom1 and iRhom2 for the activation of TACE upon pharmacological stimulation. This conclusion emanates from experiments using only pharmacological stimulation of TACE. As presented in the next section, it is clear that iRhom1 and iRhom2 are not strictly redundant for KRas-induced activation of TACE.

5.1.1. KRas-induced activation of TACE by phosphorylation of iRhom2 N-terminus

To study the role of iRhom phosphorylation in a pathological context, I focused on Ras proteins, which are one of the best characterised proto-oncogenes. I have demonstrated that Ras activity depends on iRhom2 to induce TACE-dependent shedding. As TACE is activated by both KRas or HRas, it argues that the function is conserved between Ras proteins. My results constitute further evidence that certain oncogenes induce TACE-dependent shedding of EGFR ligands. On a molecular level, I have shown that KRas-induced shedding requires identified phosphorylation sites in iRhom2 for TACE activation. Overall, my results demonstrate the requirement of iRhom2 phosphorylation for oncogene-induced shedding of EGFR ligands by TACE.

Interestingly, Ras-induced shedding of TACE ligands exhibits specificity towards iRhom2. Oncogenic KRas induces TACE shedding in DKO cells reconstituted with iRhom2, but not with iRhom1. As a result, iRhom1 is not sufficient to support KRas-induced activation of TACE. This result was unexpected, especially considering my data demonstrating that iRhom1 is sufficient for PMA-induced shedding by TACE. To understand this difference, it is interesting to focus on the phosphorylation sites in the N-terminus of iRhoms. Figure 34 presents the phosphorylation residues in mouse iRhom2, and it highlights the three sites that contribute the most to PMA-induced shedding (see Figure 7 for alignment) (Grieve et al., 2017). Comparison of mouse iRhom2 with human iRhoms shows that the residues in mouse iRhom2 are totally conserved in human iRhom2, whereas only a few are totally conserved in human iRhom1 (Figure 34). These differences between iRhom1 and iRhom2 might explain the discrepancy between KRas-induced activation in presence of either

iRhoms. By focusing on some of the non-conserved residues between iRhom1 and iRhom2, it might be possible to identify the ones that contribute the most to KRas-induced shedding. To do so, it would be interesting to mutate some of these sites in iRhom2 to investigate their respective participation. Finally, it is possible that the difference in these residues in iRhom1 and iRhom2 alters phosphorylation by the Raf/MEK/ERK cascade, one of the best characterised effector pathways of KRas. To assess its importance in KRas-induced shedding, it would be interesting to inhibit some of the components of the cascade, such as MEK1/2.

	site 1	site 2										site 3			
miR2	S60	S83	S85	S87	S99	S147	Y199	T258	S293	S295	S298	S357	S359	S360	T361
hiR2	S90	S113	S115	S117	S129	S177	Y229	T288	S323	S325	S328	S385	S387	S388	T389
hiR1	S51	S76	T78	T80	S92	T139	X	X	X	S309	X	X	X	S 390	X

Figure 34: Comparison of the phosphorylation residues of iRhoms. The conservation of putative phosphorylation sites in mouse iRhom2 (miR2) with the ones in human iRhom2 (hiR2) and human iRhom1 (hiR1) is presented according to the alignment showed in Figure 7. The fully conserved residues are shown in green, whereas the partially conserved ones are in yellow, and an 'X' in a red case denotes the absence of conservation.

As a conclusion, the observed difference in activation of TACE by KRas/iRhoms might be used to further our understanding of the precise function of iRhoms in TACE activation. Focusing on the differences in the sequences of N-termini of iRhom1 and iRhom2 might lead to the identification of binding factors that specifically target either of the iRhoms. Since the recruitment of 14-3-3 to the N-terminus of iRhom1 is not characterised, I am currently focusing on this interaction and its regulation by oncogenic KRas and PMA. However, if 14-3-3 were to show a similar recruitment to iRhom1 and iRhom2 upon KRas stimulation, this would raise the opportunity to perform a differential characterisation of iRhom interactomes upon KRas activation. Finally, the specificity of KRas activation towards iRhom2 represents a potentially fundamental opportunity. A standard method to investigate

KRas tumourigenesis is to use a mouse model with conditional expression of oncogenic KRas-G12D (see section 1.5.3). Since iRhom1/2 DKO mice are not viable, they cannot be crossed with KRas-G12D mice. However, as iRhom2 KO mice are viable, they represent a unique chance to investigate the requirement of iRhom2 for KRas-induced tumourigenesis.

5.1.2. TACE activity in KRas tumourigenesis in the lung

Given its central role in EGFR signalling, TACE is crucial for the development of several types of cancer, including KRas tumourigenesis. During the course of my project a study demonstrating the requirement of TACE for lung cancer driven by oncogenic KRas was published (Saad et al., 2019). The KRas-G12D mouse model is used to study lung adenocarcinoma (LAC). To investigate the role of TACE in tumourigenesis, TACE KO mice cannot be used as they exhibit perinatal lethality. (Chalaris et al., 2010; Jackson et al., 2003; Peschon et al., 1998). To study the *in vivo* requirement of TACE, the hypomorphic TACE mice ($TACE^{ex/ex}$) was created (Chalaris et al., 2010). KRas-G12D mice were crossed with $TACE^{ex/ex}$ to determine the importance of TACE in KRas tumourigenesis in the lung. Decreased TACE expression in KRas-G12D mice strongly reduced LAC and cell proliferation. In addition, depletion of TACE in the non-small-cell lung cancer (NSCLC) cell line A549 (expressing KRas-G12S) abolishes xenograft growth (Saad et al., 2019). Overall, these results demonstrate the requirement of TACE for KRas tumourigenesis.

To understand the participation of TACE in tumorigenesis, the effect of oncogenic KRas on TACE activity was investigated. KRas-G12D mice show higher TACE-dependent shedding of IL6R (but not of TNFα) compared to wild-type mice. In addition, the KRas mutant cell lines A549 and NCI-H23 (expressing KRas-G12C)

show higher IL6R shedding by TACE than the KRas-WT cells NIH-H2228 (Saad et al., 2019). To assess the importance of TACE activity in KRas tumorigenesis, the sheddase was inhibited in KRas-G12D mice and in A549 cells. To do so, the authors used TACE pro-domain (TPD), which can be expressed as a recombinant protein to specifically inhibit TACE activity (Wong et al., 2016). Treatment with TPD reduces LAC formation in KRas-G12D mice, and it decreases anchorage-independent growth of A549 cells (Saad et al., 2019). Overall, these results demonstrate that the activity of TACE, enhanced by oncogenic KRas, participates in tumourigenesis.

The investigation of the effects of oncogenic KRas on TACE found an increased phosphorylation of p38 and TACE in KRas-G12D mice tissues and in KRas-mutant NSCLC cell lines A549 and NCI-H23. Interestingly, the phosphorylation of TACE (at threonine 735) is dependent on p38 in these systems (Saad et al., 2019). In addition to the increase of TACE phosphorylation, these results demonstrate that a factor acting upstream of TACE, such a p38, is activated in presence of oncogenic KRas. Given the participation of p38 in LPS-induced phosphorylation of iRhom2 (Cavadas et al., 2017), it would be interesting to investigate whether p38 directly or indirectly participates in the increased activity of TACE by oncogenic KRas. Finally, the role of ERK, another kinase upstream of TACE, was investigated. Although the phosphorylation of ERK does not increase in KRas-G12D, A549 and NCI-H23 present higher level of phospho-ERK than KRas-WT NIH-H2228 (Saad et al., 2019). As a result, the precise role of oncogenic KRas on ERK phosphorylation in these contexts remains to be understood.

To conclude, Saad et al. have demonstrated the requirement of TACE for KRas tumourigenesis in lung cells and tissues. Oncogenic KRas increases TACE activity, as well as the phosphorylation of threonine 735 in TACE in a p38-dependent manner (Saad et al., 2019). However, how this phosphorylation relates to TACE activity remains to be understood ((Zunke and Rose-John, 2017), also see section 1.2.3). Molecular insights into the mechanism of TACE activation by oncogenic KRas can be informed by my results. The increase in TACE activity by oncogenic KRas is dependent on the phosphorylation of iRhom2, and oncogenic KRas induces 14-3-3 recruitment to iRhom2. As a result, it would be interesting to investigate the requirement of iRhom2 phosphorylation in KRas tumorigenesis in the lung. To do so, I am performing a xenograft with WT and iRhom1/2 DKO A549 cells. By reconstituting the latter with different iRhom2 variants, I will then be able to assess the importance of the phosphorylation of iRhom2 for KRas tumourigenesis in vivo.

5.1.3. EGFR dependence of KRas-induced tumourigenesis

Several works, including the study by Saad et al. and my results raise the question of the role of TACE-dependent signalling during KRas tumourigensis. By releasing EGFR ligands, TACE is a central regulator of EGFR signalling, which relies on four receptors: ERBB1/EGFR, ERBB2, ERBB3 and ERBB4 (Singh and Coffey, 2014). Given the importance of EGFR signalling in cancer (Sigismund et al., 2018), I will discuss in this section the role of EGFR signalling in KRas tumourigenesis. It first was shown that EGFR and KRas mutations are mutually exclusive for lung tumourigenesis (Cancer Genome Atlas Research Network, 2014). In addition, KRas-driven cancers exhibit resistance towards ERBB1 inhibition (Linardou et al., 2008; Mao et al., 2010). These findings led to the dogma that KRas

mutations are constitutively active, and that they drive tumourigenesis independently of any regulation by upstream pathways, such as EGFR signalling.

The proposed constitutive activity of KRas-G12 mutants has been challenged by the identification of inhibitors specific to KRas mutations. The development of ARS-853 was particularly important, as this inhibitor exclusively binds to the inactive form (GDP-bound) of KRas-G12C preventing further activation of the protein (Ostrem et al., 2013; Patricelli et al., 2016). This inhibitor can therefore be used to assess the proportion of KRas-G12C proteins in the cell that are into an inactive state. It was demonstrated that upon treatment with ARS-853, most of the activity of KRas-G12C in the cell is blocked within two hours (Patricelli et al., 2016). This result illustrates the fact that KRas-G12C is not constitutively active, but that it still cycles between the inactive and the active states (although at a lower rate than wild-type KRas (Hunter et al., 2015)). This means that KRas-G12 mutants cannot be considered as constitutively active, and it opens the possibility that they require upstream activation.

To study the importance of upstream signalling on the activation of KRas-G12C mutants, their dependency on EGFR signalling has been investigated in NSCLC cells. Using ARS-853 it was shown that EGF stimulation induces strong activation of KRas-G12C, whereas inhibition of EGFR signalling abolishes its activation (Lito et al., 2016; Patricelli et al., 2016). The importance of the EGFR pathway was demonstrated in A549 cells (expressing KRas-G12S) by several experiments. First, treatment with a pan-ERBB inhibitor in A549 drastically reduces the activation of KRas. Second, genetic ablation of ERBB1 is also sufficient to reduce KRas activation in A549, although it is eventually compensated at high passages by

upregulation of the other ERBBs (Moll et al., 2018). Third, the activation of KRas effectors, especially ERK, is also decreased by the pan-ERBB inhibitor. (Kruspig et al., 2018; Moll et al., 2018). Overall, these results demonstrate that oncogenic KRas requires EGFR signalling for its activity in NSCLC cells.

Experiments performed *in vivo* allowed investigation of the role of EGFR signalling on KRas-induced tumourigenesis. This has first been done for pancreatic tumourigenesis by inducing the expression of KRas-G12D in the pancreas of the mice. Depletion of either ERBB1 or TACE abolishes the development of pancreatic tumours (Ardito et al., 2012). For lung tumourigenesis, depletion of ERBB1 significantly decreases tumour growth and it increases the mouse survival (Moll et al., 2018). Treatment with a pan-ERBB inhibitor strongly decreases cell proliferation and xenograft growth of NSCLC cells, including A549 (Kruspig et al., 2018; Moll et al., 2018). In addition, ERBB1 KO in A549 also shows defect in xenograft growth (Moll et al., 2018). Overall, these findings demonstrate the requirement of EGFR signalling for KRas tumourigenesis, especially in the lung cells and tissues.

As a conclusion, KRas-G12 mutants cannot be considered as locked into an active conformation, as they still oscillate between the inactive and the active states. The latter can be induced by upstream activation, such as EGFR signalling, which is crucial for tumour growth *in vivo*. Overall, the literature on oncogenic KRas has identified two important facts: 1) TACE is required for KRas tumourigenesis, and 2) KRas activity can be amplified by upstream EGFR signalling. In addition, my results have shown that oncogenic KRas is sufficient to induce the release of EGFR ligands by TACE upon phosphorylation of iRhom2. Taken together, these conclusions highlight the presence of a possible positive feedback loop, where oncogenic KRas

activates iRhom2 to induce TACE activity, which promotes EGFR signalling to maintain KRas in an activated state. To test this hypothesis, my plan is to first assess whether the requirement of the phosphorylation of iRhom2 for TACE activity is conserved in A549. If that were to be true, it would be possible to test whether KRas-dependent phosphorylation of iRhom2 eventually leads to activation of EGFR signalling and of KRas by TACE-dependent shedding.

5.1.4. Downstream effectors of KRas as therapeutic targets

Given the importance of Ras proteins in human cancers, the development of drugs that block Ras-dependent signalling would represent a major therapeutic advance. Most of the attention has been focused on directly inhibiting Ras proteins, but there has been little success with this approach. Although KRas is no longer considered undruggable, the difficulty of developing a KRas inhibitor is exemplified by the inhibitors of the translocation of KRas to the plasma membrane. To be activated, KRas is targeted to the plasma membrane by farnesylation of its C-terminus by the farnesyltransferase (FTase) (Simanshu et al., 2017). The development and subsequent testing of FTase inhibitors (FTIs), however, did not demonstrate a decrease KRas-dependent activation of its effectors, such as ERK (Novotny et al., 2017). An explanation for this negative result is that upon FTI treatment, KRas undergoes another type of lipidation by geranylgeranyl-transferases, which allows its translocation to the plasma membrane (James et al., 1995; Rowell et al., 1997; Whyte et al., 1997). This result illustrates the plasticity of the mechanisms ensuring the activation of KRas.

Fortunately, there have been recent advances in direct KRas inhibition with the development of antibody-based approaches (Shin et al., 2017; Tanaka and

Rabbitts, 2010; Tanaka et al., 2007) and of mutation-specific inhibitors. The latter concerns the KRas-G12C mutation, which are trapped in an inactive state by the inhibitors ARS-853 and ARS-1620 (see section 5.1.3) (Janes et al., 2018; Ostrem et al., 2013; Patricelli et al., 2016). Although these inhibitors are still in pre-clinical phase, they might eventually be used in the treatment of KRas-G12C expressing cancers, which represent 11% of all KRas-mutant cancers (Cosmic database, (Forbes et al., 2017)).

To target the other KRas mutations and to develop complementary treatments, an option consists in focusing on the upstream pathways, such as EGFR, which ensures constitutive activation of oncogenic KRas variants (section 5.1.3). However, to specifically target the pathways that contribute to KRas tumourigenesis, focusing on the factors downstream of KRas would be more advantageous. It would allow for the specific targeting of the cellular pathways that contribute to tumourigenesis, while leaving intact the other functions of KRas. One of the best characterised effector pathways for KRas tumourigenesis is the Raf/MEK/ERK cascade. Unfortunately, inhibition of Raf or MEK showed high toxicity, and it also leads to paradoxical activation of the cascade due to the presence of negative feedback loops (Holderfield et al., 2014; Karoulia et al., 2017; Kohler et al., 2018). Although therapies with multiple inhibitors are in development, the complex regulations within the Raf/MEK/ERK cascade make this complicated.

Given the importance of TACE in cancer development, several inhibitors have been developed to prevent the activity of the sheddase enzyme. However, due to the structural conservation between the active site of TACE and ADAM10 (Moss et al., 2008), most of these inhibitors target both shedding enzymes. This lack of

specificity has resulted in off-target effects. For example, the small molecule inhibitors INCB3619 and INCB7839 were promising as they decreased cell proliferation and xenograft growth of breast cancer cells and NSCLC cells (Giricz et al., 2013; Witters et al., 2008; Zhou et al., 2006). However, these inhibitors are not considered fit for clinical use due to their toxic effect upon injection (Infante et al., 2007). Fortunately, this lack of specificity has been overcome by the development of the recombinant TACE pro-domain (TPD), which targets TACE but not ADAM10 (Wong et al., 2016). Although the TPD is still at the preclinical stage, it opens the possibility for the specific inhibition of TACE to block tumourigenesis.

Even with the ongoing development of TACE specific inhibitors, the question of their potential toxicity in heathy tissues remains, as TACE activity is critical during development (Zunke and Rose-John, 2017). The development of a TACE drug that does not cause non-selective damage therefore appears very challenging. My results have demonstrated that Ras-induced shedding by TACE specifically requires the phosphorylation of the N-terminus of iRhom2, but not of iRhom1. As a result, the development of a drug targeting iRhom2 might bypass the problems that current TACE drugs are facing. To target iRhom2, it could be suggested that its interface with TACE represents an interesting target. However, as this interface is considered to mostly involve the first transmembrane domain (TMD1) of iRhom2, this strategy poses two problems: i) the technical difficulty of preventing an interaction in a lipidic environment; and ii) the specific targeting of the TMD1 of iRhom2, which shares high sequence similarity with TMD1 of iRhom1 (Düsterhöft et al., 2019). Focusing on the phosphorylation sites in the cytoplasmic N-terminus of iRhom2 would solve these problems. As these phosphorylation sites are not well conserved with iRhom1 (Figure 34), this strategy would specifically target the

cytoplasmic sites of iRhom2 to prevent the activation of TACE by oncogenic KRas. In addition, the importance of these phosphorylation sites for inflammation (see section 1.2.3) raises the possibility that the drugs might be used for both cancer and inflammatory therapies. Two main challenges will have to be overcome to target the phosphorylation sites of iRhoms: i) the absence of an active site to target; and ii) the requirement of the drug to access the cytoplasm. Given the ongoing development on intracellular antibodies (intrabodies) for clinical use (Slastnikova et al., 2018), it could be proposed that phosphospecific intrabodies (similar to the recently designed for STAT3 (Koo et al., 2014)) might be used to target the phosphorylation sites of iRhom2 N-terminus, and eventually for therapies of KRas-induced cancers.

5.2. iRhom-driven degradation of EGFR ligands

5.2.1. iRhom-driven degradation of Myc-EGF from the endoplasmic reticulum (ER) in a Beclin-1 dependent manner

The roles of iRhoms are superficially confusing, since they are both positive regulators of EGFR signalling as TACE cofactors, and negative regulators of this very pathway by destabilising EGFR ligands (Zettl et al., 2011). In this second project, I focused on the molecular mechanism by which iRhoms induce the degradation of EGFR ligands. To do so, I used Myc-EGF as a reporter of this degradation mechanism. I first demonstrated that expression of iRhom1 or iRhom2 leads to a dose-dependent decrease in Myc-EGF in HEK293T cells. To identify the molecular machinery of this degradation, the contribution of the proteasome and the lysosome was assessed. My results consistently show the contribution of the lysosome and the proteasome for iRhom-driven degradation of Myc-EGF. Of note, the balance between the degradation machineries exhibits cell-specificity, as the proteasomal degradation partially contributes to clearance of Myc-EGF in HEK293T, whereas the proteasome is considered responsible for all of Myc-EGF degradation in COS-7 cells (Zettl et al., 2011).

As the lysosomal degradation of Myc-EGF triggered by iRhoms has not been characterised, I decided to focus on this mechanism. To assess whether Myc-EGF is sent for degradation directly from the ER, or whether it requires to traffic through the secretory pathway before being degraded, two complementary approaches were performed. First, I focused on the pool of Myc-EGF that is rescued from iRhom-driven lysosomal degradation. This pool is sensitive to Endo H treatment, thereby presenting the glycosylation signature characteristic of an ER-resident protein. This result demonstrates that Myc-EGF is sent for lysosomal degradation by iRhoms

directly from the ER. Second, I added an ER-retention signal to EGF to create an ER-retained variant (ER-EGF). As ER-EGF still undergoes lysosomal degradation triggered by iRhoms, this is the second evidence that iRhom-driven lysosomal degradation occurs directly from the ER.

The direct trafficking of Myc-EGF from the ER to the lysosome in presence of iRhoms bears striking similarity with the described routes for the autophagy of the ER (called ER-phagy). It was thus investigated whether iRhom-driven degradation of Myc-EGF requires autophagy core components, such as Beclin-1 (see Figure 5). Knockdown of Beclin-1 leads to the stabilisation of Myc-EGF, even upon expression of iRhom1-WT. Although addressing the stability of Myc-EGF in Beclin-1 KO cells would allow us to definitively conclude on its requirement, my data support the hypothesis that iRhoms promote ER-phagy routes for the degradation of Myc-EGF (see section 5.2.3).

5.2.2. Dual degradation of ER proteins

Since the recent discovery of the role of autophagy for the degradation of ER proteins (ER-phagy), it has become increasingly evident that ERAD and ER-phagy cooperate to maintain the proteostasis of the ER (De Leonibus et al., 2019; Fregno and Molinari, 2019; Sun and Brodsky, 2019). In addition to iRhom-driven degradation of Myc-EGF, several cases illustrate this shared role for the clearance of ER proteins.

One of the examples pointing toward a dual degradation of ER proteins concerns the gonadotropin-releasing hormone receptor (GnRHR). This seven transmembrane protein is a G protein-coupled receptor (GPCR), for which several human disease-causing mutations have been identified, including E90K and S168R

(Conn and Ulloa-Aguirre, 2011). Interestingly, the presence of these mutations is sufficient to induce a change in the required degradation machinery (Houck et al., 2014). GnRHR-WT and GnRHR-S168R are degraded by the proteasome in a VCP/p97 dependent-manner, indicating that they undergo ERAD. Conversely, GnRHR-E90K is predominantly degraded by the lysosome. Multiple lines of evidence suggest that GnRHR-E90K undergoes an ER-phagy pathway. First, degradation of GnRHR-E90K does not require its trafficking through the Golgi. Second, targeting of GnRHR-E90K to the lysosome is abolished upon inhibition of PI3Ks, including the autophagy-core component Vps34. Third, it was shown that GnRHR-E90K is present in Beclin-1 complexes (Houck et al., 2014). Overall, these results demonstrate that different variants of a protein can be processed either by ERAD, or by an ER-phagy-like mechanism.

The concept of dual degradation has recently been characterised in detail for the protein NCP1 (Schultz et al., 2018). NPC1 is a 13 transmembrane protein, which is involved in the intracellular trafficking of cholesterol to allow its esterification (Chang et al., 2006; McKay Bounford and Gissen, 2014). NPC1 derives its name from the neurogenerative disease called Niemann–Pick type C, which is caused by point mutations, such as I1061T (Vanier, 2010). Although NPC1-I1061T retains some activity when it is overexpressed, this mutant is partially misfolded (Gelsthorpe et al., 2008). It has been shown that NPC1-I1061T exhibits an ER localisation and is partially degraded by the proteasome, suggesting that this mutant undergoes an ERAD pathway (Gelsthorpe et al., 2008; Nakasone et al., 2014).

To identify the required components of NPC1-I1061T degradation, Schultz et al. focused on the turnover of the endogenous proteins NPC1-WT and NPC1-I1061T

(Schultz et al., 2018). Surprisingly, both variants are degraded by both the proteasome and the lysosome. In the case of NPC1-I1061T, lysosomal activity accounts for most of its degradation. These results demonstrate that the proteasome and the lysosome cooperate for the clearance of NCP1-WT and NPC1-I1061T. To characterise the molecular mechanism of the proteasomal degradation of NPC1-I1061T, the authors focused on the role of ERAD components. Although the depletion of Hrd1, gp78 or Derlin1 does not affect the stability of NPC1-I1061T, knockdown of the E3 ligase MARCH6 strongly increases it. In addition, the inhibition of VCP/p97 supports its involvement in the degradation of NPC1-I1061T (Schultz et al., 2018). These results therefore demonstrate that the proteasomal degradation of NPC1-I1061T represents a MARCH6-dependent ERAD.

To investigate the role of the lysosome in the degradation of NPC1-I1061T, the glycosylation of the protein was investigated. The pool of protein rescued by lysosomal inhibition displays the characteristic signature of an ER-resident protein (Schultz et al., 2018). This result demonstrates that NPC1-I1061T does not require trafficking through the secretory pathway for lysosomal degradation. Depletion of Beclin1 or FAM134B strongly increases NPC1-I1061T level. In addition, NPC1-I1061T is destabilised by expression of FAM134B-WT, but not by FAM134B-ΔLIR (in which the LC3-interacting motif has been removed). These results demonstrate that endogenous NPC1-I1061T is degraded by ER-phagy.

It has been suggested that protein aggregation is one of the characteristics which direct proteins towards the lysosome, instead of the proteasome (Sun and Brodsky, 2019). Therefore, focusing on proteins that form detergent-insoluble complexes is one way to investigate the importance of aggregation during dual degradation. The

first example is dysferlin, a type II transmembrane protein for which several mutations have been identified, such as L1341P, to cause dystrophy (Jin et al., 2016). Both dysferlin-WT and dysferlin-L1341P form detergent-insoluble aggregates. However, although proteasomal inhibition stabilises the aggregates of both variants, dysferlin-L1341P, but not dysferlin-WT, is also stabilised either by lysosomal inhibition or by Atg5 depletion (Fujita et al., 2007). Another example of dual degradation of an aggregate-forming protein is mutant α1-antitrypsin Z (ATZ), which misfolds and forms aggregates in the lumen of the ER (Teckman and Perlmutter, 2000). As for dysferlin-L1341P, ATZ is independently stabilised by proteasomal and lysosomal inhibition, and by depletion of several autophagy components such as Atg5 and Atg7 (Fregno et al., 2018; Hidvegi et al., 2010; Houck et al., 2014; Kamimoto et al., 2006; Qu et al., 1996). Although the role of aggregation for lysosomal degradation remains to be understood for these proteins, these results demonstrate that the proteasome and the lysosome cooperate for the degradation of proteins that form insoluble aggregates.

The most conclusive example of the importance of aggregation in dual degradation is the proinsulin mutant Akita, as the degradation of the aggregates and the soluble fraction has been separately characterised (Cunningham et al., 2019). Soluble Akita is rescued by the depletion of Beclin-1 and Hrd1, which demonstrates the requirement of ERAD and ER-phagy components for the dual degradation of this fraction(Cunningham et al., 2019; He et al., 2015). However, detergent insoluble Akita is rescued by the depletion of ER-phagy components (including Beclin-1), but not upon knockdown of Hrd1 (Cunningham et al., 2019). These results demonstrate that the aggregation status of Akita is crucial to determine which degradation machinery it will be processed by. To explain that Akita aggregates are degraded

by ER-phagy but not by ERAD, it was suggested that the size of the aggregates preclude their retro-translocation, whereas the trafficking to the lysosome is still possible (Sun and Brodsky, 2019).

As a conclusion, the study by Schultz et al. established the dual degradation of an ER-localised transmembrane protein (Schultz et al., 2018). By characterising the molecular mechanism of both ERAD and ER-phagy of NPC1-I1061T, it illustrates the cooperation of the two mechanisms to maintain the proteostasis in the ER. This bears strong similarities to my work: i) the dual degradation by the lysosome and the proteasome; ii) the Endo H sensitivity of the lysosome-rescued pool; and iii) the Beclin-1 dependency (Schultz et al., 2018). However, crucial differences also exist between the degradation of Myc-EGF and NPC1-I1061T. In the latter case, an endogenous, mutant, polytopic protein is degraded in the absence of the expression of another factor. The expression and the structure of the substrate, as well as the requirement for a stimulation, therefore distinguish iRhom-driven degradation of Myc-EGF from the degradation of NPC1-I1061T. At most, it might therefore be suggested that iRhoms highjack existing pathways for the clearance of transmembrane proteins to ensure the degradation of Myc-EGF. Finally, the mechanisms that determine the dual degradation remain to be understood in most cases, including for the degradation of Myc-EGF and of NPC1-I1061T. Although the aggregation status constitutes an emerging theme for the preferential degradation by the lysosome, this has not been checked in the case of iRhom-driven degradation of EGFR ligands. In addition, it is possible that the balance between the dual forms of degradation is directed by other criteria, such as the thermodynamics of the folding, or the kinetics of the trafficking (Sun and Brodsky, 2019). Due to the early interruption of the project, the contribution of these factors, including the aggregation

status of Myc-EGF, could however not be investigated. In addition, identification of endogenous substrates targeted by iRhom-driven degradation could not be performed either.

5.2.3. ER-phagy

ER-phagy is a mechanism by which a specific receptor in the ER membrane recruits the autophagy machinery to trigger the lysosomal degradation of ER proteins (Figure 5). Two findings of my project support the hypothesis that iRhom-driven lysosomal degradation is an ER-phagy process. The first is that iRhoms trigger the lysosomal degradation of the ER-localised pool of Myc-EGF. This is demonstrated by the glycosylation signature of the targeted pool, and by the degradation of ER-retained Myc-EGF. The second finding of my project is that the autophagy core component Beclin-1 stabilises Myc-EGF, even upon expression of iRhom1. Interestingly, the knockdown of FIP200 or Atg7 does not affect Myc-EGF level. Overall, these results demonstrate that iRhoms target ER-localised Myc-EGF to lysosomal degradation, and they suggest that an autophagy core component participates in this mechanism.

The unchanged Myc-EGF level upon FIP200 or ATG7 siRNA is surprising given the strong increase in Myc-EGF level by Beclin1 siRNA. These results suggest that some autophagy core components, such as Beclin1, are required for Myc-EGF degradation, whereas others, such as FIP200 and ATG7, are not (see Figure 5 for their respective role in ER-phagy). To explain this discrepancy in the requirement of different autophagy components, several explanations can be proposed. The first one is technical as it concerns the minimum protein level required to ensure autophagy. The efficiency of the siRNA was high as evidenced by the strong

decrease in protein level of FIP200 and ATG7 (see section 4.2.3). However, it has been demonstrated that even when the protein level of autophagy components is too low to be detected by western blot, it is still sufficient to support autophagy (Hosokawa et al., 2006). As a result, it is necessary to assess Myc-EGF stability in KO cell lines to definitively conclude on the requirement of FIP200 and Atg7 for iRhom-driven degradation of Myc-EGF.

To solve the discrepancy, it might be suggested that iRhoms trigger non-autophagic degradation of Myc-EGF in a Beclin-1 dependent manner. In addition to its crucial role in autophagy, Beclin-1 has been reported to participate in other cellular processes, such as cytokinesis, apoptosis and phagocytosis (Levine and Kroemer, 2019; Wirawan et al., 2012). As the latter requires other autophagy components, including the Atg8 conjugation system, it has been coined the term LC3-associated phagocytosis (LAP). Although LAP involves degradation of components, including proteins, they are of extracellular origin (Martinez et al., 2011, 2015; Sanjuan et al., 2007). As a result, it is hard to reconcile the role of Beclin-1 in LAP with the clearance of ER-localised Myc-EGF. The most elegant explanation therefore remains that Beclin-1 probably acts as an autophagy component during iRhom-driven degradation of Myc-EGF.

Assuming that the absence of requirement of FIP200 and ATG7 was confirmed, the most likely explanation would be that iRhom-driven degradation of Myc-EGF constitutes a non-canonical autophagy pathway. It has been demonstrated that some autophagy routes bypass the requirement of autophagy core components, such as members of the Atg8 conjugation system (Nishida et al., 2009) or constituents of the ULK1 complex (Figure 5) (Cheong et al., 2011). One of the best

characterised examples of non-canonical ER-phagy is the degradation of the mutant α1-antitrypsin Z (ATZ) triggered by FAM134B. The lysosomal degradation of ATZ requires Vps34, Atg7 and LC3, but not FIP200 or ULK1/2 (Fregno et al., 2018). As a result, only some autophagy components are involved in FAM134B-driven degradation of ATZ. Similar to this case, the degradation of Myc-EGF triggered by iRhoms might require only some of the constituents of the autophagy machinery (such as Beclin-1). If this hypothesis were to be proven, iRhom-driven degradation of Myc-EGF might constitute a new example of non-canonical ER-phagy.

As a conclusion, the most likely explanation for the participation of Beclin-1 is that iRhom-driven lysosomal degradation might represent an ER-phagy route, whether it is canonical or not. In support of this model are two features of iRhoms. The first its long cytoplasmic, unstructured N-terminus, as the presence of such domains in ER-phagy receptors is proposed to be crucial for the recruitment of the autophagy machinery (An et al., 2019). The second characteristic of ER-phagy receptors that is shared with iRhoms is their eventual clearance by the lysosome. The degradation of receptors at the end of ER-phagy has been observed for RTN4 (Grumati et al., 2017), Sec62 (Fumagalli et al., 2016), CCPG1 (Smith et al., 2018) and TEX264 (An et al., 2019; Chino et al., 2019). As a result, the stabilisation of iRhom1 upon lysosomal inhibition or Beclin-1 depletion (see section 4.2.3) suggests that iRhom1 shares this feature with the ER-phagy receptors. Finally, although further experiments are required to definitively conclude whether iRhoms drive an ER-phagy route, the elements presented in this section argue in favour of this hypothesis.

5.2.4. The role of endogenous iRhoms in Myc-EGF degradation

To conclude this discussion about iRhom-driven degradation, this project has brought interesting insights into a potential novel ER-phagy route. However, it is important to note that all experiments were performed using Myc-EGF as a reporter. To place my findings in a physiological context will require the identification of endogenous substrates of this pathway. The second limitation of this project consists in the absence of a reliable method to investigate the requirement of endogenous iRhoms for Myc-EGF degradation. The most surprising finding emanates from the siRNA of iRhoms. Although knockdowns of iRhoms lead to an accumulation of Myc-EGF, this is not due to its role in protein stability. The increase in Myc-EGF signal is already detected by qPCR using a probe that specifically recognises transfected Myc-EGF. As most of the increase due to iRhom2 siRNA is DNase-sensitive, this result demonstrates that the effect concerns the cDNA of Myc-EGF (section 4.2.4). As a conclusion, the apparent increase in Myc-EGF protein level is not due to increased protein stability, but to an effect at the cDNA level.

To explain this puzzling result, it could be suggested that this effect is due to a loss of function of iRhoms on the transfected cDNA (similar to the action of cytoplasmic nucleases (Lechardeur et al., 1999; Rattan et al., 2013)). However, there is no supporting evidence for a role of iRhoms on transfection efficiency or cDNA stability. In addition, it has been demonstrated that the decrease of Myc-EGF level upon expression of iRhoms is due to an effect at the protein level, and not at the cDNA or mRNA level (Zettl et al., 2011). As a result, the effect of iRhom2 siRNA on Myc-EGF cDNA is distinct from the established role of iRhom in protein degradation. As a conclusion, the most likely explanation is that the increased Myc-

EGF cDNA is due to off-target effects of the siRNA itself, rather than the depletion of endogenous iRhom2.

Design of a HEK293T cell line depleted for the expression of iRhom1 and iRhom2 allowed me to abrogate some functions of iRhoms, such as TACE maturation. However, no increased Myc-EGF level is visible in the double KO (DKO) cell line. It could be suggested that the DKO cells underwent adaptation to prevent the accumulation of the substrates of iRhom-driven degradation. Such adaptation has recently been described upon loss of the rhomboid-like protein derlin Dfm1 in *Saccharomyces cerevisiae* (Neal et al., 2018). Dfm1 is a required component for ERAD of Hmg2, a polytopic protein crucial for sterol synthesis (Hampton, 2002). Dfm1 presents the characteristic motifs of the rhomboid-like superfamily, such as GxxxG and WR, which are required for the retrotranslocation of Hmg2 (Neal et al., 2018). Upon loss of Dfm1, the retrotranslocation and degradation of Hmg2 are first abrogated. However, high passage of dfm1Δ cells show restored degradation of Hmg2 due to the duplication of the chromosome expressing Hrd1 (Neal et al., 2018). As a result, the increased expression of the central ERAD E3 ligase in yeast is sufficient to compensate for the loss of Dfm1. It could be suggested that a similar adaptation occurred in HEK293T iRhom1/2 DKO. To test this hypothesis, the expression of the 19 ERAD-related E3 ligases in mammalian cells would have to be assessed (Preston and Brodsky, 2017).

Appendix

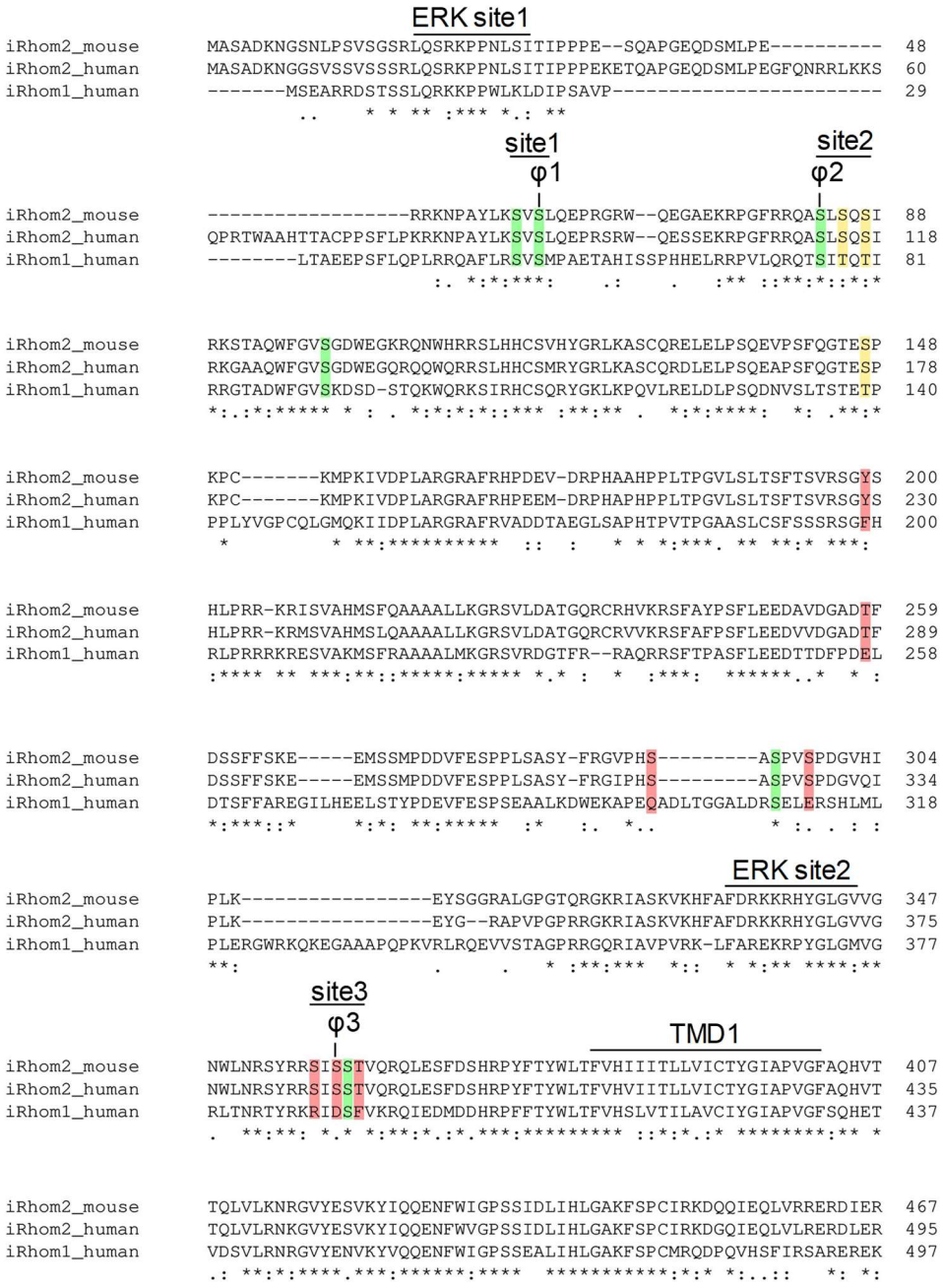
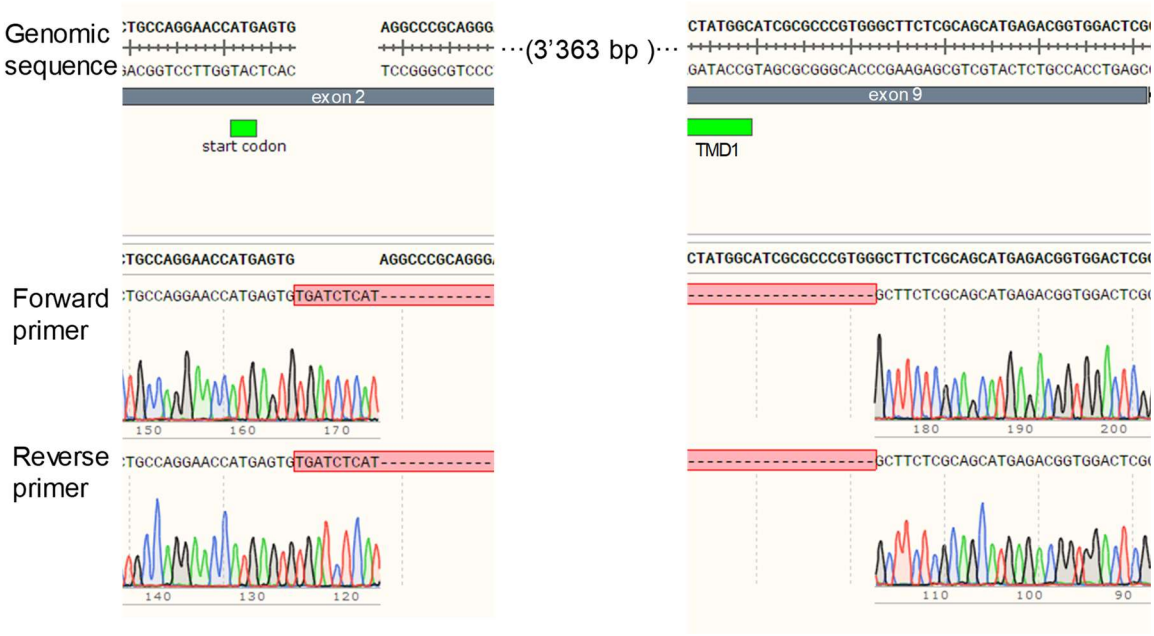




Figure 35: Alignment of full-length mouse iRhom2, human iRhom2 and human iRhom1. Conservation of the phosphorylation residues identified in mouse iRhom2 (Cavadas et al., 2017; Grieve et al., 2017) is indicated as in Figure 7: total conservation (identical amino acid) in green, partial conservation (serine-threonine conversion) in yellow, and absence of conservation in red. The three main phosphorylation sites identified in mouse iRhom2 (Grieve et al., 2017), the first transmembrane domain (TMD1), the predicted ERK docking sites and 14-3-3 binding sites (denoted by φ) (Cavadas et al., 2017) are annotated. The alignment was performed with Clustal Omega using the following notation: an asterisk (*) for fully conserved residue, a colon (:) for residues with similar properties and a period (.) for residues with weakly similar properties.

A) Deletion in RHBDF1



B) Deletion in RHBDF2



Figure 36: Genomic deletion of RHBDF1 and RHBDF2 in HEK293T DKO cell line. A) Alignment of the genomic sequence of human RHBDF1 based on the Ensembl browser (Yates et al., 2016) with the sequence reads from the PCR using forward and reverse primers to amplify the targeted region in the DNA extract. Due to the size of the deletion (3'395 bp), only the boundaries are shown. **B)** Sequence of the mutation in RHBDF2 cDNA sequence based on the sequence reads from the PCR using forward and reverse primers to amplify the targeted region in the DNA extract. The early stop codon after iRhom2 TMD1 is shown below the cDNA sequence. Alignments and visualisations in this figure were performed using SnapGene 3.2.

References

Adrain, C., and Freeman, M. (2012). New lives for old: evolution of pseudoenzyme function illustrated by iRhoms. Nat. Rev. Mol. Cell Biol. *13*, 489–498.

Adrain, C., and Freeman, M. (2014). Regulation of receptor tyrosine kinase ligand processing. Cold Spring Harb. Perspect. Biol. *6*.

Adrain, C., Strisovsky, K., Zettl, M., Hu, L., Lemberg, M.K., and Freeman, M. (2011). Mammalian EGF receptor activation by the rhomboid protease RHBDL2. EMBO Rep. *12*, 421–427.

Adrain, C., Zettl, M., Christova, Y., Taylor, N., and Freeman, M. (2012). Tumor necrosis factor signaling requires iRhom2 to promote trafficking and activation of TACE. Science *335*, 225–228.

An, H., Ordureau, A., Paulo, J.A., Shoemaker, C.J., Denic, V., and Harper, J.W. (2019). TEX264 Is an Endoplasmic Reticulum-Resident ATG8-Interacting Protein Critical for ER Remodeling during Nutrient Stress. Mol. Cell *74*, 891-908.e10.

Ardito, C.M., Grüner, B.M., Takeuchi, K.K., Lubeseder-Martellato, C., Teichmann, N., Mazur, P.K., DelGiorno, K.E., Carpenter, E.S., Halbrook, C.J., Hall, J.C., et al. (2012). EGF Receptor Is Required for KRAS-Induced Pancreatic Tumorigenesis. Cancer Cell *22*, 304–317.

Bai, J., Chiu, W., Wang, J., Tzeng, T., Perrimon, N., and Hsu, J. (2001). The cell adhesion molecule Echinoid defines a new pathway that antagonizes the Drosophila EGF receptor signaling pathway. Dev. Camb. Engl. *128*, 591–601.

Baumgart, A., Seidl, S., Vlachou, P., Michel, L., Mitova, N., Schatz, N., Specht, K., Koch, I., Schuster, T., Grundler, R., et al. (2010). ADAM17 regulates epidermal growth factor receptor expression through the activation of Notch1 in non-small cell lung cancer. Cancer Res. *70*, 5368–5378.

Ben-Shem, A., Fass, D., and Bibi, E. (2007). Structural basis for intramembrane proteolysis by rhomboid serine proteases. Proc. Natl. Acad. Sci. U. S. A. *104*, 462–466.

Black, R.A., Rauch, C.T., Kozlosky, C.J., Peschon, J.J., Slack, J.L., Wolfson, M.F., Castner, B.J., Stocking, K.L., Reddy, P., Srinivasan, S., et al. (1997). A metalloproteinase disintegrin that releases tumour-necrosis factor-α from cells. Nature *385*, 729–733.

Blaydon, D.C., Etheridge, S.L., Risk, J.M., Hennies, H.-C., Gay, L.J., Carroll, R., Plagnol, V., McRonald, F.E., Stevens, H.P., Spurr, N.K., et al. (2012). RHBDF2 Mutations Are Associated with Tylosis, a Familial Esophageal Cancer Syndrome. Am. J. Hum. Genet. *90*, 340–346.

Brooke, M.A., Etheridge, S.L., Kaplan, N., Simpson, C., O'Toole, E.A., Ishida-Yamamoto, A., Marches, O., Getsios, S., and Kelsell, D.P. (2014). iRHOM2-

dependent regulation of ADAM17 in cutaneous disease and epidermal barrier function. Hum. Mol. Genet. *23*, 4064–4076.

Caescu, C.I., Jeschke, G.R., and Turk, B.E. (2009). Active-site determinants of substrate recognition by the metalloproteinases TACE and ADAM10. Biochem. J. *424*, 79–88.

Cancer Genome Atlas Research Network (2014). Comprehensive molecular profiling of lung adenocarcinoma. Nature *511*, 543–550.

Cavadas, M., Oikonomidi, I., Gaspar, C.J., Burbridge, E., Badenes, M., Félix, I., Bolado, A., Hu, T., Bileck, A., Gerner, C., et al. (2017). Phosphorylation of iRhom2 Controls Stimulated Proteolytic Shedding by the Metalloprotease ADAM17/TACE. Cell Rep. *21*, 745–757.

Chalaris, A., Adam, N., Sina, C., Rosenstiel, P., Lehmann-Koch, J., Schirmacher, P., Hartmann, D., Cichy, J., Gavrilova, O., Schreiber, S., et al. (2010). Critical role of the disintegrin metalloprotease ADAM17 for intestinal inflammation and regeneration in mice. J. Exp. Med. *207*, 1617–1624.

Chang, T.-Y., Chang, C.C.Y., Ohgami, N., and Yamauchi, Y. (2006). Cholesterol Sensing, Trafficking, and Esterification. Annu. Rev. Cell Dev. Biol. *22*, 129–157.

Chen, X., Tukachinsky, H., Huang, C.-H., Jao, C., Chu, Y.-R., Tang, H.-Y., Mueller, B., Schulman, S., Rapoport, T.A., and Salic, A. (2011). Processing and turnover of the Hedgehog protein in the endoplasmic reticulum. J. Cell Biol. *192*, 825–838.

Cheong, H., Lindsten, T., Wu, J., Lu, C., and Thompson, C.B. (2011). Ammonia-induced autophagy is independent of ULK1/ULK2 kinases. Proc. Natl. Acad. Sci. *108*, 11121–11126.

Cheung, W.K.C., and Nguyen, D.X. (2015). Lineage factors and differentiation states in lung cancer progression. Oncogene *34*, 5771–5780.

Chino, H., Hatta, T., Natsume, T., and Mizushima, N. (2019). Intrinsically Disordered Protein TEX264 Mediates ER-phagy. Mol. Cell *74*, 909-921.e6.

Christianson, J.C., Olzmann, J.A., Shaler, T.A., Sowa, M.E., Bennett, E.J., Richter, C.M., Tyler, R.E., Greenblatt, E.J., Harper, J.W., and Kopito, R.R. (2011). Defining human ERAD networks through an integrative mapping strategy. Nat. Cell Biol. *14*, 93–105.

Christova, Y., Adrain, C., Bambrough, P., Ibrahim, A., and Freeman, M. (2013). Mammalian iRhoms have distinct physiological functions including an essential role in TACE regulation. EMBO Rep. *14*, 884–890.

Ciardiello, F., and Tortora, G. (2008). EGFR antagonists in cancer treatment. N. Engl. J. Med. *358*, 1160–1174.

Conn, P.M., and Ulloa-Aguirre, A. (2011). Pharmacological Chaperones for Misfolded Gonadotropin-Releasing Hormone Receptors. Adv. Pharmacol. San Diego Calif *62*, 109–141.

Cristea, S., and Sage, J. (2016). Is the Canonical RAF/MEK/ERK Signaling Pathway a Therapeutic Target in SCLC? J. Thorac. Oncol. *11*, 1233–1241.

Cunningham, C.N., Williams, J.M., Knupp, J., Arunagiri, A., Arvan, P., and Tsai, B. (2019). Cells Deploy a Two-Pronged Strategy to Rectify Misfolded Proinsulin Aggregates. Mol. Cell.

Das, S., Czarnek, M., Bzowska, M., Mężyk-Kopeć, R., Stalińska, K., Wyroba, B., Sroka, J., Jucha, J., Deneka, D., Stokłosa, P., et al. (2012). ADAM17 Silencing in Mouse Colon Carcinoma Cells: The Effect on Tumoricidal Cytokines and Angiogenesis. PLoS ONE *7*.

De Leonibus, C., Cinque, L., and Settembre, C. (2019). Emerging Lysosomal Pathways for Quality Control at the Endoplasmic Reticulum. FEBS Lett.

Dempsey, P.J., Meise, K.S., Yoshitake, Y., Nishikawa, K., and Coffey, R.J. (1997). Apical enrichment of human EGF precursor in Madin-Darby canine kidney cells involves preferential basolateral ectodomain cleavage sensitive to a metalloprotease inhibitor. J. Cell Biol. *138*, 747–758.

Der, C.J., Krontiris, T.G., and Cooper, G.M. (1982). Transforming genes of human bladder and lung carcinoma cell lines are homologous to the ras genes of Harvey and Kirsten sarcoma viruses. Proc. Natl. Acad. Sci. U. S. A. *79*, 3637–3640.

Dikic, I., and Elazar, Z. (2018). Mechanism and medical implications of mammalian autophagy. Nat. Rev. Mol. Cell Biol.

Díaz-Rodríguez, E., Montero, J.C., Esparís-Ogando, A., Yuste, L., Pandiella, A., and Mumby, M. (2002). Extracellular Signal-regulated Kinase Phosphorylates Tumor Necrosis Factor α-converting Enzyme at Threonine 735: A Potential Role in Regulated Shedding. Mol. Biol. Cell *13*, 2031–2044.

Doedens, J.R., Mahimkar, R.M., and Black, R.A. (2003). TACE/ADAM-17 enzymatic activity is increased in response to cellular stimulation. Biochem. Biophys. Res. Commun. *308*, 331–338.

Doudna, J.A., and Charpentier, E. (2014). Genome editing. The new frontier of genome engineering with CRISPR-Cas9. Science *346*, 1258096.

Dulloo, I., Muliyil, S., and Freeman, M. (2019). The molecular, cellular and pathophysiological roles of iRhom pseudoproteases. Open Biol. *9*, 190003.

DuPage, M., Dooley, A.L., and Jacks, T. (2009). Conditional mouse lung cancer models using adenoviral or lentiviral delivery of Cre recombinase. Nat. Protoc. *4*, 1064–1072.

Düsterhöft, S., Babendreyer, A., Giese, A.A., Flasshove, C., and Ludwig, A. (2019). Status update on iRhom and ADAM17: It's still complicated. Biochim. Biophys. Acta BBA - Mol. Cell Res.

Ellgaard, L., and Helenius, A. (2003). Quality control in the endoplasmic reticulum. Nat. Rev. Mol. Cell Biol. *4*, 181–191.

Ellis, A., Risk, J.M., Maruthappu, T., and Kelsell, D.P. (2015). Tylosis with oesophageal cancer: Diagnosis, management and molecular mechanisms. Orphanet J. Rare Dis. *10*, 126.

Endres, K., Anders, A., Kojro, E., Gilbert, S., Fahrenholz, F., and Postina, R. (2003). Tumor necrosis factor-α converting enzyme is processed by proprotein-convertases to its mature form which is degraded upon phorbol ester stimulation. Eur. J. Biochem. *270*, 2386–2393.

Fan, H., Turck, C.W., and Derynck, R. (2003). Characterization of growth factor-induced serine phosphorylation of tumor necrosis factor-alpha converting enzyme and of an alternatively translated polypeptide. J. Biol. Chem. *278*, 18617–18627.

Farnsworth, C.L., and Feig, L.A. (1991). Dominant inhibitory mutations in the Mg(2+)-binding site of RasH prevent its activation by GTP. Mol. Cell. Biol. *11*, 4822–4829.

Feig, L.A., and Cooper, G.M. (1988). Inhibition of NIH 3T3 cell proliferation by a mutant ras protein with preferential affinity for GDP. Mol. Cell. Biol. *8*, 3235–3243.

Fernández-Medarde, A., and Santos, E. (2011). Ras in Cancer and Developmental Diseases. Genes Cancer *2*, 344–358.

Fleig, L., Bergbold, N., Sahasrabudhe, P., Geiger, B., Kaltak, L., and Lemberg, M.K. (2012). Ubiquitin-dependent intramembrane rhomboid protease promotes ERAD of membrane proteins. Mol. Cell *47*, 558–569.

Foltenyi, K., Greenspan, R.J., and Newport, J.W. (2007). Activation of EGFR and ERK by rhomboid signaling regulates the consolidation and maintenance of sleep in Drosophila. Nat. Neurosci. *10*, 1160–1167.

Forbes, S.A., Beare, D., Boutselakis, H., Bamford, S., Bindal, N., Tate, J., Cole, C.G., Ward, S., Dawson, E., Ponting, L., et al. (2017). COSMIC: somatic cancer genetics at high-resolution. Nucleic Acids Res. *45*, D777–D783.

Forrester, A., De Leonibus, C., Grumati, P., Fasana, E., Piemontese, M., Staiano, L., Fregno, I., Raimondi, A., Marazza, A., Bruno, G., et al. (2019). A selective ER-phagy exerts procollagen quality control via a Calnexin-FAM134B complex. EMBO J. *38*, e99847.

Fraser, J., Cabodevilla, A.G., Simpson, J., and Gammoh, N. (2017). Interplay of autophagy, receptor tyrosine kinase signalling and endocytic trafficking. Essays Biochem. *61*, 597–607.

Freeman, M. (1994). Misexpression of the Drosophila argos gene, a secreted regulator of cell determination. Dev. Camb. Engl. *120*, 2297–2304.

Fregno, I., and Molinari, M. (2019). Proteasomal and lysosomal clearance of faulty secretory proteins: ER-associated degradation (ERAD) and ER-to-lysosome-associated degradation (ERLAD) pathways. Crit. Rev. Biochem. Mol. Biol. *54*, 153–163.

Fregno, I., Fasana, E., Bergmann, T.J., Raimondi, A., Loi, M., Soldà, T., Galli, C., D'Antuono, R., Morone, D., Danieli, A., et al. (2018). ER-to-lysosome-associated degradation of proteasome-resistant ATZ polymers occurs via receptor-mediated vesicular transport. EMBO J. e99259.

Fujita, E., Kouroku, Y., Isoai, A., Kumagai, H., Misutani, A., Matsuda, C., Hayashi, Y.K., and Momoi, T. (2007). Two endoplasmic reticulum-associated degradation (ERAD) systems for the novel variant of the mutant dysferlin: ubiquitin/proteasome ERAD(I) and autophagy/lysosome ERAD(II). Hum. Mol. Genet. *16*, 618–629.

Fumagalli, F., Noack, J., Bergmann, T.J., Cebollero, E., Pisoni, G.B., Fasana, E., Fregno, I., Galli, C., Loi, M., Soldà, T., et al. (2016). Translocon component Sec62 acts in endoplasmic reticulum turnover during stress recovery. Nat. Cell Biol. *18*, 1173–1184.

Gauss, R., Sommer, T., and Jarosch, E. (2006). The Hrd1p ligase complex forms a linchpin between ER-lumenal substrate selection and Cdc48p recruitment. EMBO J. *25*, 1827–1835.

Gazdar, A.F., Girard, L., Lockwood, W.W., Lam, W.L., and Minna, J.D. (2010). Lung Cancer Cell Lines as Tools for Biomedical Discovery and Research. JNCI J. Natl. Cancer Inst. *102*, 1310–1321.

Gelsthorpe, M.E., Baumann, N., Millard, E., Gale, S.E., Langmade, S.J., Schaffer, J.E., and Ory, D.S. (2008). Niemann-Pick Type C1 I1061T Mutant Encodes a Functional Protein That Is Selected for Endoplasmic Reticulum-associated Degradation Due to Protein Misfolding. J. Biol. Chem. *283*, 8229–8236.

Giricz, O., Calvo, V., Peterson, E.A., Abouzeid, C.M., and Kenny, P.A. (2013). TACE-dependent TGF-alpha shedding drives triple-negative breast cancer cell invasion. Int. J. Cancer J. Int. Cancer *133*, 2587–2595.

Greenblatt, E.J., Olzmann, J.A., and Kopito, R.R. (2011). Derlin-1 is a rhomboid pseudoprotease required for the dislocation of mutant α-1 antitrypsin from the endoplasmic reticulum. Nat. Struct. Mol. Biol. *18*, 1147–1152.

Grieve, A.G., Xu, H., Künzel, U., Bambrough, P., Sieber, B., and Freeman, M. (2017). Phosphorylation of iRhom2 at the plasma membrane controls mammalian TACE-dependent inflammatory and growth factor signalling. ELife *6*.

Grumati, P., Morozzi, G., Hölper, S., Mari, M., Harwardt, M.-L.I., Yan, R., Müller, S., Reggiori, F., Heilemann, M., and Dikic, I. (2017). Full length RTN3 regulates turnover of tubular endoplasmic reticulum via selective autophagy. ELife *6*.

Haigis, K.M. (2017). KRAS Alleles: The Devil Is in the Detail. Trends Cancer *3*, 686–697.

Hall, K.C., and Blobel, C.P. (2012). Interleukin-1 stimulates ADAM17 through a mechanism independent of its cytoplasmic domain or phosphorylation at threonine 735. PloS One *7*, e31600.

Hampton, R.Y. (2002). Proteolysis and sterol regulation. Annu. Rev. Cell Dev. Biol. *18*, 345–378.

Hanahan, D., and Weinberg, R.A. (2011). Hallmarks of Cancer: The Next Generation. Cell *144*, 646–674.

He, K., Cunningham, C.N., Manickam, N., Liu, M., Arvan, P., and Tsai, B. (2015). PDI reductase acts on Akita mutant proinsulin to initiate retrotranslocation along the Hrd1/Sel1L-p97 axis. Mol. Biol. Cell *26*, 3413–3423.

Heigener, D.F., Gandara, D.R., and Reck, M. (2015). Targeting of MEK in lung cancer therapeutics. Lancet Respir. Med. *3*, 319–327.

Hennies, H.C., Hagedorn, M., and Reis, A. (1995). Palmoplantar keratoderma in association with carcinoma of the esophagus maps to chromosome 17q distal to the keratin gene cluster. Genomics *29*, 537–540.

Hidvegi, T., Ewing, M., Hale, P., Dippold, C., Beckett, C., Kemp, C., Maurice, N., Mukherjee, A., Goldbach, C., Watkins, S., et al. (2010). An autophagy-enhancing drug promotes degradation of mutant alpha1-antitrypsin Z and reduces hepatic fibrosis. Science *329*, 229–232.

Hobbs, G.A., Der, C.J., and Rossman, K.L. (2016). RAS isoforms and mutations in cancer at a glance. J. Cell Sci. *129*, 1287–1292.

Holderfield, M., Deuker, M.M., McCormick, F., and McMahon, M. (2014). Targeting RAF kinases for cancer therapy: BRAF-mutated melanoma and beyond. Nat. Rev. Cancer *14*, 455–467.

Hosokawa, N., Hara, Y., and Mizushima, N. (2006). Generation of cell lines with tetracycline-regulated autophagy and a role for autophagy in controlling cell size. FEBS Lett. *580*, 2623–2629.

Hosur, V., Johnson, K.R., Burzenski, L.M., Stearns, T.M., Maser, R.S., and Shultz, L.D. (2014). Rhbdf2 mutations increase its protein stability and drive EGFR hyperactivation through enhanced secretion of amphiregulin. Proc. Natl. Acad. Sci. U. S. A. *111*, E2200-2209.

Hosur, V., Low, B.E., Shultz, L.D., and Wiles, M.V. (2017). Genetic deletion of amphiregulin restores the normal skin phenotype in a mouse model of the human skin disease tylosis. Biol. Open *6*, 1174–1179.

Houck, S.A., Ren, H.Y., Madden, V.J., Bonner, J.N., Conlin, M.P., Janovick, J.A., Conn, P.M., and Cyr, D.M. (2014). Quality control autophagy degrades soluble

ERAD-resistant conformers of the misfolded membrane protein GnRHR. Mol. Cell *54*, 166–179.

Hunter, J.C., Manandhar, A., Carrasco, M.A., Gurbani, D., Gondi, S., and Westover, K.D. (2015). Biochemical and Structural Analysis of Common Cancer-Associated KRAS Mutations. Mol. Cancer Res. MCR *13*, 1325–1335.

Ihle, N.T., Byers, L.A., Kim, E.S., Saintigny, P., Lee, J.J., Blumenschein, G.R., Tsao, A., Liu, S., Larsen, J.E., Wang, J., et al. (2012). Effect of KRAS oncogene substitutions on protein behavior: implications for signaling and clinical outcome. J. Natl. Cancer Inst. *104*, 228–239.

Infante, J., Burris, H., Lewis, N., Donehower, R., Redman, J., Friedman, S., Scherle, P., Fridman, J., Li, J., Emm, T., et al. (2007). A multicenter phase Ib study of the safety, pharmacokinetics, biological activity and clinical efficacy of INCB7839, a potent and selective inhibitor of ADAM10 and ADAM17. Breast Cancer Res. Treat. *106*.

Issuree, P.D.A., Maretzky, T., McIlwain, D.R., Monette, S., Qing, X., Lang, P.A., Swendeman, S.L., Park-Min, K.-H., Binder, N., Kalliolias, G.D., et al. (2013). iRHOM2 is a critical pathogenic mediator of inflammatory arthritis. J. Clin. Invest. *123*, 928–932.

Jackson, E.L., Willis, N., Mercer, K., Bronson, R.T., Crowley, D., Montoya, R., Jacks, T., and Tuveson, D.A. (2001). Analysis of lung tumor initiation and progression using conditional expression of oncogenic K-ras. Genes Dev. *15*, 3243–3248.

Jackson, L.F., Qiu, T.H., Sunnarborg, S.W., Chang, A., Zhang, C., Patterson, C., and Lee, D.C. (2003). Defective valvulogenesis in HB-EGF and TACE-null mice is associated with aberrant BMP signaling. EMBO J. *22*, 2704–2716.

James, G.L., Goldstein, J.L., and Brown, M.S. (1995). Polylysine and CVIM sequences of K-RasB dictate specificity of prenylation and confer resistance to benzodiazepine peptidomimetic in vitro. J. Biol. Chem. *270*, 6221–6226.

Janes, M.R., Zhang, J., Li, L.-S., Hansen, R., Peters, U., Guo, X., Chen, Y., Babbar, A., Firdaus, S.J., Darjania, L., et al. (2018). Targeting KRAS Mutant Cancers with a Covalent G12C-Specific Inhibitor. Cell *172*, 578-589.e17.

Jin, S.-Q., Yu, M., Zhang, W., Lyu, H., Yuan, Y., and Wang, Z.-X. (2016). Dysferlin Gene Mutation Spectrum in a Large Cohort of Chinese Patients with Dysferlinopathy. Chin. Med. J. (Engl.) *129*, 2287–2293.

Jinek, M., Chylinski, K., Fonfara, I., Hauer, M., Doudna, J.A., and Charpentier, E. (2012). A programmable dual-RNA-guided DNA endonuclease in adaptive bacterial immunity. Science *337*, 816–821.

Jürgens, G., Wieschaus, E., Nüsslein-Volhard, C., and Kluding, H. (1984). Mutations affecting the pattern of the larval cuticle inDrosophila melanogaster. Wilhelm Rouxs Arch. Dev. Biol. *193*, 283–295.

Kamimoto, T., Shoji, S., Hidvegi, T., Mizushima, N., Umebayashi, K., Perlmutter, D.H., and Yoshimori, T. (2006). Intracellular inclusions containing mutant alpha1-antitrypsin Z are propagated in the absence of autophagic activity. J. Biol. Chem. *281*, 4467–4476.

Karoulia, Z., Gavathiotis, E., and Poulikakos, P.I. (2017). New perspectives for targeting RAF kinase in human cancer. Nat. Rev. Cancer *17*, 676–691.

Kenny, P.A., and Bissell, M.J. (2007). Targeting TACE-dependent EGFR ligand shedding in breast cancer. J. Clin. Invest. *117*, 337–345.

Killock, D.J., and Ivetić, A. (2010). The cytoplasmic domains of TNFα-converting enzyme (TACE/ADAM17) and L-selectin are regulated differently by p38 MAPK and PKC to promote ectodomain shedding. Biochem. J. *428*, 293–304.

Knop, M., Finger, A., Braun, T., Hellmuth, K., and Wolf, D.H. (1996). Der1, a novel protein specifically required for endoplasmic reticulum degradation in yeast. EMBO J. *15*, 753–763.

Kohler, J., Catalano, M., and Ambrogio, C. (2018). Back to the Bench? MEK and ERK Inhibitors for the Treatment of KRAS Mutant Lung Adenocarcinoma. Curr. Med. Chem. *25*, 558–574.

Koo, M.Y., Park, J., Lim, J.M., Joo, S.Y., Shin, S.-P., Shim, H.B., Chung, J., Kang, D., Woo, H.A., and Rhee, S.G. (2014). Selective inhibition of the function of tyrosine-phosphorylated STAT3 with a phosphorylation site-specific intrabody. Proc. Natl. Acad. Sci. U. S. A. *111*, 6269–6274.

Kruspig, B., Monteverde, T., Neidler, S., Hock, A., Kerr, E., Nixon, C., Clark, W., Hedley, A., Laing, S., Coffelt, S.B., et al. (2018). The ERBB network facilitates KRAS-driven lung tumorigenesis. Sci. Transl. Med. *10*.

Künzel, U., Grieve, A.G., Meng, Y., Sieber, B., Cowley, S.A., and Freeman, M. (2018). FRMD8 promotes inflammatory and growth factor signalling by stabilising the iRhom/ADAM17 sheddase complex. ELife *7*.

Le Gall, S.M.L., Maretzky, T., Issuree, P.D.A., Niu, X.-D., Reiss, K., Saftig, P., Khokha, R., Lundell, D., and Blobel, C.P. (2010). ADAM17 is regulated by a rapid and reversible mechanism that controls access to its catalytic site. J Cell Sci *123*, 3913–3922.

Lechardeur, D., Sohn, K.-J., Haardt, M., Joshi, P.B., Monck, M., Graham, R.W., Beatty, B., Squire, J., O'Brodovich, H., and Lukacs, G.L. (1999). Metabolic instability of plasmid DNA in the cytosol: a potential barrier to gene transfer. Gene Ther. *6*, 482–497.

Lee, J.R., Urban, S., Garvey, C.F., and Freeman, M. (2001). Regulated Intracellular Ligand Transport and Proteolysis Control EGF Signal Activation in Drosophila. Cell *107*, 161–171.

Lee, W., Kim, Y., Park, J., Shim, S., Lee, J., Hong, S., Ahn, H.-H., Lee, H., and Jung, Y.-K. (2015). iRhom1 regulates proteasome activity via PAC1/2 under ER stress. Sci. Rep. *5*, 11559.

Lemberg, M.K., and Adrain, C. (2016). Inactive rhomboid proteins: New mechanisms with implications in health and disease. Semin. Cell Dev. Biol. *60*, 29–37.

Lemberg, M.K., and Freeman, M. (2007). Functional and evolutionary implications of enhanced genomic analysis of rhomboid intramembrane proteases. Genome Res. *17*, 1634–1646.

Lemberg, M.K., Menendez, J., Misik, A., Garcia, M., Koth, C.M., and Freeman, M. (2005). Mechanism of intramembrane proteolysis investigated with purified rhomboid proteases. EMBO J. *24*, 464–472.

Levine, B., and Kroemer, G. (2019). Biological Functions of Autophagy Genes: A Disease Perspective. Cell *176*, 11–42.

Li, X., Maretzky, T., Weskamp, G., Monette, S., Qing, X., Issuree, P.D.A., Crawford, H.C., McIlwain, D.R., Mak, T.W., Salmon, J.E., et al. (2015). iRhoms 1 and 2 are essential upstream regulators of ADAM17-dependent EGFR signaling. Proc. Natl. Acad. Sci. *112*, 6080–6085.

Li, X., Maretzky, T., Perez-Aguilar, J.M., Monette, S., Weskamp, G., Le Gall, S., Beutler, B., Weinstein, H., and Blobel, C.P. (2017). Structural modeling defines transmembrane residues in ADAM17 that are crucial for Rhbdf2-ADAM17-dependent proteolysis. J. Cell Sci. *130*, 868–878.

Lilley, B.N., and Ploegh, H.L. (2004). A membrane protein required for dislocation of misfolded proteins from the ER. Nature *429*, 834–840.

Linardou, H., Dahabreh, I.J., Kanaloupiti, D., Siannis, F., Bafaloukos, D., Kosmidis, P., Papadimitriou, C.A., and Murray, S. (2008). Assessment of somatic k-RAS mutations as a mechanism associated with resistance to EGFR-targeted agents: a systematic review and meta-analysis of studies in advanced non-small-cell lung cancer and metastatic colorectal cancer. Lancet Oncol. *9*, 962–972.

Lito, P., Solomon, M., Li, L.-S., Hansen, R., and Rosen, N. (2016). Allele-specific inhibitors inactivate mutant KRAS G12C by a trapping mechanism. Science *351*, 604–608.

Loegering, D.J., and Lennartz, M.R. (2011). Protein Kinase C and Toll-Like Receptor Signaling.

Lorenzen, I., Lokau, J., Korpys, Y., Oldefest, M., Flynn, C.M., Künzel, U., Garbers, C., Freeman, M., Grötzinger, J., and Düsterhöft, S. (2016). Control of ADAM17 activity by regulation of its cellular localisation. Sci. Rep. *6*, 35067.

Lu, X.-L., Zhao, C.-H., Zhang, H., and Yao, X.-L. (2017). iRhom2 is involved in lipopolysaccharide-induced cardiac injury in vivo and in vitro through regulating inflammation response. Biomed. Pharmacother. *86*, 645–653.

Luo, W.-W., Li, S., Li, C., Lian, H., Yang, Q., Zhong, B., and Shu, H.-B. (2016). iRhom2 is essential for innate immunity to DNA viruses by mediating trafficking and stability of the adaptor STING. Nat. Immunol. *17*, 1057–1066.

Luo, W.-W., Li, S., Li, C., Zheng, Z.-Q., Cao, P., Tong, Z., Lian, H., Wang, S.-Y., Shu, H.-B., and Wang, Y.-Y. (2017). iRhom2 is essential for innate immunity to RNA virus by antagonizing ER- and mitochondria-associated degradation of VISA. PLoS Pathog. *13*, e1006693.

Maney, S.K., McIlwain, D.R., Polz, R., Pandyra, A.A., Sundaram, B., Wolff, D., Ohishi, K., Maretzky, T., Brooke, M.A., Evers, A., et al. (2015). Deletions in the cytoplasmic domain of iRhom1 and iRhom2 promote shedding of the TNF receptor by the protease ADAM17. Sci. Signal. *8*, ra109.

Mao, C., Qiu, L.-X., Liao, R.-Y., Du, F.-B., Ding, H., Yang, W.-C., Li, J., and Chen, Q. (2010). KRAS mutations and resistance to EGFR-TKIs treatment in patients with non-small cell lung cancer: a meta-analysis of 22 studies. Lung Cancer Amst. Neth. *69*, 272–278.

Maretzky, T., McIlwain, D.R., Issuree, P.D.A., Li, X., Malapeira, J., Amin, S., Lang, P.A., Mak, T.W., and Blobel, C.P. (2013). iRhom2 controls the substrate selectivity of stimulated ADAM17-dependent ectodomain shedding. Proc. Natl. Acad. Sci. U. S. A. *110*, 11433–11438.

Martinez, J., Almendinger, J., Oberst, A., Ness, R., Dillon, C.P., Fitzgerald, P., Hengartner, M.O., and Green, D.R. (2011). Microtubule-associated protein 1 light chain 3 alpha (LC3)-associated phagocytosis is required for the efficient clearance of dead cells. Proc. Natl. Acad. Sci. *108*, 17396–17401.

Martinez, J., Malireddi, R.K.S., Lu, Q., Cunha, L.D., Pelletier, S., Gingras, S., Orchard, R., Guan, J.-L., Tan, H., Peng, J., et al. (2015). Molecular characterization of LC3-associated phagocytosis reveals distinct roles for Rubicon, NOX2 and autophagy proteins. Nat. Cell Biol. *17*, 893–906.

Martinez, J.D., Parker, M.T., Fultz, K.E., Ignatenko, N.A., and Gerner, E.W. (2003). Molecular Biology of Cancer. In Burger's Medicinal Chemistry and Drug Discovery, (American Cancer Society), pp. 1–50.

McCubrey, J.A., Steelman, L.S., Chappell, W.H., Abrams, S.L., Wong, E.W.T., Chang, F., Lehmann, B., Terrian, D.M., Milella, M., Tafuri, A., et al. (2007). Roles of the Raf/MEK/ERK pathway in cell growth, malignant transformation and drug resistance. Biochim. Biophys. Acta *1773*, 1263–1284.

McIlwain, D.R., Lang, P.A., Maretzky, T., Hamada, K., Ohishi, K., Maney, S.K., Berger, T., Murthy, A., Duncan, G., Xu, H.C., et al. (2012). iRhom2 regulation of TACE controls TNF-mediated protection against Listeria and responses to LPS. Science *335*, 229–232.

McKay Bounford, K., and Gissen, P. (2014). Genetic and laboratory diagnostic approach in Niemann Pick disease type C. J. Neurol. *261*, 569–575.

Medzihradszky, K.F. (2005). Characterization of protein N-glycosylation. Methods Enzymol. *405*, 116–138.

Mehnert, M., Sommer, T., and Jarosch, E. (2014). Der1 promotes movement of misfolded proteins through the endoplasmic reticulum membrane. Nat. Cell Biol. *16*, 77–86.

Mizushima, N. (2018). A Dual Binding Receptor for ER-phagy. Dev. Cell *44*, 133–135.

Mochizuki, S., and Okada, Y. (2007). ADAMs in cancer cell proliferation and progression. Cancer Sci. *98*, 621–628.

Mokoena, T., Smit, J.G.M., Karusseit, V.O., Dorfling, C.M., and van Rensburg, E.J. (2018). Tylosis associated with squamous cell carcinoma of the oesophagus (TOC): Report of an African family with a novel RHBDF2 variant. Clin. Genet.

Moll, H.P., Pranz, K., Musteanu, M., Grabner, B., Hruschka, N., Mohrherr, J., Aigner, P., Stiedl, P., Brcic, L., Laszlo, V., et al. (2018). Afatinib restrains K-RAS-driven lung tumorigenesis. Sci. Transl. Med. *10*.

Moon, H.W., Han, H.G., and Jeon, Y.J. (2018). Protein Quality Control in the Endoplasmic Reticulum and Cancer. Int. J. Mol. Sci. *19*.

Moss, M.L., Jin, S.-L.C., Milla, M.E., Burkhart, W., Carter, H.L., Chen, W.-J., Clay, W.C., Didsbury, J.R., Hassler, D., Hoffman, C.R., et al. (1997). Cloning of a disintegrin metalloproteinase that processes precursor tumour-necrosis factor-α. Nature *385*, 733–736.

Moss, M.L., Sklair-Tavron, L., and Nudelman, R. (2008). Drug Insight: tumor necrosis factor-converting enzyme as a pharmaceutical target for rheumatoid arthritis. Nat. Clin. Pract. Rheumatol. *4*, 300–309.

Nakasone, N., Nakamura, Y.S., Higaki, K., Oumi, N., Ohno, K., and Ninomiya, H. (2014). Endoplasmic reticulum-associated degradation of Niemann-Pick C1: evidence for the role of heat shock proteins and identification of lysine residues that accept ubiquitin. J. Biol. Chem. *289*, 19714–19725.

Nassar, N., Singh, K., and Garcia-Diaz, M. (2010). Structure of the dominant negative S17N mutant of Ras. Biochemistry *49*, 1970–1974.

Neal, S., Jaeger, P.A., Duttke, S.H., Benner, C.K., Glass, C., Ideker, T., and Hampton, R. (2018). The Dfm1 Derlin Is Required for ERAD Retrotranslocation of Integral Membrane Proteins. Mol. Cell *69*, 306-320.e4.

Nishida, Y., Arakawa, S., Fujitani, K., Yamaguchi, H., Mizuta, T., Kanaseki, T., Komatsu, M., Otsu, K., Tsujimoto, Y., and Shimizu, S. (2009). Discovery of Atg5/Atg7-independent alternative macroautophagy. Nature *461*, 654–658.

Novotny, C.J., Hamilton, G.L., McCormick, F., and Shokat, K.M. (2017). Farnesyltransferase-Mediated Delivery of a Covalent Inhibitor Overcomes Alternative Prenylation to Mislocalize K-Ras. ACS Chem. Biol. *12*, 1956–1962.

Nussinov, R., Tsai, C.-J., and Jang, H. (2019). Does Ras Activate Raf and PI3K Allosterically? Front. Oncol. *9*.

Oikonomidi, I., Burbridge, E., Cavadas, M., Sullivan, G., Collis, B., Naegele, H., Clancy, D., Brezinova, J., Hu, T., Bileck, A., et al. (2018). iTAP, a novel iRhom interactor, controls TNF secretion by policing the stability of iRhom/TACE. ELife *7*, e35032.

Olzmann, J.A., Kopito, R.R., and Christianson, J.C. (2013). The mammalian endoplasmic reticulum-associated degradation system. Cold Spring Harb. Perspect. Biol. *5*.

Ostrem, J.M.L., and Shokat, K.M. (2016). Direct small-molecule inhibitors of KRAS: from structural insights to mechanism-based design. Nat. Rev. Drug Discov. *15*, 771–785.

Ostrem, J.M., Peters, U., Sos, M.L., Wells, J.A., and Shokat, K.M. (2013). K-Ras(G12C) inhibitors allosterically control GTP affinity and effector interactions. Nature *503*, 548–551.

Parada, L.F., Tabin, C.J., Shih, C., and Weinberg, R.A. (1982). Human EJ bladder carcinoma oncogene is homologue of Harvey sarcoma virus ras gene. Nature *297*, 474–478.

Park, J., Throop, A.L., and LaBaer, J. (2015). Site-Specific Recombinational Cloning Using Gateway and In-Fusion Cloning Schemes. Curr. Protoc. Mol. Biol. *110*, 3.20.1-3.20.23.

Patricelli, M.P., Janes, M.R., Li, L.-S., Hansen, R., Peters, U., Kessler, L.V., Chen, Y., Kucharski, J.M., Feng, J., Ely, T., et al. (2016). Selective Inhibition of Oncogenic KRAS Output with Small Molecules Targeting the Inactive State. Cancer Discov. *6*, 316–329.

Peiretti, F., Canault, M., Deprez-Beauclair, P., Berthet, V., Bonardo, B., Juhan-Vague, I. rène, and Nalbone, G. (2003). Intracellular maturation and transport of tumor necrosis factor alpha converting enzyme. Exp. Cell Res. *285*, 278–285.

Peschon, J.J., Slack, J.L., Reddy, P., Stocking, K.L., Sunnarborg, S.W., Lee, D.C., Russell, W.E., Castner, B.J., Johnson, R.S., Fitzner, J.N., et al. (1998). An essential role for ectodomain shedding in mammalian development. Science *282*, 1281–1284.

Preston, G.M., and Brodsky, J.L. (2017). The evolving role of ubiquitin modification in endoplasmic reticulum-associated degradation. Biochem. J. *474*, 445–469.

Qu, D., Teckman, J.H., Omura, S., and Perlmutter, D.H. (1996). Degradation of a Mutant Secretory Protein, α1-Antitrypsin Z, in the Endoplasmic Reticulum Requires Proteasome Activity. J. Biol. Chem. *271*, 22791–22795.

Qu, L., Sha, S., Zou, Q.-L., Gao, X.-H., Xiao, T., Chen, H.-D., and He, C.C. (2019). Whole Exome Sequencing Identified a Novel Mutation of the RHBDF2 Gene

in a Chinese Family of Tylosis with Esophageal Cancer. Acta Derm. Venereol. *99*, 699–700.

Rattan, R., Vaidyanathan, S., Wu, G.S.-H., Shakya, A., Orr, B.G., and Banaszak Holl, M.M. (2013). Polyplex-induced cytosolic nuclease activation leads to differential transgene expression. Mol. Pharm. *10*, 3013–3022.

Roskoski, R. (2012). ERK1/2 MAP kinases: structure, function, and regulation. Pharmacol. Res. *66*, 105–143.

Rousselet, E., Benjannet, S., Marcinkiewicz, E., Asselin, M.-C., Lazure, C., and Seidah, N.G. (2011). Proprotein convertase PC7 enhances the activation of the EGF receptor pathway through processing of the EGF precursor. J. Biol. Chem. *286*, 9185–9195.

Rovida, E., Paccagnini, A., Rosso, M.D., Peschon, J., and Sbarba, P.D. (2001). TNF-α-Converting Enzyme Cleaves the Macrophage Colony-Stimulating Factor Receptor in Macrophages Undergoing Activation. J. Immunol. *166*, 1583–1589.

Rowell, C.A., Kowalczyk, J.J., Lewis, M.D., and Garcia, A.M. (1997). Direct demonstration of geranylgeranylation and farnesylation of Ki-Ras in vivo. J. Biol. Chem. *272*, 14093–14097.

Ruggiano, A., Foresti, O., and Carvalho, P. (2014). Quality control: ER-associated degradation: protein quality control and beyond. J. Cell Biol. *204*, 869–879.

Saad, M.I., Alhayyani, S., McLeod, L., Yu, L., Alanazi, M., Deswaerte, V., Tang, K., Jarde, T., Smith, J.A., Prodanovic, Z., et al. (2019). ADAM17 selectively activates the IL-6 trans-signaling/ERK MAPK axis in KRAS-addicted lung cancer. EMBO Mol. Med. e9976.

Saarinen, S., Vahteristo, P., Lehtonen, R., Aittomäki, K., Launonen, V., Kiviluoto, T., and Aaltonen, L.A. (2012). Analysis of a Finnish family confirms RHBDF2 mutations as the underlying factor in tylosis with esophageal cancer. Fam. Cancer *11*, 525–528.

Sahin, U., Weskamp, G., Kelly, K., Zhou, H.-M., Higashiyama, S., Peschon, J., Hartmann, D., Saftig, P., and Blobel, C.P. (2004). Distinct roles for ADAM10 and ADAM17 in ectodomain shedding of six EGFR ligands. J. Cell Biol. *164*, 769–779.

Sander, J.D., and Joung, J.K. (2014). CRISPR-Cas systems for editing, regulating and targeting genomes. Nat. Biotechnol. *32*, 347–355.

Sanjuan, M.A., Dillon, C.P., Tait, S.W.G., Moshiach, S., Dorsey, F., Connell, S., Komatsu, M., Tanaka, K., Cleveland, J.L., Withoff, S., et al. (2007). Toll-like receptor signalling in macrophages links the autophagy pathway to phagocytosis. Nature *450*, 1253–1257.

Santos, E., Tronick, S.R., Aaronson, S.A., Pulciani, S., and Barbacid, M. (1982). T24 human bladder carcinoma oncogene is an activated form of the normal human homologue of BALB- and Harvey-MSV transforming genes. Nature *298*, 343–347.

Schlöndorff, J., Becherer, J.D., and Blobel, C.P. (2000). Intracellular maturation and localization of the tumour necrosis factor α convertase (TACE). Biochem. J. *347*, 131–138.

Schmidt, S., Schumacher, N., Schwarz, J., Tangermann, S., Kenner, L., Schlederer, M., Sibilia, M., Linder, M., Altendorf-Hofmann, A., Knösel, T., et al. (2018). ADAM17 is required for EGF-R–induced intestinal tumors via IL-6 trans-signaling. J. Exp. Med. *215*, 1205–1225.

Scholl, C., Fröhling, S., Dunn, I.F., Schinzel, A.C., Barbie, D.A., Kim, S.Y., Silver, S.J., Tamayo, P., Wadlow, R.C., Ramaswamy, S., et al. (2009). Synthetic lethal interaction between oncogenic KRAS dependency and STK33 suppression in human cancer cells. Cell *137*, 821–834.

Schubbert, S., Shannon, K., and Bollag, G. (2007). Hyperactive Ras in developmental disorders and cancer. Nat. Rev. Cancer *7*, 295–308.

Schultz, M.L., Krus, K.L., Kaushik, S., Dang, D., Chopra, R., Qi, L., Shakkottai, V.G., Cuervo, A.M., and Lieberman, A.P. (2018). Coordinate regulation of mutant NPC1 degradation by selective ER autophagy and MARCH6-dependent ERAD. Nat. Commun. *9*, 3671.

Schwarz, J., Broder, C., Helmstetter, A., Schmidt, S., Yan, I., Müller, M., Schmidt-Arras, D., Becker-Pauly, C., Koch-Nolte, F., Mittrücker, H.-W., et al. (2013). Short-term TNFα shedding is independent of cytoplasmic phosphorylation or furin cleavage of ADAM17. Biochim. Biophys. Acta BBA - Mol. Cell Res. *1833*, 3355–3367.

Sharma, A., Bender, S., Zimmermann, M., Riesterer, O., Broggini-Tenzer, A., and Pruschy, M.N. (2016). Secretome Signature Identifies ADAM17 as Novel Target for Radiosensitization of Non-Small Cell Lung Cancer. Clin. Cancer Res. Off. J. Am. Assoc. Cancer Res. *22*, 4428–4439.

Shin, S.-M., Choi, D.-K., Jung, K., Bae, J., Kim, J.-S., Park, S.-W., Song, K.-H., and Kim, Y.-S. (2017). Antibody targeting intracellular oncogenic Ras mutants exerts anti-tumour effects after systemic administration. Nat. Commun. *8*, 15090.

Siegel, R.L., Miller, K.D., and Jemal, A. (2017). Cancer statistics, 2017. CA. Cancer J. Clin. *67*, 7–30.

Sigismund, S., Avanzato, D., and Lanzetti, L. (2018). Emerging functions of the EGFR in cancer. Mol. Oncol. *12*, 3–20.

Simanshu, D.K., Nissley, D.V., and McCormick, F. (2017). RAS Proteins and Their Regulators in Human Disease. Cell *170*, 17–33.

Singh, B., and Coffey, R.J. (2014). Trafficking of Epidermal Growth Factor Receptor Ligands in Polarized Epithelial Cells. Annu. Rev. Physiol. *76*, 275–300.

Slastnikova, T.A., Ulasov, A.V., Rosenkranz, A.A., and Sobolev, A.S. (2018). Targeted Intracellular Delivery of Antibodies: The State of the Art. Front. Pharmacol. *9*.

Smith, M., and Wilkinson, S. (2017). ER homeostasis and autophagy. Essays Biochem. *61*, 625–635.

Smith, M.D., Harley, M.E., Kemp, A.J., Wills, J., Lee, M., Arends, M., von Kriegsheim, A., Behrends, C., and Wilkinson, S. (2018). CCPG1 Is a Non-canonical Autophagy Cargo Receptor Essential for ER-Phagy and Pancreatic ER Proteostasis. Dev. Cell *44*, 217-232.e11.

Smith, M.J., Neel, B.G., and Ikura, M. (2013). NMR-based functional profiling of RASopathies and oncogenic RAS mutations. Proc. Natl. Acad. Sci. *110*, 4574–4579.

Song, B.-L., Sever, N., and DeBose-Boyd, R.A. (2005). Gp78, a membrane-anchored ubiquitin ligase, associates with Insig-1 and couples sterol-regulated ubiquitination to degradation of HMG CoA reductase. Mol. Cell *19*, 829–840.

Speiseder, T., Hofmann-Sieber, H., Rodríguez, E., Schellenberg, A., Akyüz, N., Dierlamm, J., Spruss, T., Lange, C., and Dobner, T. (2017). Efficient Transformation of Primary Human Mesenchymal Stromal Cells by Adenovirus Early Region 1 Oncogenes. J. Virol. *91*.

Stanley, A.M., Carvalho, P., and Rapoport, T. (2011). Recognition of an ERAD-L substrate analyzed by site-specific in vivo photocrosslinking. FEBS Lett. *585*, 1281–1286.

Stanley, P., Schachter, H., and Taniguchi, N. (2009). N-Glycans. In Essentials of Glycobiology, A. Varki, R.D. Cummings, J.D. Esko, H.H. Freeze, P. Stanley, C.R. Bertozzi, G.W. Hart, and M.E. Etzler, eds. (Cold Spring Harbor (NY): Cold Spring Harbor Laboratory Press), p.

Stolz, A., and Grumati, P. (2019). The various shades of ER-phagy. FEBS J.

Stolz, A., Schweizer, R.S., Schäfer, A., and Wolf, D.H. (2010). Dfm1 forms distinct complexes with Cdc48 and the ER ubiquitin ligases and is required for ERAD. Traffic Cph. Den. *11*, 1363–1369.

Sturtevant, M.A., Roark, M., and Bier, E. (1993). The Drosophila rhomboid gene mediates the localized formation of wing veins and interacts genetically with components of the EGF-R signaling pathway. Genes Dev. *7*, 961–973.

Sun, Z., and Brodsky, J.L. (2019). Protein quality control in the secretory pathway. J. Cell Biol. jcb.201906047.

Tanaka, T., and Rabbitts, T.H. (2010). Interfering with RAS–effector protein interactions prevent RAS-dependent tumour initiation and causes stop–start control of cancer growth. Oncogene *29*, 6064–6070.

Tanaka, T., Williams, R.L., and Rabbitts, T.H. (2007). Tumour prevention by a single antibody domain targeting the interaction of signal transduction proteins with RAS. EMBO J. *26*, 3250–3259.

Taparowsky, E., Suard, Y., Fasano, O., Shimizu, K., Goldfarb, M., and Wigler, M. (1982). Activation of the T24 bladder carcinoma transforming gene is linked to a single amino acid change. Nature *300*, 762–765.

Teckman, J.H., and Perlmutter, D.H. (2000). Retention of mutant alpha(1)-antitrypsin Z in endoplasmic reticulum is associated with an autophagic response. Am. J. Physiol. Gastrointest. Liver Physiol. *279*, G961-974.

Terrell, E.M., and Morrison, D.K. (2019). Ras-Mediated Activation of the Raf Family Kinases. Cold Spring Harb. Perspect. Med. *9*.

Tichá, A., Collis, B., and Strisovsky, K. (2018). The Rhomboid Superfamily: Structural Mechanisms and Chemical Biology Opportunities. Trends Biochem. Sci. *43*, 726–739.

Twomey, E.C., Ji, Z., Wales, T.E., Bodnar, N.O., Ficarro, S.B., Marto, J.A., Engen, J.R., and Rapoport, T.A. (2019). Substrate processing by the Cdc48 ATPase complex is initiated by ubiquitin unfolding. Science *365*, eaax1033.

Urban, S., Lee, J.R., and Freeman, M. (2001). Drosophila Rhomboid-1 Defines a Family of Putative Intramembrane Serine Proteases. Cell *107*, 173–182.

Urban, S., Lee, J.R., and Freeman, M. (2002). A family of Rhomboid intramembrane proteases activates all Drosophila membrane-tethered EGF ligands. EMBO J. *21*, 4277–4286.

Vanier, M.T. (2010). Niemann-Pick disease type C. Orphanet J. Rare Dis. *5*, 16.

Vetter, I.R., and Wittinghofer, A. (2001). The guanine nucleotide-binding switch in three dimensions. Science *294*, 1299–1304.

Voice, J.K., Klemke, R.L., Le, A., and Jackson, J.H. (1999). Four human ras homologs differ in their abilities to activate Raf-1, induce transformation, and stimulate cell motility. J. Biol. Chem. *274*, 17164–17170.

Walter, P., and Ron, D. (2011). The unfolded protein response: from stress pathway to homeostatic regulation. Science *334*, 1081–1086.

Wang, Y., Zhang, Y., and Ha, Y. (2006). Crystal structure of a rhomboid family intramembrane protease. Nature *444*, 179–180.

van de Weijer, M.L., Bassik, M.C., Luteijn, R.D., Voorburg, C.M., Lohuis, M.A.M., Kremmer, E., Hoeben, R.C., LeProust, E.M., Chen, S., Hoelen, H., et al. (2014). A high-coverage shRNA screen identifies TMEM129 as an E3 ligase involved in ER-associated protein degradation. Nat. Commun. *5*, 3832.

Whyte, D.B., Kirschmeier, P., Hockenberry, T.N., Nunez-Oliva, I., James, L., Catino, J.J., Bishop, W.R., and Pai, J.-K. (1997). K- and N-Ras are geranylgeranylated in cells treated with farnesyl protein transferase inhibitors. J. Biol. Chem. *272*, 14459–14464.

Wilson, K.J., Gilmore, J.L., Foley, J., Lemmon, M.A., and Riese, D.J. (2009). Functional selectivity of EGF family peptide growth factors: Implications for cancer. Pharmacol. Ther. *122*, 1–8.

Wirawan, E., Lippens, S., Vanden Berghe, T., Romagnoli, A., Fimia, G.M., Piacentini, M., and Vandenabeele, P. (2012). Beclin1: a role in membrane dynamics and beyond. Autophagy *8*, 6–17.

Witters, L., Scherle, P., Friedman, S., Fridman, J., Caulder, E., Newton, R., and Lipton, A. (2008). Synergistic Inhibition with a Dual Epidermal Growth Factor Receptor/HER-2/neu Tyrosine Kinase Inhibitor and a Disintegrin and Metalloprotease Inhibitor. Cancer Res. *68*, 7083–7089.

Wong, E., Cohen, T., Romi, E., Levin, M., Peleg, Y., Arad, U., Yaron, A., Milla, M.E., and Sagi, I. (2016). Harnessing the natural inhibitory domain to control TNFα Converting Enzyme (TACE) activity *in vivo*. Sci. Rep. *6*, 35598.

Wu, Z., Yan, N., Feng, L., Oberstein, A., Yan, H., Baker, R.P., Gu, L., Jeffrey, P.D., Urban, S., and Shi, Y. (2006). Structural analysis of a rhomboid family intramembrane protease reveals a gating mechanism for substrate entry. Nat. Struct. Mol. Biol. *13*, 1084–1091.

Xu, P., and Derynck, R. (2010). Direct activation of TACE-mediated ectodomain shedding by p38 MAP kinase regulates EGF receptor-dependent cell proliferation. Mol. Cell *37*, 551–566.

Yan, J., Roy, S., Apolloni, A., Lane, A., and Hancock, J.F. (1998). Ras Isoforms Vary in Their Ability to Activate Raf-1 and Phosphoinositide 3-Kinase. J. Biol. Chem. *273*, 24052–24056.

Yan, Z., Zou, H., Tian, F., Grandis, J.R., Mixson, A.J., Lu, P.Y., and Li, L.-Y. (2008). Human rhomboid family-1 gene silencing causes apoptosis or autophagy to epithelial cancer cells and inhibits xenograft tumor growth. Mol. Cancer Ther. *7*, 1355–1364.

Yates, A., Akanni, W., Amode, M.R., Barrell, D., Billis, K., Carvalho-Silva, D., Cummins, C., Clapham, P., Fitzgerald, S., Gil, L., et al. (2016). Ensembl 2016. Nucleic Acids Res. *44*, D710-716.

Ye, Y., Shibata, Y., Yun, C., Ron, D., and Rapoport, T.A. (2004). A membrane protein complex mediates retro-translocation from the ER lumen into the cytosol. Nature *429*, 841–847.

Yuan, H., Wei, R., Xiao, Y., Song, Y., Wang, J., Yu, H., Fang, T., Xu, W., and Mao, S. (2018). RHBDF1 regulates APC-mediated stimulation of the epithelial-to-mesenchymal transition and proliferation of colorectal cancer cells in part via the Wnt/β-catenin signalling pathway. Exp. Cell Res. *368*, 24–36.

Zerangue, N., Malan, M.J., Fried, S.R., Dazin, P.F., Jan, Y.N., Jan, L.Y., and Schwappach, B. (2001). Analysis of endoplasmic reticulum trafficking signals by combinatorial screening in mammalian cells. Proc. Natl. Acad. Sci. U. S. A. *98*, 2431–2436.

Zettl, M., Adrain, C., Strisovsky, K., Lastun, V., and Freeman, M. (2011). Rhomboid Family Pseudoproteases Use the ER Quality Control Machinery to Regulate Intercellular Signaling. Cell *145*, 79–91.

Zhang, T., Xu, Y., Liu, Y., and Ye, Y. (2015). gp78 functions downstream of Hrd1 to promote degradation of misfolded proteins of the endoplasmic reticulum. Mol. Biol. Cell *26*, 4438–4450.

Zhang, Y., Li, Y., Yang, X., Wang, J., Wang, R., Qian, X., Zhang, W., and Xiao, W. (2018). Uev1A-Ubc13 catalyzes K63-linked ubiquitination of RHBDF2 to promote TACE maturation. Cell. Signal. *42*, 155–164.

Zheng, X., Jiang, F., Katakowski, M., Zhang, Z.G., Lu, Q., and Chopp, M. (2009). ADAM17 promotes breast cancer cell malignant phenotype through EGFR-PI3K-AKT activation. Cancer Biol. Ther. *8*, 1045–1054.

Zheng, X., Jiang, F., Katakowski, M., Lu, Y., and Chopp, M. (2012). ADAM17 promotes glioma cell malignant phenotype. Mol. Carcinog. *51*, 150–164.

Zhou, B.-B.S., Peyton, M., He, B., Liu, C., Girard, L., Caudler, E., Lo, Y., Baribaud, F., Mikami, I., Reguart, N., et al. (2006). Targeting ADAM-mediated ligand cleavage to inhibit HER3 and EGFR pathways in non-small cell lung cancer. Cancer Cell *10*, 39–50.

Zhou, Z., Liu, F., Zhang, Z.-S., Shu, F., Zheng, Y., Fu, L., and Li, L.-Y. (2014). Human rhomboid family-1 suppresses oxygen-independent degradation of hypoxia-inducible factor-1α in breast cancer. Cancer Res. *74*, 2719–2730.

Zou, H., Thomas, S.M., Yan, Z.-W., Grandis, J.R., Vogt, A., and Li, L.-Y. (2009). Human rhomboid family-1 gene RHBDF1 participates in GPCR-mediated transactivation of EGFR growth signals in head and neck squamous cancer cells. FASEB J. Off. Publ. Fed. Am. Soc. Exp. Biol. *23*, 425–432.

Zunke, F., and Rose-John, S. (2017). The shedding protease ADAM17: Physiology and pathophysiology. Biochim. Biophys. Acta BBA - Mol. Cell Res. *1864*, 2059–2070.